UNIVERSITY OF
LIVERPOOL

Invariants of Lagrangian Mappings

Thesis submitted in accordance with the requirements of the University of Liverpool for the degree of Doctor in Philosophy

by

Katy Gallagher

September 2016

Abstract

In this thesis we study the space $\mathcal{L} = \mathcal{L}(M, N)$ of all Lagrangian mappings of a fixed closed surface or 3-manifold M to respectively another surface or 3-manifold N. In most cases we are assuming both M and N oriented. We are looking for local (order 1) invariants of such generic maps, that is, for those whose increments along generic paths in $\mathcal{L}$ are completely determined by diffeomorphism types of the local bifurcations of the caustics in N. Such invariants are dual to trivial cycles supported on the discriminantal hypersurface Ξ in $\mathcal{L}$. The duality here is in the sense of the increment of an invariant along a generic path γ in $\mathcal{L}$ is the index of intersection of γ with the cycle, and the triviality means that if γ is a loop then its index of intersection with the cycle must vanish.

For surfaces, we obtain a complete description of the spaces of discriminantal cycles, possibly non-trivial. For $N = \mathbb{R}^2$ and the subset of maps in $\mathcal{L}$ without corank 2 singularities, this description implies that any rational local invariant itself is a linear combinations of the numbers of various singular points of the caustics and of the Ohmoto-Aicardi linking invariant of ordinary maps between surfaces. Using our discriminantal cycles, we also prove Ohmoto's conjecture about non-contractability of a certain loop in $\mathcal{L}(S^2, \mathbb{R}^2)$. Our surface results are now published in [16].

For oriented 3-manifolds, we prove that the space of all rational local invariants is ten-dimensional and spanned by the numbers of various isolated-

type singularities of the caustics and the Euler characteristic of the critical point set. We also show that the rank of the space of the mod2 invariants has dimension 16.

The results of the thesis are based on our study of generic one- and two-parameter families of caustics. In our 3-dimensional constructions, we had to analyse generic projections of the D_6 and E_6 caustics to the plane. Nothing anyhow close to this rather delicate analysis has been done before, and it occupies nearly half the thesis.

Acknowledgements

I would like to express my gratitude to my supervisor Professor Victor Goryunov for all his help, support and guidance over the past four years and in particular for his patience. I would also like to thank my second supervisor Dr Anna Pratoussevitch for her kind words and support.

Thanks are also due to the University of Liverpool and to EPSRC for funding my research and providing me with the opportunity to travel to conferences.

I must thank the friends I have made over the past four years in the department for their support and advice. In particular to those I have had the joy of sharing office 523 with for their words of encouragement and friendships.

Finally I would like to thank my family and close friends for their unconditional love and support. Words cannot express how grateful I am to you all and this work is dedicated to you.

Contents

Chapter 0

Introduction

Vassiliev's famous singularity theory approach to knot invariants [22] has been successfully applied to the study of invariants of generic maps in some other low-dimensional problems.

The interest in this direction was initiated by Arnold's introduction in [5] of three order 1 Vassiliev-type invariants of regular planar curves. Two of Arnold's invariants, those dual to triple point and direct self-tangency bifurcations, were then generalised to the higher order settings [23, 18, 12].

Arnold gave also a classification of order 1 invariants of planar wave fronts [6], which was refined by Aicardi in [1]. A few years later followed Chernov's classification of similar invariants of fronts on arbitrary surfaces [21].

Victor Goryunov classified the local invariants of mappings of oriented surfaces into $\mathbb{R}^3$ in [11] and local invariants of mappings between 3-manifolds in [13].

To add to this list, we must mention the Ohmoto-Aicardi classification of local invariants of maps of surfaces to a plane done in [19] in terms of bifurcations of the critical value curves.

The locality of the invariants in the papers quoted and in this thesis means that the values of the invariants in generic one-parameter families of maps change at the moments of bifurcations by the amounts completely defined by the local types of the bifurcations.

In this thesis we classify local invariants of two other natural sets of low-dimensional maps, namely, of Lagrangian maps between surfaces and between 3-manifolds. We do this in terms of the geometry of their caustics, that is, of their critical value sets. In this sense the main themes of the thesis are the Lagrangian analogues of papers [19] and [13]. However, the Lagrangian geometry turns out to be much richer and more complicated than that of ordinary smooth maps.

To allow comparison of our results with those from papers [19] and [13], we recall in the next two sections the main results of these papers, and some ideas they used.

0.1 Mappings between surfaces

In [19], Toru Ohmoto and Francesca Aicardi considered C^∞ maps of a closed (i.e. compact without boundary) surface M to oriented $\mathbb{R}^2$. For a generic such map, its critical value set (also called the *apparent contour*) has local shapes

depicted in Figure 1. The co-orientation of the branches there are towards the sides with more preimages, and it induces the orientation of the apparent contour as shown in the figure.

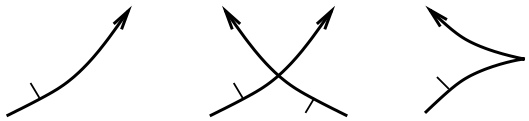

Figure 1: Local singularities of the apparent contour of a generic map from a surface to $\mathbb{R}^2$

Figure 1 immediately suggests two invariants of generic maps in this case: numbers d and v of respectively double points and cusps of the apparent contour.

One can also define a third invariant: the self-linking number ℓ of the Legendrian lift of the contour to $PT^*\mathbb{R}^2$. However, we prefer to postpone its exact definition till Section 1.2.

The main result of [19] is

Theorem 0.1.1. *The invariants d, v and ℓ form a basis of the space of rational-valued local invariants of smooth maps of a non-oriented surface to $\mathbb{R}^2$.*

Introduction of orientation on the source surface allows one to introduce the local degrees, $+1$ or -1, at the cusp points. This splits the invariant v into two, v^+ and v^-, the numbers of positive and negative cusps.

The approach used in [19] for proving Theorem 0.1.1 is based − similar

to other papers on local invariants − on the detailed study of generic one-parameter families of maps and of their interactions in generic two-parameter families.

For a non-oriented source surface, one distinguishes ten generic one-parameter local bifurcations of apparent contours. They are all shown in Figure 2. The notations there are of a mixed English-Russian origin: Lips, Beaks,

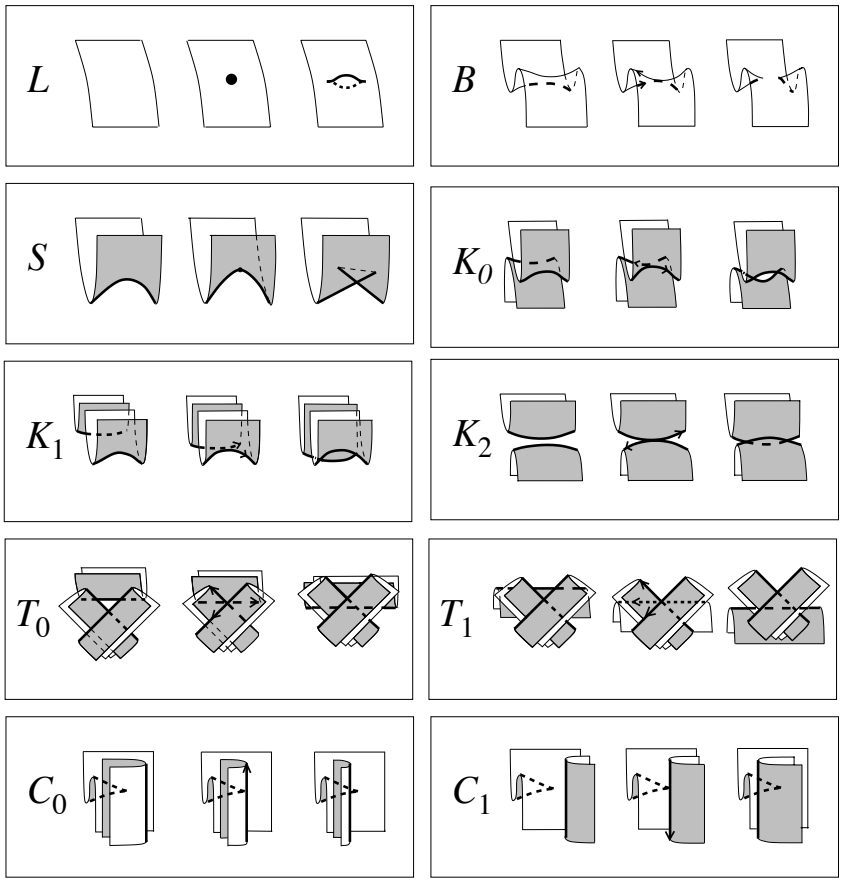

Figure 2: Bifurcations in generic one-parameter families of maps of a surface to $\mathbb{R}^2$.

Swallowtail, Kasanie (translation of the word 'tangency' to Russian), Triple point and Cusp crossing. In each case the middle picture is for a non-generic map which belongs to the discriminantal hypersurface Γ in the space Ω of all smooth maps from M to $\mathbb{R}^2$.

It is convenient to denote the strata of Γ of codimension 1 in Ω by the letters used for the corresponding bifurcations. Each of these strata is co-oriented in the direction where the number of cusps, double points or the preimages of a newly formed region is higher. The increments of the local invariants at crossings of the ten strata in the co-orienting directions are the values to find if we want to construct the invariants.

The increments are subject to equations known as the consistency or coherence equations. To add to the list of synonyms, we call them *roundabout* equations. Their meaning is that the total increment of an invariant along a generic loop in Ω must be zero. Since Ω is contractible, it is sufficient to consider here only small loops around strata of Γ having codimension 2 in Ω. Therefore, one has to consider bifurcations in generic two-parameter families of maps and take small loops around the origin in the parameter spaces.

As an example, we show in Figure 3 the bifurcation diagrams for a few generic two-parameter families of maps. These particular diagrams give us respectively the following equations on the increments of our invariants

$$\text{I.} \quad \ell - b = 0, \qquad \text{II.} \quad 0 = 0, \qquad \text{III.} \quad s - k_1 + s = 0.$$

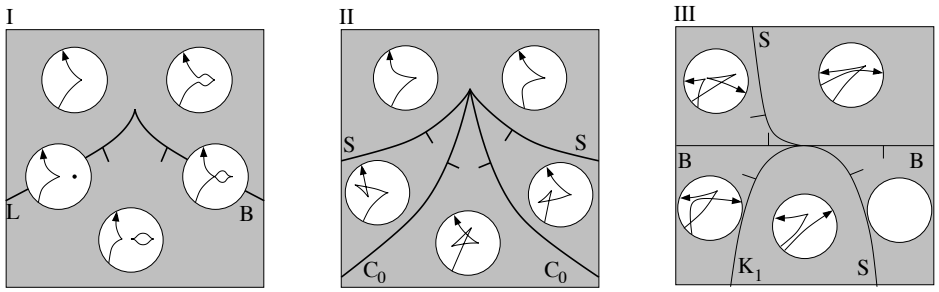

Figure 3: Some bifurcation diagrams from [19].

We denote here by x the increment of a local invariant across the stratum X at its crossing in the direction of its co-orientation.

The first equation here allows us to 'glue up' the strata L and B in one 'big stratum' LB and carry it as a whole through all our further analysis. This is a simplification method we shall use later in the thesis. The second equation is trivial and we will have similar outcomes for quite a few bifurcation diagrams throughout the thesis. Finally, the third equation is a typical example of the constraints we will be dealing with.

In [19], the analysis of all possible generic 2-parameter families of maps yields a rank 7 system of linear equations on the 10 unknown increments. The solution space is therefore of dimension 3. It can be checked that the sets of the increments of the invariants d, v and ℓ form a basis of this space over the rationals. This proves Theorem 0.1.1.

The versions of the three invariants for the Lagrangian case will appear in our Chapter 1.

0.2 Maps between 3-manifolds

Another set of results that we should quote in detail are those from [13] on local invariants of smooth maps between oriented 3-manifolds. Similar to the previous section, we continue to assume the source M closed and target N having no boundary. Once again, we are looking for invariants expressed in terms of the geometry of the critical value sets.

The local geometry of a generic critical value set in the current setting is depicted in Figure 4. Following the pattern of the previous section, we define this time the discriminantal hypersurface Γ in the space Ω of all smooth maps from M to N as the set of all maps with more complicated critical sets.

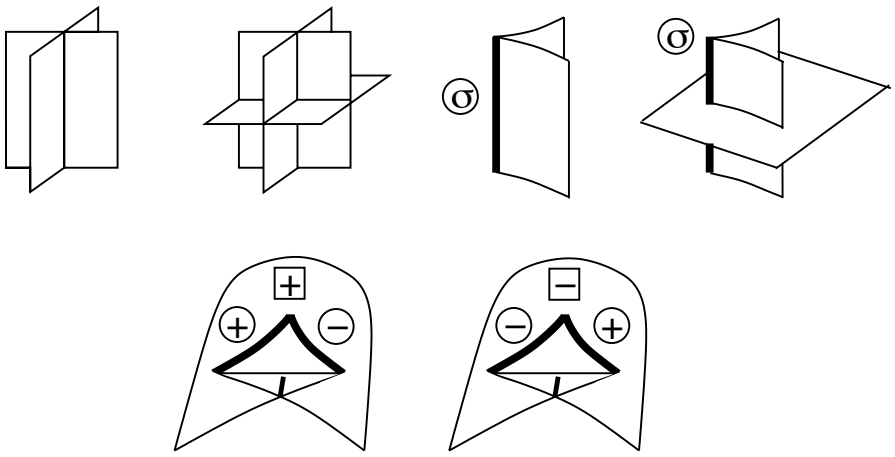

Figure 4: Local singularities of the critical value sets of generic maps between 3-manifolds. The value $\sigma = \pm$ indicates the local degree ± 1 of the map at the cuspidal edge.

Figure 4 immediately suggests five local invariants in the current setting,

all of them counting the numbers of various points of the critical value sets:

i) I_t, the number of triple points;

ii) I_{s_+}, the number of positive swallowtails;

iii) I_{s_-}, the number of negative swallowtails;

iv) I_{c_+}, the number of intersection points of a positive cuspidal edge with a smooth sheet;

v) I_{c_-}, the number of intersection points of a negative cuspidal edge with a smooth sheet.

We also have another obvious invariant:

vi) I_χ, half of the Euler characteristic of the critical locus.

Moreover, one more local invariant was introduced in [13]:

vii) I_{Σ^2}, the linking number in $J^1(M,N)$ of the image of the 1-jet extension of a map with the set of all 1-jets of corank ≥ 2.

The main result of [13] is:

Theorem 0.2.1. *The space of integer local invariants of C^∞ maps between oriented 3-manifolds is seven-dimensional. It is spanned by the invariants*

$$(I_{s_+} \pm I_{s_-})/2, \qquad (I_{c_+} + I_{c_-})/2, \qquad I_t, \qquad (I_t + I_{c_+})/2, \qquad I_\chi, \qquad I_{\Sigma^2}.$$

The theorem is proved in [13] by the methods described in Section 0.1 for the 2-dimensional case: via analysis of generic one- and two-parameter families of maps. The main difference is that such families and bifurcations of them are much more complicated in dimension three.

Notice that the theorem is valid for any connected component of the space of all maps, and the invariants are considered up to an arbitrary choice of individual additive constants 'of integration' on such connected components. All original results of this thesis about dimensions of spaces of local invariants will be formulated within the same approach.

A mod2 analogue of the last theorem obtained in [13] is more convenient to state for $\mathbb{R}^3$ as the target. This is because the space Ω of all maps is contractible in this case, and hence any solution of the system of roundabout equations coming from generic 2-parameter bifurcations can be integrated (see Section 0.3 for the integrability notion). So, we have in [13]

Theorem 0.2.2. *The space of mod2 local invariants of C^∞ maps from a closed oriented 3-manifold to oriented $\mathbb{R}^3$ has dimension 11.*

Of course, the mod2 reduction of the integer invariants from the previous theorem provides a seven-dimensional subspace in this mod2 space. It has also been possible to define three further linearly independent $\mathbb{Z}_2$-invariants. Introduced in [13] and [2], each of these three invariants combines the number of components and the self-linking of one of the three framed links in $\mathbb{R}^3$ constructed from the cuspidal edge and self-intersection locus of the critical

value set. An integral interpretation of an eleventh basic invariant is still missing.

Paper [13] also considers cases of non-oriented source and/or target. However, we do not recall the results of this since we are not going to consider their Lagrangian analogues in this thesis.

Except for its main theorems, paper [13] is quite useful for this dissertation since there is basically no difference between ordinary and Lagrangian maps as long as their coranks are at most one. Therefore the bifurcations considered in [13] partly cover the range we have to analyse in Chapter 2.

0.3 Results of the thesis

In this dissertation we study the space $\mathcal{L} = \mathcal{L}(M, E, N)$ of all Lagrangian immersions of a closed (that is, compact without boundary) surface or 3-manifold M to the total space E of a Lagrangian fibration $E \to N$, where N is respectively another surface or 3-manifold. In most cases we are assuming both the source and target oriented. We are looking for invariants of such Lagrangian maps whose increments along generic paths in $\mathcal{L}$ are completely determined by diffeomorphism types of the local bifurcations of the caustics in N. These are what should be called local order 1 invariants of the caustics (cf. [22]), but we call them just *local* since no higher-order invariants will be considered. We denote by $\Xi \subset \mathcal{L}$ the set of Lagrangian maps at which the caustics bifurcate, and call this set the *discriminant.* We should remark that

Ξ is not what one would consider as a complete discriminant in the space of all Lagrangian maps since it ignores bifurcations of self-intersection points in E of the immersed manifolds M. Respectively, our space of local invariants of caustics is a subset of the space of all local order 1 invariants of Lagrangian maps.

Up to a choice of an additive constant (individual for each connected component of $\mathcal{L}$), any numerical local invariant I is defined by its *derivative* $I' = \sum x_i X_i$, where the $X_i \subset \Xi$ are discriminantal strata of codimension 1 in $\mathcal{L}$, and the x_i are the increments of I across them. This linear combination is a *trivial* codimension 1 *cycle* in $\mathcal{L}$, that is, its index of intersection with any loop in $\mathcal{L}$ vanishes since this index is the total increment of the invariant along a closed path. Therefore, construction of such linear combinations (without an a priori knowledge of the invariants) splits into two parts:

i) establishing conditions on linear combinations of the codimension 1 strata to be cycles (we call them *discriminantal cycles*), and

ii) checking the triviality of the discriminantal cycles.

The first part is approachable via an appropriate development of singularity theory methods, and does not depend on the choice of M, E and N (except for the orientability) and of a particular connected component of $\mathcal{L}(M, E, N)$. The second part is either sufficiently straightforward (when an integral, that is, homotopy-free interpretation of a relevant invariant is available), or quite hard (when there is no such interpretation, and this is a general situation). In

the latter case, knowledge of the fundamental group of a particular connected component of $\mathcal{L}(M, E, N)$ could be helpful, but calculation of this group is an even more complicated task. On the other hand, discriminantal cycles themselves may be used for testing non-contractibility of certain loops in $\mathcal{L}$, and we give examples of this in Section 1.5.

In this thesis we describe the integer and mod2 invariants for Lagrangian maps between 2-manifolds followed by maps between 3-manifolds. In the two-dimensional case we also describe the rational invariants. These two cases are presented in separate chapters, followed by three additional chapters that look at in-depth calculations regarding the D_6 and E_6 singularities in the 3-dimensional case.

The first main result of this thesis, Theorem 1.3.3, is a complete description of the spaces of discriminantal cycles for caustics on surfaces. Translation of this description to the local invariants themselves has turned out to be the most complete for the target $N = \mathbb{R}^2$ and the subset $\mathcal{L}_1$ of $\mathcal{L}(M, T^*\mathbb{R}^2, \mathbb{R}^2)$ consisting of maps without corank 2 singularities. According to Theorem 1.3.6, for such a setting, up to a choice of additive constants on connected components of $\mathcal{L}_1$, all rational local invariants of caustics are linear combinations of the numbers of various singular points of the caustics and of the linking invariant ℓ of ordinary maps between surfaces mentioned in Section 0.1. For other targets, the question of triviality of certain discriminantal cycles is open, which allows to only bound the dimensions of the invariant spaces.

The second main result of this thesis, Theorem 2.2.3, states that the space

of rational discriminantal cycles in $\mathcal{L}(M, T^*N, N)$, where M and N are oriented 3-manifolds, has rank 10. All discriminantal cycles turn out to be integrable, and generators of the rank 10 lattice of integer local invariants are described in Corollary 2.2.6. The mod2 analogue of Theorem 2.2.3 is Theorem 2.2.7 which states that the space of $\mathbb{Z}_2$ discriminantal cycles in $\mathcal{L}(M, T^*N, N)$ has rank 16. This contains the ten dimensional space spanned by the mod2 reductions of the invariants in Corollary 2.2.2, however in the case of ordinary maps between 3-manifolds with the target $\mathbb{R}^3$ or S^3 there are three further invariants which results in a 13 dimensional space inside our rank 16 space. Hence the corresponding space of $\mathbb{Z}_2$-invariants has dimension at most 16, and at least 10 since it contains the 10-dimensional subspace spanned by the mod2 reductions of the invariants from Corollary 2.2.6. For the target manifold $\mathbb{R}^3$ or S^3, one can increase the lower bound on the dimension to 13 by adding Lagrangian generalizations of the three link invariants from [13] and [2] mentioned in Section 0.2. However, we are not including these generalisations in this thesis.

The thesis is organised as follows:

Chapter 1: the local invariants in two dimensions are studied. In Section 1.1 we recall basic definitions regarding Lagrangian mappings. The singularities of a generic caustic are the same as those in [19]. Section 1.2 lists discriminantal strata of codimension 1 in $\mathcal{L}$, and formulates the first main results, Theorems 1.3.3, 1.3.4 and 1.3.6, stated in Subsection 1.3.4. Section 1.4 proves our main theorems via analysis of generic 2-parameter families of

caustics. Its Subsection 1.4.4 considers adjustments needed if at least one of the source and target surfaces is not oriented. Finally, in Section 1.5, we use the discriminantal cycles corresponding to corank 2 degenerations of maps to prove non-contractibility of certain loops in the spaces of Lagrangian maps of the 2-sphere. It would be very interesting to see to what extent the results of this section could be generalised to loops in other connected components of $\mathcal{L}(S^2, E, N)$ and to the source different from S^2.

Chapter 2: we consider the local invariants in three dimensions. Section 2.1 gives a description of strata we distinguish in the singular locus of the caustic of a generic Lagrangian map between two oriented 3-manifolds following page 18 of [4]. We also introduce there some obvious invariants. Section 2.2 lists the discriminantal strata of codimensional 1 in $\mathcal{L}$, and formulates the second set of main results, Theorem 2.2.3 and 2.2.7, stated in Subsection 2.2.4. Section 2.3 lists the generic 2-parameter families of caustics which are then analysed in Section 2.4 to prove our main Theorems from this chapter.

Chapters 3 - 5 are devoted to a proof of Theorem 2.3.3 from Section 2.3.2.7 on the roundabout equations coming from the D_6 and E_6 isolated function singularities. To obtain these equations, one considers the 'big' caustics $\tilde{C} \subset \mathbb{R}^5$ of D_6 and E_6, and analyse their generic projections π to $\mathbb{R}^2$. The critical value sets of various π's give rise to the equations we are looking for. The analysis of each of the three cases (D_6^+, D_6^- and E_6) turns out to be rather lengthy and delicate, and occupies Chapters 3, 4 and 5 respectively. The main difficulty there is that the principal quasihomogeneous part π_0 of a generic π

is not a generic map of $\tilde{\mathcal{C}}$ on its own. Therefore we have to consider terms of π of a few further quasi-homogeneous degrees to extract the sufficiently generic information needed. The expositions in Chapters 3 - 5 are very similar: they all start with checking the behaviour of the relevant π_0 on various strata of $\tilde{\mathcal{C}}$, and then add to the consideration new terms degree by degree. In our analysis, we are using parametrisations of various strata of $\tilde{\mathcal{C}}$. In the $D_6^{\pm}$ cases such parametrisations come from the well-known reduction to the polynomials in one variable (see, for example [26] and [14]). In the E_6 case, such a universal approach does not exist, and we resort to construction of rather individual parametrisations of different strata of $\tilde{\mathcal{C}}$. Chapter 5 on the E_6 caustic is perhaps the most technical part of the thesis. We should remark that the only study of the E_6 caustic is somehow (but rather distantly) relevant to our needs that is known to us is [9].

Chapter 1

Local invariants of Lagrangian mappings between surfaces

1.1 Lagrangian mappings: general definitions

We start with recalling a series of standard definitions which may be found, for example, in [7] or [4].

A *symplectic structure* on a manifold E^{2n} is a closed non-degenerate differential 2-form ω.

A *Lagrangian submanifold* of a symplectic manifold (E^{2n}, ω) is an n-dimensional submanifold on which the pullback of the symplectic form vanishes.

A *fibration* $p : E^{2n} \to N^n$ of a symplectic manifold E over a base N is called *Lagrangian* if all its fibres are Lagrangian submanifolds. A composition

$M \xrightarrow{i} E \xrightarrow{p} N$ where i is an embedding of a manifold M^n into E^{2n} as a Lagrangian submanifold is what is usually called a *Lagrangian map.* However, we allow i to be a Lagrangian immersion.

The critical value set $\mathcal{C} \subset N$ of a Lagrangian map $p \circ i$ is called the *caustic* of the map.

All Lagrangian fibrations of the same dimension are locally isomorphic. In this chapter we will be mostly considering the $n = 2$ case, and in all our local normal forms, we will be using the standard local model of $T^*\mathbb{R}^2$ fibred over $\mathbb{R}^2$. The symplectic form here is $\omega = dU \wedge du + dV \wedge dv$, where u, v and U, V are coordinates respectively on the plane and along the fibres of the fibration.

A germ of a Lagrangian surface $L \subset T^*\mathbb{R}^2_{u,v}$ is defined by its *generating family of functions* $F(x, u, v)$:

$$L = \{(u, v, U, V) \,|\, \exists\, x \in \mathbb{R}^k : F_x = 0, U = F_u, V = F_v\}\,.$$

The minimal dimension k of the variable x here is the corank of the derivative of the projection $L \to \mathbb{R}^2_{u,v}$ at the base point. The smoothness of L requires that the rank of the matrix $(F_x)_{x,u,v}$ of the second derivatives at the base point must be equal to the dimension of x. The caustic $\mathcal{C} \subset \mathbb{R}^2_{u,v}$ consists of those points (u, v) for which the member $F(\cdot, u, v)$ of the generating family has non-Morse critical points.

An equivalence of two Lagrangian maps $L_j \to E_j \to N_j$, $j = 1, 2$, is a

commutative diagram

$$\begin{array}{ccccc} L_1 & \to & E_1 & \to & N_1 \\ \downarrow & & \varphi\downarrow & & \downarrow \\ L_2 & \to & E_2 & \to & N_2 \end{array}$$

in which all vertical arrows are diffeomorphisms, and $\varphi^*(\omega_2) = \omega_1$ holds for the corresponding symplectic structures. In terms of the local generating families $F(x, u, v)$ of functions this corresponds to the stable $\mathcal{R}_+$-equivalence preserving the fibration $(x, u, v) \mapsto (u, v)$ (see [7]). The stability here is in the sense of addition of non-degenerate quadratic forms in extra x-variables.

In this chapter, we will be using $N = \mathbb{R}^2$ for the target surface and $T^*\mathbb{R}^2 \to \mathbb{R}^2$ for the Lagrangian fibration. The differences existing with more general settings will be addressed in the remarks. All the local normal forms of maps or families of maps that we will be using will be considered near the origins of the source, target and parameter spaces.

1.2 Generic planar caustics and their local invariants

According to the classical result of Whitney [25], the critical point set of a generic C^∞ map (not necessarily Lagrangian) between surfaces is a smooth curve. At isolated points on this curve the map has the *pleat* singularity,

for which one can choose local coordinates in the source and target so that the map is $(z_1, z_2) \mapsto (t_1, t_2) = (z_1^3 + z_1 z_2, z_2)$. At all other points of the critical curve, the map has the *fold* singularity, with the local normal form $(z_1, z_2) \mapsto (z_1^2, z_2)$. See Figure 5. Fold singularities correspond to regular branches of the critical value set, while pleat points provide semi-cubical cusps of this set. If both the source and target surfaces are oriented, we distinguish two types of pleats, of local degrees $+1$ and -1. Regular branches of a generic critical value set meet transversally.

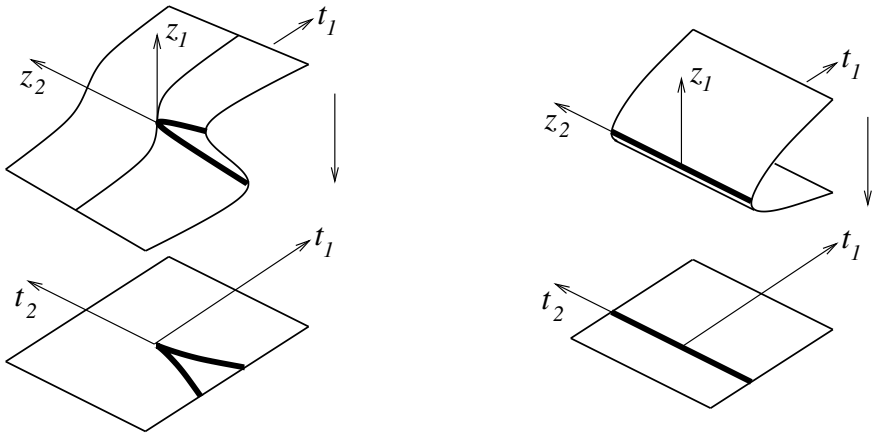

Figure 5: Pleat and fold singularities.

Similarly, in the case of Lagrangian maps from surfaces to the plane, a generic caustic $\mathcal{C}$ (that is, the critical value set) is a planar curve whose only singularities are points of transversal self-intersection and semi-cubical cusps. Translating the above normal forms of maps to the Lagrangian language of local generating families and using the standard notations of the corresponding function singularities (see page 32 of [4]), we introduce the following notations

for the points of $\mathcal{C}$:

A_2, regular points of a caustic, with a local generating family $x^3 + ux$;

A_2^2, points of transversal intersection of two regular local branches;

$A_3^{s,\sigma}$, $s = \pm$, $\sigma = \pm$, semi-cubical cusps, with a local generating family $sx^4 + ux^2 + vx$, and the sign σ indicating the local degree ± 1 of the Lagrangian map.

Remark 1.2.1. We emphasise that the Lagrangian pleats A_3 with different choices of the sign $s = \pm$ are *not* Lagrangian equivalent, in spite of being equivalent in the oriented Whitney setting. The reason is that the function x^4 cannot be transformed to $-x^4$ by a change of the real coordinate x (see page 18 of [4] for details).

Following [19], we co-orient a caustic $\mathcal{C} \subset \mathbb{R}^2$ to its side with a higher number of local pre-images. We will also show the same information by orienting $\mathcal{C}$ so that its (orientation, co-orientation) frame gives the orientation of the plane, as in Figure 6.

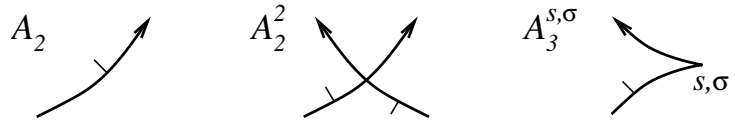

Figure 6: Singularities of generic caustics.

Consider the space $\mathcal{L} = \mathcal{L}(M, T^*\mathbb{R}^2, \mathbb{R}^2)$ of all Lagrangian maps $M \looparrowright T^*\mathbb{R}^2 \to \mathbb{R}^2$, where the first arrow is a Lagrangian immersion of a compact

surface and the second the canonical projection. Maps whose caustics have more complicated singularities than those described above form the *discriminantal* hypersurface Ξ in $\mathcal{L}$.

Consider connected components of $\mathcal{L} \setminus \Xi$. A numerical *invariant* is a way to assign numbers to each of them. Along a generic path in $\mathcal{L}$, the values of an invariant change at the moments of discriminant crossings.

Definition 1.2.2. We say that an *invariant is local* if every increment of the invariant is completely determined by the diffeomorphism type of the local bifurcation of the caustic at the crossing.

For non-$\mathbb{Z}_2$-valued invariants, the discriminant should be locally co-oriented.

A local invariant I defines its *derivative* $I' = \sum_i x_i X_i$, where the $X_i \subset \Xi$ are the strata of codimension 1 in $\mathcal{L}$ we are able to distinguish for the needs of Definition 1.2.2, and the x_i are the local increments of I along generic paths in $\mathcal{L}$ crossing the X_i in the co-orienting direction. On the other hand, I is defined by I' on each connected component $\mathcal{L}_j$ of $\mathcal{L}$ up to an arbitrary choice of the value of I at a non-discriminantal base point in $\mathcal{L}_j$.

Since the total increment of I along any loop in $\mathcal{L}_j$ vanishes, the derivative $\sum_i x_i X_i$ must be a trivial codimension 1 cycle in $\mathcal{L}_j$. The vanishing of the total increment on contractible loops (that is, the derivative being a cycle, maybe non-trivial) is equivalent to its vanishing on small loops in $\mathcal{L}$ around codimension 2 strata of the discriminant. Finding the relevant cyclicity constraints on the increments x_i is the problem we are mainly concentrating on in this thesis. Cycles of the form $\sum_i x_i X_i$ will be called *discriminantal*.

To establish the non-triviality of a discriminantal cycle, one should point out a loop in $\mathcal{L}$ with a non-zero index of intersection with the cycle. The loop itself is then non-contractible. We will give examples of this in Section 1.5.

On the other hand, one of the ways to establish the triviality of a cycle $I' = \sum_i x_i X_i$ is to find an *integral* (that is, path-independent) interpretation of its antiderivative I in terms of the geometry of individual caustics.

Examples 1.2.3. The number of isolated singularities of a caustic $\mathcal{C}$ of a particular type is, of course, a local invariant. We have five such invariants:

I_d, *the number of double points* A_2^2*;*

$I^c_{s,\sigma}$, $s, \sigma = \pm$, *the numbers of* (s,σ)*-cusps.*

For Lagrangian maps to a plane but not to a more complicated surface, we have a sixth local invariant. It is the restriction to the set of Lagrangian maps $\mathcal{L}(M, T^*\mathbb{R}^2, \mathbb{R}^2)$ of the self-linking invariant of the critical value sets of generic smooth maps from M to the plane, as introduced by Ohmoto and Aicardi in [19]. Basically, this Bennequin-type invariant is the writhe of a ribbon defined by the critical value set in $PT^*\mathbb{R}^2$ which is then embedded into $\mathbb{R}^3$. We recall its exact definition now.

Let $\mathcal{C}$ be this time the critical value set of a generic C^∞ map from a surface M to oriented $\mathbb{R}^2$. The curve $\mathcal{C}$ is oriented in the way we oriented caustics earlier. Considering each point of $\mathcal{C}$ with its normal direction to the curve, we lift $\mathcal{C}$ to a link $\widetilde{\mathcal{C}}$ in $PT^*\mathbb{R}^2 \simeq \mathbb{R}^2 \times S^1$. Now, for a fixed small $\varepsilon > 0$ and each point $c \in \mathcal{C}$, take the two points on the normal to $\mathcal{C}$ at c at the distance ε

from c. Let $\mathcal{C}_\varepsilon \subset \mathbb{R}^2$ be the curve formed by all such points, and $\widetilde{\mathcal{C}}_\varepsilon \subset PT^*\mathbb{R}^2$ the corresponding link. Choose a small $\varepsilon_0 > 0$. The union $\widetilde{C}$ of all the $\widetilde{\mathcal{C}}_\varepsilon$ for $0 \leq \varepsilon \leq \varepsilon_0$ is an oriented multi-component ribbon in $PT^*\mathbb{R}^2$ with the core $\widetilde{\mathcal{C}}$.

We orient the solid torus $PT^*\mathbb{R}^2$ as $\mathbb{R}^2 \times S^1$, with the circular factor oriented by the positive rotational direction in the plane. We embed $PT^*\mathbb{R}^2$ unknottedly into $\mathbb{R}^3$ which we take with the orientation coming from the solid torus, and define the linking number $\ell(\mathcal{C})$ as the writhe of the ribbon $\widetilde{C} \subset \mathbb{R}^3$. Following the standard algorithmical definition of the writhe of a framed knot (see for example [17]), we consider the diagram of $\widetilde{C}$ obtained from a generic projection of the $\mathbb{R}^3$ to a plane. We calculate the linking number $\ell_0(\widetilde{\mathcal{C}})$ as the usual algebraic sum of positive and negative crossings in the link diagram of $\widetilde{\mathcal{C}}$, and we also calculate the algebraic number $\ell_1(\widetilde{C})$ of signed half-twists by which the ribbon diagram differs from the blackboard one, that is, from the ribbon following the link diagram of $\tilde{\mathcal{C}}$ and lying flat on the plane. Finally, $\ell(\mathcal{C}) := \ell_0(\widetilde{\mathcal{C}}) + \ell_1(\widetilde{C})/2$.

1.3 Generic codimension 1 bifurcations of planar caustics

We will now describe the strata from which we will be building up discriminantal cycles in $\mathcal{L} = \mathcal{L}(M, T^*\mathbb{R}^2, \mathbb{R}^2)$. They correspond to bifurcations met in generic one-parameter families of caustics. Wherever the letters s or σ appear in the notations below, they always mean $\pm$ like in the previous section. The

indices e and h distinguish between the elliptic and hyperbolic versions of similar bifurcations.

1.3.1 Corank 1 multi- and uni-germs

First of all we list all (see [4], pages 32 and 33) bifurcations in generic 1-parameter families which involve only *corank 1 singularities* of the corresponding Lagrangian maps. By this we mean that the corank of the derivative of a map at any critical point is 1.

We start with bifurcations of multi-germs. In each of them, one of the participating local components is a smooth A_2 branch of the caustic. We illustrate such a bifurcation in Figure 7 only with the final curve (that is, the one to the positive side of the corresponding discriminantal stratum in $\mathcal{L}$) and indicate the shift of the smooth branch during the transition. The notations we are introducing are self-explanatory, with the letter T standing for the tangency of the caustic components.

We have (see Figure 7):

$A_2^{3,k}$, $k = 2, 3$, triple point of a caustic. The post-bifurcational triangular region has k sides co-oriented outwards. Respectively, for the pre-bifurcational triangle, this number is $3 - k$.

$TA_2^{2,k}$, $k = 0, 1, 2$, tangency of two smooth branches. Here k is the number of sides of the new-born bi-gon co-oriented outwards.

$A_3^{s,\sigma}A_2^k$, $k = 0, 1$, an (s, σ)-cusp passes through a smooth branch of a caustic.

Here the value of k distinguishes between the two co-orientation possibilities of the regular curve.

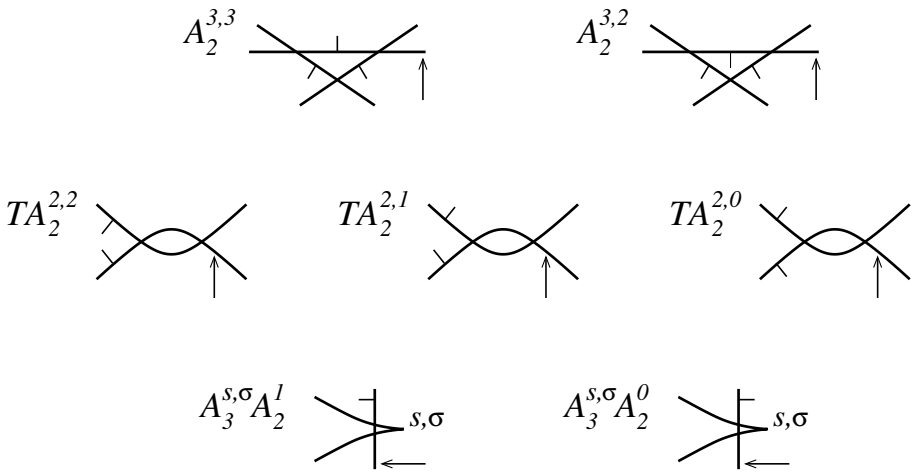

Figure 7: Generic bifurcations of multi-germ caustics.

For the uni-germs, we have the following transformations of the caustics (see Figure 8 where the directions of the positive moves are from the left to the right):

$A_3^{s,\sigma;e}$, birth of a lips component, with two (s,σ)-cusps.

$A_3^{s,\sigma;h}$, a beaks bifurcation of the caustic, with two (s,σ)-cusps appearing.

$A_4^{s,\sigma}$, a swallowtail bifurcation. The (s,σ)-cusp is the first of the two cusps on the local post-bifurcational curve if we follow its conventional orientation.

Normal forms of the generating family bifurcations in the last three cases

respectively are

$$s(x^4+(v^2-\lambda)x^2)+ux\,,\qquad s(x^4+(\lambda-v^2)x^2)+ux\,,\qquad x^5-\lambda x^3+vx^2+ux\,,$$

where λ is the parameter increasing in the bifurcation (see [3, 26]).

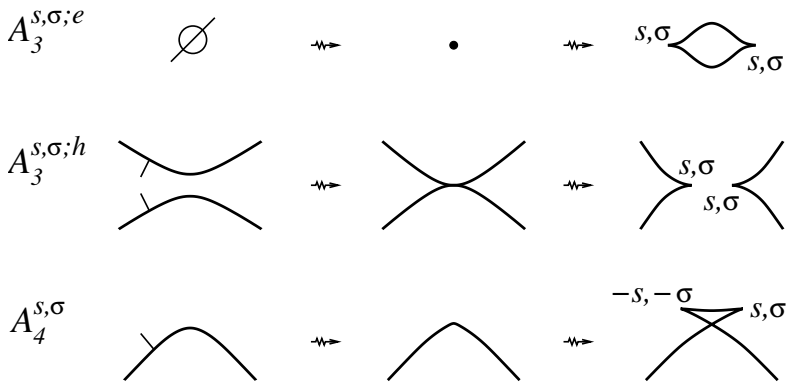

Figure 8: Generic corank 1 bifurcations of uni-germ caustics.

1.3.2 Corank 2 bifurcations in one-parameter families

We now allow the derivatives of the maps to have corank 2 at some critical points. According to [26], any local bifurcation of caustics in this case may be obtained as a generic one-parameter family of planar sections of the spatial caustics of the $\mathcal{R}_+$-miniversal deformations of the $D_4^{\pm}$ function singularities:

$$F(x,y;u,v,w)=\pm x^2y+\frac{1}{3}y^3+\frac{1}{2}wy^2+vy+ux\,.$$

These two caustics are shown in Figure 9. The parameter of such a sectional family reduces to $\lambda = w + \alpha u + \beta v$, $\alpha, \beta \in \mathbb{R}$, $\alpha^2 \mp \beta^2 \neq 0$. The presence of w in this expression for λ implies that the sections are transversal to the cuspidal edges. On the other hand, the inequality condition here means that the sectional surface passing through the origin should not be tangent to the self-intersection locus (real for D_4^+ and imaginary for D_4^-) of the spatial caustic. The families are actually uni-modular: if one of the coefficients α and β is not zero, it may be normalised to ± 1, the other staying arbitrary.

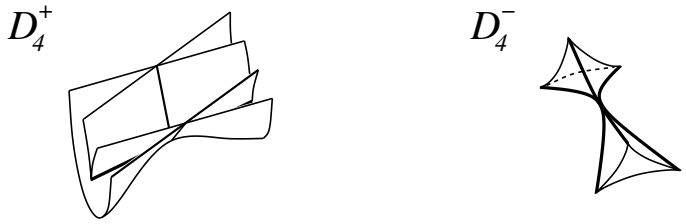

Figure 9: The $D_4^\pm$ caustics in $\mathbb{R}^3$.

We co-orient the corresponding discriminantal strata in $\mathcal{L}$ by the *decrease* of the above parameter λ, which means that in the sectional planar caustics the $(-,\sigma)$-cusps change to the $(+,\sigma)$-cusps. We distinguish five pairs of corank 2 bifurcations shown in Figure 10. The subscripts in the notations of the first four of them store the information about the post-bifurcational double points: either their number, or the right/left position of the only point.

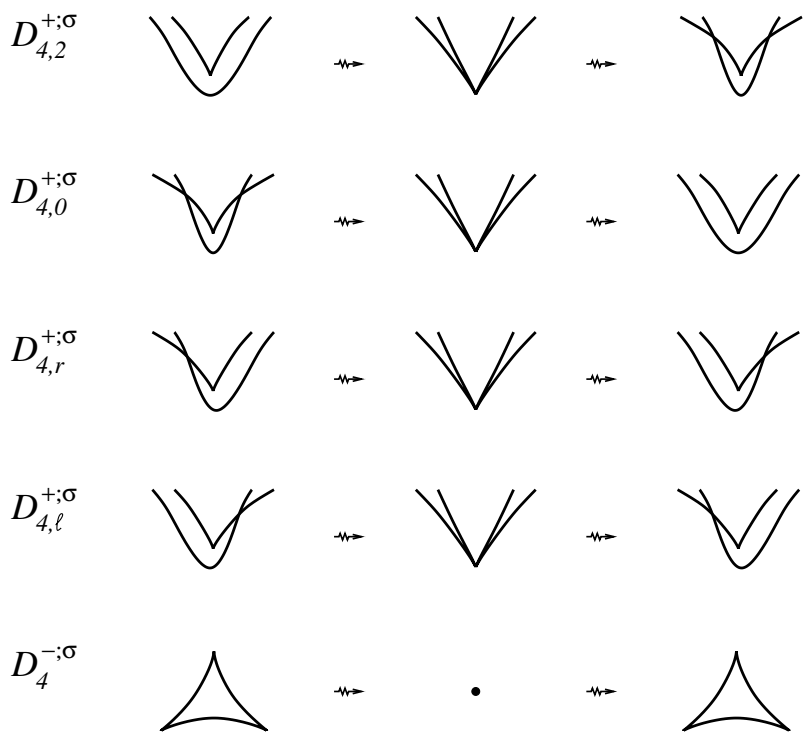

Figure 10: Generic corank 2 bifurcations of caustics. All cusps of the curves on the left are $(-, \sigma)$, and all of the curves on the right are $(+, \sigma)$.

1.3.3 Derivatives of the standard invariants

In what follows, it will be convenient for us to operate with sums of the above elementary discriminantal strata differing only in certain indices in their notation. In such cases we will omit the corresponding signs or letter and assume that the summation is done across the whole range of the omitted symbols, for example:

$$A_2^3 = A_2^{3,3} + A_2^{3,2}\,, \quad A_3A_2 = \sum_{s,\sigma=\pm} (A_3^{s,\sigma}A_2^1 + A_3^{s,\sigma}A_2^0)\,, \quad D_{4,2}^+ = D_{4,2}^{+;+} + D_{4,2}^{+;-}\,.$$

However, to avoid notational confusion, we will use

$$A_3^{s,\sigma;e/h} = A_3^{s,\sigma;e} + A_3^{s,\sigma;h} \quad \text{and} \quad A_3^{e/h} = A_3^e + A_3^h\,.$$

Within these settings we have the following summary of the increments of the invariants introduced in Section 1.2.

Lemma 1.3.1. *The derivatives of the invariants counting the double points and various cusps of planar caustics, and of their linking invariant are*

$$\begin{aligned} I_d' &= 2TA_2^2 + 2A_3A_2 + A_4 + 2D_{4,2}^+ - 2D_{4,0}^+\,, \\ I_{s,\sigma}^{c\,\prime} &= 2A_3^{s,\sigma;e/h} + A_4^{s,\sigma} + A_4^{-s,-\sigma} + sD_4^{+;\sigma} + 3sD_4^{-;\sigma}\,, \\ I_\ell' &= 2TA_2^{2,2} - 2TA_2^{2,1} + 2TA_2^{2,0} + A_3^{e/h} - 2D_{4,2}^+ + 2D_{4,0}^+\,. \end{aligned}$$

Proof. The expressions for the first five derivatives, I_d' and $I_{s,\sigma}^{c\,\prime}$, are provided by a simple inspection of the bifurcation figures.

The A-part of the linking derivative I'_ℓ, is a translation to our notations of the increment count done in [19] for the linking invariant of critical value sets of maps from surfaces to the plane.

To obtain the D-part, we consider the set of all Lagrangian maps $M \looparrowright T^*\mathbb{R}^2 \to \mathbb{R}^2$ as a subset of the space $\Omega(M, \mathbb{R}^2)$ of all smooth maps from M to $\mathbb{R}^2$. In Ω, the bifurcations of Figure 10 are no longer stable as one-parameter families, and we deform them into generic paths along which the planar critical value sets undergo sequences of local corank 1 transitions shown in Figure 11 (deformed $D^+_{4,0}$ and $D^+_{4,\ell}$ paths are opposite to the two in the Figure). Now the D-part of the expression follows from its A-part. □

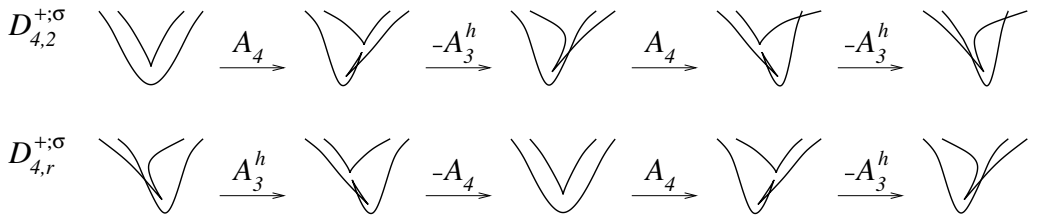

Figure 11: The D-moves of the caustics as sequences of transitions of the critical value sets of arbitrary (not necessarily Lagrangian) smooth maps. The notation of the steps is in terms of their Lagrangian analogues. Notice that the s signs of the cusps should not be used now since they are not defined in $\Omega(M, \mathbb{R}^2)$ (see Remark 1.2.1).

Remark 1.3.2. The $D^\pm_4$ caustics of Figure 9 are stable as critical value sets of Lagrangian maps between 3-manifolds. However, the corresponding local singularities of maps are of codimension 1 in the space of all smooth maps

between these manifolds. In particular, a small generic perturbation within smooth maps deforms the D_4^+ caustic to the left surface in Figure 12 [8, 13]. The sequences in Figure 11 are generic 1-parameter families of planar sections of this surface.

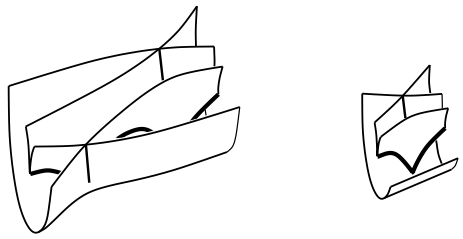

Figure 12: Stable perturbation of the D_4^+ caustic via a smooth non-Lagrangian deformation of a map between 3-manifolds. The surface has the axial symmetry which produces the whole surface from its swallowtail half shown on the right.

1.3.4 Classification of the discriminantal cycles and invariants

All statements in this section refer to any closed oriented surface M and any connected component of $\mathcal{L}(M, T^*\mathbb{R}^2, \mathbb{R}^2)$. The target plane is oriented. All invariants are considered up to a choice of additive constants on connected components of the spaces of maps.

The main result of this chapter is

Theorem 1.3.3. *The space of rational discriminantal cycles in* $\mathcal{L}(M, T^*\mathbb{R}^2, \mathbb{R}^2)$ *has rank 8. It is spanned by the derivatives of the six invariants* $I_d, I^c_{s,\sigma}, I_\ell$ *and the two cycles*

$$D_4^{\pm;\sigma} = D_{4,2}^{+;\sigma} + D_{4,0}^{+;\sigma} + D_{4,r}^{+;\sigma} + D_{4,\ell}^{+;\sigma} + D_4^{-;\sigma}, \quad \sigma = \pm\,.$$

For a basis of the discriminantal cycles in $\mathcal{L}(M, T^*\mathbb{R}^2, \mathbb{R}^2)$ in the integer case one can, for example, take the derivatives of

$$\begin{gathered} I^c/2 = (I^c_{+,+} + I^c_{+,-} + I^c_{-,+} + I^c_{-,-})/2, \qquad (I_d - I^c_{+,+} - I^c_{-,+})/2, \\ (I_\ell - I^c/2 + I^c_{+,+} + I^c_{-,+})/2, \qquad I^c_{+,+}, \qquad I^c_{+,-}, \end{gathered} \tag{1}$$

and the cycles

$$((I^c_{+,-} - I^c_{-,+})' - D_4^{\pm;+} - D_4^{\pm;-})/2, \qquad D_4^{\pm;+}, \qquad D_4^{\pm;-}\,. \tag{2}$$

Passing to the mod2 coefficients, we have

Theorem 1.3.4. *The space of* $\mathbb{Z}_2$ *discriminantal cycles in* $\mathcal{L}(M, T^*\mathbb{R}^2, \mathbb{R}^2)$ *has rank 9. It is spanned by the mod2 reductions of the above 8 integer cycles and* $A_2^3 + A_3^{\pm,+}A_2$.

Among the cycles appearing in these two theorems, the triviality of the $D_4^{\pm;\sigma}$ and $A_2^3 + A_3^{\pm,+}A_2$ is not known. Their triviality may also depend on the choice of a particular connected component of $\mathcal{L}(M, T^*\mathbb{R}^2, \mathbb{R}^2)$. Therefore,

passing from discriminantal cycles to invariants, we have only estimates:

Corollary 1.3.5. *The rank of the space of integer local invariants on a particular connected component of $\mathcal{L}(M, T^*\mathbb{R}^2, \mathbb{R}^2)$ is at least 6 and at most 8. For mod2-valued invariants, the bounds are respectively 6 and 9.*

In Section 1.5 we will have an example when the rank in the integer case is less than 8.

The minimal invariant spaces guaranteed by the corollary are spanned, for example, by the five invariants in (1) and $I^c_{-,+}$.

Let $\mathcal{L}_1(M, T^*\mathbb{R}^2, \mathbb{R}^2) \subset \mathcal{L}(M, T^*\mathbb{R}^2, \mathbb{R}^2)$ be the set of all Lagrangian maps without corank 2 points. Discriminantal cycles in $\mathcal{L}_1$ do not contain any D-summands.

Theorem 1.3.6. *The space of integer discriminantal cycles in $\mathcal{L}_1(M, T^*\mathbb{R}^2, \mathbb{R}^2)$ has rank 6. Its basis is formed, for example, by the derivatives of the invariants (1) and $(I^c_{+,-} - I^c_{-,+})/2$. Respectively, these six invariants form a basis of the space of all integer local invariants on $\mathcal{L}_1(M, T^*\mathbb{R}^2, \mathbb{R}^2)$.*

The mod2 setting adds here two linearly independent cycles, $A_2^3 + A_3^{\pm,+}A_2$ and $A_3^{+,+}A_2 + A_3^{-,-}A_2$, whose triviality is not known.

Remark 1.3.7. All the statements of the above three theorems about the discriminantal cycles stay valid if we replace Lagrangian maps $M \looparrowright T^*\mathbb{R}^2 \to \mathbb{R}^2$ with Lagrangian maps $M \looparrowright E^4 \to N$, where N is an arbitrary oriented surface. The upper bounds for the ranks of the invariant spaces stated in

the corollary and last theorem also stay true, but the lower bounds should be reduced by 1 since the cycle I'_ℓ may no longer be trivial.

Theorems 1.3.3, 1.3.4 and 1.3.6 are proved in Section 1.4.3, with the preparations occupying Sections 1.4.1 and 1.4.2.

1.4 Bifurcations in 2-parameter families of Lagrangian maps

Our proof of the classification theorems of the previous section is based on the study of bifurcations in generic 2-parameter families of caustics in the next two subsections. The bifurcation diagram of each family yields a linear equation on the increments of our local invariants across the codimension 1 strata: the equation states that the total increment along a small generic loop in $\mathcal{L}$ around the codimension 2 stratum must vanish. The whole system of these equations guarantees that the corresponding linear combination of codimension 1 strata is a discriminantal cycle in $\mathcal{L}$.

The generating families will now depend on four parameters: local coordinates u and v on the target plane, and bifurcational parameters λ_1 and λ_2. The value range for the variables s and σ is always $\{+,-\}$, tracing the (s,σ)-types of the cusps in the bifurcations.

We follow the general approach to the study of bifurcations in families of caustics developed in [26]. Namely, a local family of caustics in $\mathbb{R}^n$ depending

on k bifurcational parameters collects to one *big caustic* $\tilde{\mathcal{C}} \subset \mathbb{R}^{n+k}$. If the family is generic, $\tilde{\mathcal{C}}$ is the caustic of a generic Lagrangian map germ to $\mathbb{R}^{n+k}$. If the germ is actually a uni-germ, then within the dimensional range considered in this thesis such a map is stable and $\tilde{\mathcal{C}}$ is the caustic of an $\mathcal{R}_+$-versal deformation of one of the A_μ, D_μ, E_μ isolated function singularities with $\mu \leq n+k+1$. To understand all possible k-parameter bifurcations of uni-germ caustics, we must understand all generic maps π of the pair $(\mathbb{R}^{n+k}, \tilde{\mathcal{C}})$ to $\mathbb{R}^k$. Of course, such maps are submersive on $\mathbb{R}^{n+k}$, and therefore we frequently call them projections. The critical value set of π on $\tilde{\mathcal{C}}$ is the bifurcation diagram of the corresponding family of caustics in $\mathbb{R}^n$.

The $k = 1$ case, as far as we need it, has been considered completely in [26], and we have already quoted some of the relevant results from there. The $k = 2$ case is what we will need to analyse in this section, Section 2.3 and Chapters 3 - 5. We would like to notice that our genuine aim in the analysis is to obtain the incremental equations. This does not require exact normal forms of the projections π. The most we need is a qualitative bifurcation diagram for π. In some later cases we will not even need the relative positions of all the branches of the diagram - only relative positions in certain subsets of these branches will be crucial.

In Section 1.3 we singled out 35 discriminantal strata which we will call *elementary.* A part of our strategy to choose a particular sequence of bifurcations will be to show as soon as possible that the increments across some of them must coincide and, therefore, such strata may be united into sums like

those used in Lemma 1.3.1. We call these sums *big* strata. We denote the increment across a particular elementary or big stratum as the stratum itself, but in small characters.

Quite a few bifurcations in our analysis will be of the form $S{\cdot}A_2$, by which we mean a generic A_2 line passing through a generic codimension 1 bifurcation S. The co-orientation of the A_2 line will not be important.

1.4.1 Corank 1 maps

The bifurcations we are considering in this subsection differ from those considered in [19] for non-Lagrangian maps by the involvement of the sign σ of the cusps.

a) The simplest $S{\cdot}A_2$ bifurcations have the diagram shown in the left of Figure 13, which gives us the equation $g = h$. In particular, this happens if the codimension 1 bifurcation S is of types **1** or **2** of the table below. Our conclusion in case **1** is that the triple point stratum A_2^3 may participate in discriminantal cycles only over $\mathbb{Z}_2$, which will be noted by the square brackets in the formulas (but not in the diagrams).

The middle bifurcation diagram in Figure 13 is of the $A_4^{s,\sigma}{\cdot}A_2$ degeneration, corresponding to case **3** of the table.

The last diagram of Figure 13 serves the codimension 2 cubic versions of the codimension 1 'quadratic' degenerations $A_3^{s,\sigma;e}$ and $TA_2^{2,1}$. Namely, the first cubic bifurcation has generating family $sx^4 + (v^3 + \lambda_2 v + \lambda_1)x^2 + ux$, while the second is the interaction of the curves $v = 0$ and $v = u^3 + \lambda_2 u + \lambda_1$

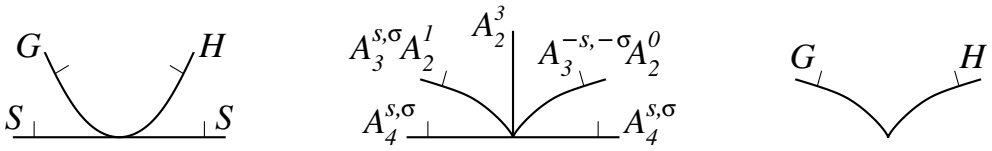

Figure 13: The diagrams of the simplest $S \cdot A_2$ singularities, of the $A_4^{s,\sigma} \cdot A_2$ bifurcations, and of the simplest cubic degenerations. They correspond to the equations **1**–**5**.

with opposite co-orientations. The conclusions derived from these two cases are in lines **4** and **5** of the table. The superscripts *opp* and *dir* are used there for opposite and direct tangencies.

	S	Equation			Big stratum		
1.	$TA_2^{2,2}$	$a_2^{3,3}$	$=$	$a_2^{3,2}$			
	$TA_2^{2,1}$	$2a_2^{3,2}$	$=$	0	$[A_2^3]$	$=$	$A_2^{3.3} + A_2^{3,2}$
2.	$A_3^{s,\sigma;e}$	$a_3^{s,\sigma}a_2^1$	$=$	$a_3^{s,\sigma}a_2^0$	$A_3^{s,\sigma}A_2$	$=$	$A_3^{s,\sigma}A_2^1 + A_3^{s,\sigma}A_2^0$
3.	$A_4^{s,\sigma}$	$a_3^{s,\sigma}a_2$	$-$	$a_3^{-s,-\sigma}a_2 = [a_2^3]$	$A_3^{\pm(+,\sigma)}A_2$	$=$	$A_3^{+,\sigma}A_2 + A_3^{-,-\sigma}A_2$
							over $\mathbb{Z}$
4.	$A_3^{s,\sigma;e}$	$a_3^{s,\sigma;e}$	$=$	$a_3^{s,\sigma;h}$	$A_3^{s,\sigma;e/h}$	$=$	$A_3^{s,\sigma;e} + A_3^{s,\sigma;h}$
5.	$TA_2^{2,0}$	$ta_2^{2,2}$	$=$	$ta_2^{2,0}$	$TA_2^{2,opp}$	$=$	$TA_2^{2,2} + TA_2^{2,0}$
	$TA_2^{2,1}$				$TA_2^{2,dir}$	$=$	$TA_2^{2,1}$

b) In Figures 14 and 15, we show bifurcation diagrams of three more codimension 2 degeneration. The corresponding incremental equations are

6–**8** below.

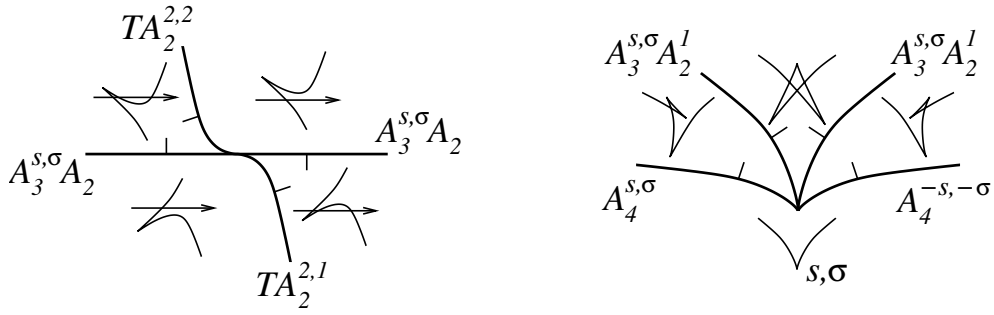

Figure 14: The line-and-cusp tangency bifurcation, and a family $F = sx^6 + \lambda_1 x^4 + \lambda_2 x^3 + vx^2 + ux$ of planar sections of the A_5 caustic in $\mathbb{R}^4$. Trying to normalize the map ($\mathbb{R}^4_{\lambda,u,v}$, 3-dimensional caustic) $\Rightarrow \mathbb{R}^2_\lambda$, similar to [26], we would get coefficients of x^3 and x^4 not just the λ_i, but also involving certain dependence on u, v. However, the dependence will not affect the "roundabout" equation.

	Equation	Big stratum
6.	$2a_3^{s,\sigma}a_2 = ta_2^{2,opp} + ta_2^{2,dir}$	$A_3A_2 = \sum_{s,\sigma=\pm} A_3^{s,\sigma}A_2$ over $\mathbb{Z}$
7.	$a_4^{s,\sigma} = a_4^{-s,-\sigma}$	$A_4^{\pm(+,\sigma)} = A_4^{+,\sigma} + A_4^{-,-\sigma}$
8.	$2a_4^{\pm(+,\sigma)} = a_3^{+,\sigma;h} + a_3^{-,-\sigma;h} + ta_2^{2,dir}$	

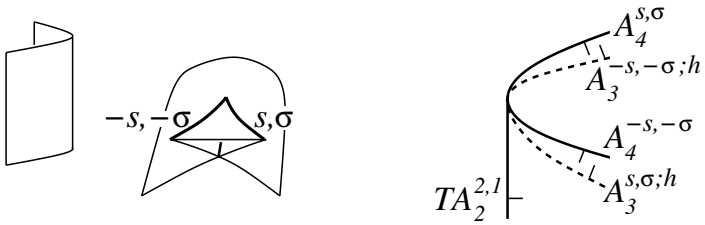

Figure 15: Bifurcations of a swallowtail section by a smooth surface tangent to the self-intersection line and generic in any other sense [13].

1.4.2 Corank 2 bifurcations

a) *The* $D_{4,r}^{+;\sigma}\cdot A_2$ *family.* Comparing the events on the left and on the right in Figure 16 during the motion of the additional A_2 component and recalling from equations **1** above that $2a_2^3 = 0$, we conclude that the incremental equation here reduces to

$$\mathbf{9}. \quad a_3^{-,\sigma} a_2 = a_3^{+,\sigma} a_2 \,.$$

This provides us with a big stratum $A_3^{\pm,\sigma}A_2 = A_3^{+,\sigma}A_2 + A_3^{-,\sigma}A_2$ over $\mathbb{Z}_2$. (We already have A_3A_2 over the integers.) All the other versions of the $D_4^+\cdot A_2$ bifurcations yield the same.

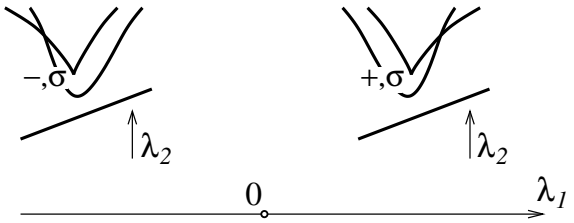

Figure 16: The $D_{4,r}^{+;\sigma}\cdot A_2$ bifurcation.

b) *Degenerate sections of the D_4^+ caustic.* In Section 1.3.2 we quoted the normal form of a generic function on $\mathbb{R}^3$ in presence of the D_4^+ caustic. We will now denote this caustic $\mathcal{C}(D_4^+)$. A standard argument using the description from [26] of the vector fields tangent to $\mathcal{C}(D_4^+)$ shows that the functions next in the hierarchy in this case can be reduced to the normal forms

$$w \pm u \pm v + \gamma v^2\,, \quad \gamma \in \mathbb{R} \setminus \{0\}\,.$$

Here γ is a modular coefficient. The zero level of such a function is tangent at the origin to one of the two rays of the self-intersection locus of $\mathcal{C}(D_4^+)$. Making use of a natural notion of a versal deformation of a function germ on $\mathbb{R}^3$ with respect to the group of diffeomorphisms preserving the caustic, we see that the functions above give us two-parameter families of caustics defined by generating families of functions depending on two additional parameters (λ_1, λ_2):

$$x^2y + \frac{1}{3}y^3 + \frac{1}{2}(\pm u \pm v + \gamma v^2 + \lambda_2 v + \lambda_1)y^2 + vy + ux\,. \tag{3}$$

Various choices of the signs in this formula (including the sign of γ) give us the bifurcation diagrams in the (λ_1, λ_2)-plane shown in Figure 17. Comparison of the first two diagrams there implies $d_{4,r}^{+;\sigma} = d_{4,\ell}^{+;\sigma}$, which allows us to introduce a big stratum

$$D_{4,r/\ell}^{+;\sigma} = D_{4,r}^{+;\sigma} + D_{4,\ell}^{+;\sigma}\,.$$

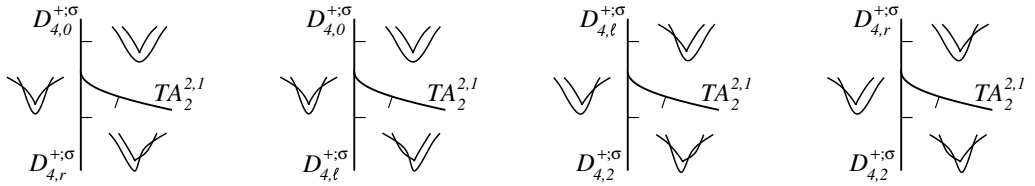

Figure 17: Bifurcation diagrams of the families (3). In each diagram, the cusp on the left of the vertical strata is $(-,\sigma)$ and the cusps on the right are $(+,\sigma)$. The opposite cusp option is not shown since it yields the same set of four incremental equations.

Now Figure 17 provides two linearly independent incremental equations for each $\sigma = \pm$:

$$\textbf{10}. \qquad ta_2^{2,1} = d^{+;\sigma}_{4,r/\ell} - d^{+;\sigma}_{4,0}$$

$$= d^{+;\sigma}_{4,2} - d^{+;\sigma}_{4,r/\ell}$$

We remark that we are not considering here functions on $(\mathbb{R}^3, \mathcal{C}(D_4))$ whose zero level is tangent at the origin to the cuspidal edge of the caustic since such functions would correspond to the change of topology of the source surface of our Lagrangian maps. However, such functions will appear in Section 1.5 where they will be used for constructing non-contractible loops in the spaces of Lagrangian maps.

c) *The D_5 family.* In Figure 18 we are showing the bifurcation diagrams of two-parameter families of caustics coming from the deformations

$$x^2y \pm y^4 + \lambda_1 y^3 + \lambda_2 y^2 + vy + ux$$

of the $D_5^{\pm}$ function singularities. Since each diagram has two pairs of double strata, these two-parameter families of planar caustics are infinitely degenerate. However, these families are the principal quasi-homogeneous parts of generic two-parameter slicings of the big $D_5^{\pm}$ caustics in $\mathbb{R}^4$, and yield the same incremental equations as such generic slicings do, namely:

$$\textbf{11}. \qquad d_{4,2}^{+;\sigma} - d_4^{-;\sigma} + a_3^{+,\sigma;e} + a_3^{+.-\sigma;h} - 2a_4^{+,-\sigma} = 0$$

$$-d_{4,0}^{+;\sigma} + d_4^{-;\sigma} + a_3^{-,\sigma;e} + a_3^{-.-\sigma;h} - 2a_4^{-,-\sigma} = 0$$

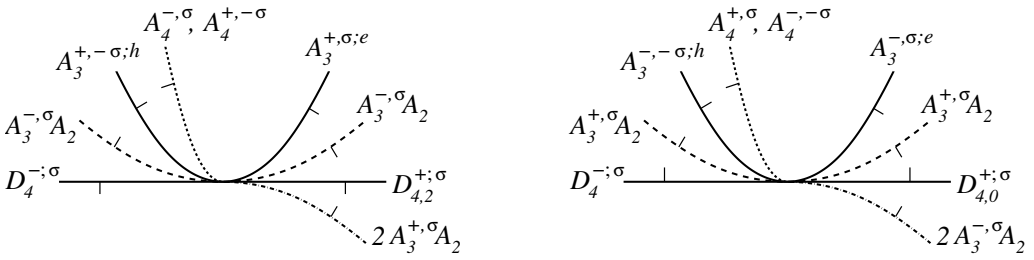

Figure 18: The D_5^+ and D_5^- bifurcation diagrams.

This finishes the process of deriving the incremental equations. It is not very difficult to show that no other stable codimension 2 bifurcation of planar caustics delivers an equation linearly independent (both mod2 and over the integers) from the equations already listed.

1.4.3 Proofs of the classification theorems

We initially had 35 elementary discriminantal strata. Over the previous two subsections we have been able to join them, both over $\mathbb{Z}$ and $\mathbb{Z}_2$, into 19

bigger. Equations on the increments of the invariants across these 19 strata obtained during the bifurcation analysis are collected in the columns of Table 1e below. Equations which are integer linear combinations of the others are not included there. That is why only one of the equations **6** and only the first pair of the equations **11** are in the table. We are using dots instead of zeros.

With 11 linearly independent equations in 19 unknowns, we have a rank 8 solution space. The 8 columns of Table 1s contain the coefficients of the discriminantal cycles mentioned in Theorem 1.3.3. They are easily seen to form a basis of the solution space over the rationals, which proves the theorem.

The rank of the mod2 solutions matrix in Table 1s is 5. This yields a few parity conservation laws for appropriate linear combinations of numbers of double points and various cusps of caustics in homotopies. The most obvious one is that the parity of the total number of cusps stays the same.

To produce an integer solution basis from the rational one we can, for example, consider its modification (1–2) from Section 1.3.4.

The mod2 reduction of the incremental equations drops the rank of the coefficient matrix by 1, due to the elimination of equation **1**. Therefore, a mod2 solution basis may be obtained by addition to the reduced basis (1–2) of one cycle, for example, $A_2^3 + A_3^{\pm,+}A_2$ (or $A_2^3 + A_3^{\pm,-}A_2$). This proves Theorem 1.3.4.

Table 1e	1	3	6	8	8	10	10	10	10	11	11
A_2^3	2	1	.	.	.	.	.	.	.	.	.
$TA_2^{2,opp}$	.	.	-1	.	.	.	.	.	.	.	.
$TA_2^{2,dir}$	.	.	-1	-1	-1	1	1	1	1	.	.
$A_3^{\pm,+}A_2$	.	1	2	.	.	.	.	.	.	.	.
$A_3^{\pm,-}A_2$	.	-1	.	.	.	.	.	.	.	.	.
$A_3^{+,+;e/h}$	.	.	.	-1	.	.	.	.	.	1	1
$A_3^{+,-;e/h}$	.	.	.	.	-1	.	.	.	.	1	1
$A_3^{-,+;e/h}$	.	.	.	.	-1	.	.	.	.	.	.
$A_3^{-,-;e/h}$	.	.	.	-1	.	.	.	.	.	.	.
$A_4^{\pm(+,+)}$	.	.	.	2	.	.	.	.	.	.	-2
$A_4^{\pm(+,-)}$	.	.	.	.	2	.	.	.	.	-2	.
$D_{4,2}^{+;+}$	.	.	.	.	.	.	.	-1	.	1	.
$D_{4,2}^{+;-}$	.	.	.	.	.	.	.	.	-1	.	1
$D_{4,r/\ell}^{+;+}$	.	.	.	.	.	-1	.	1	.	.	.
$D_{4,r/\ell}^{+;-}$	.	.	.	.	.	.	-1	.	1	.	.
$D_{4,0}^{+;+}$	.	.	.	.	.	1	.	.	.	.	.
$D_{4,0}^{+;-}$	.	.	.	.	.	.	1	.	.	.	.
$D_4^{-;+}$	.	.	.	.	.	.	.	.	.	-1	.
$D_4^{-;-}$	.	.	.	.	.	.	.	.	.	.	-1

Table 1s	I'_d	$I^{c\,\prime}_{+,+}$	$I^{c\,\prime}_{+,-}$	$I^{c\,\prime}_{-,+}$	$I^{c\,\prime}_{-,-}$	I'_ℓ	$D_4^{\pm;+}$	$D_4^{\pm;-}$
A_2^3	.	.	.	.	.	.	.	.
$TA_2^{2,opp}$	2	.	.	.	.	2	.	.
$TA_2^{2,dir}$	2	.	.	.	.	-2	.	.
$A_3^{\pm,+}A_2$	2	.	.	.	.	.	.	.
$A_3^{\pm,-}A_2$	2	.	.	.	.	.	.	.
$A_3^{+,+;e/h}$	.	2	.	.	.	1	.	.
$A_3^{+,-;e/h}$	.	.	2	.	.	1	.	.
$A_3^{-,+;e/h}$	.	.	.	2	.	1	.	.
$A_3^{-,-;e/h}$	.	.	.	.	2	1	.	.
$A_4^{\pm(+,+)}$	1	1	.	.	1	.	.	.
$A_4^{\pm(+,-)}$	1	.	1	1	.	.	.	.
$D_{4,2}^{+;+}$	2	1	.	-1	.	-2	1	.
$D_{4,2}^{+;-}$	2	.	1	.	-1	-2	.	1
$D_{4,r/\ell}^{+;+}$	.	1	.	-1	.	.	1	.
$D_{4,r/\ell}^{+;-}$	.	.	1	.	-1	.	.	1
$D_{4,0}^{+;+}$	-2	1	.	-1	.	2	1	.
$D_{4,0}^{+;-}$	-2	.	1	.	-1	2	.	1
$D_4^{-;+}$	.	3	.	-3	.	.	1	.
$D_4^{-;-}$	.	.	3	.	-3	.	.	1

For Theorem 1.3.6, avoiding corank 2 maps, we have to restrict our atten-

tion to the A-strata and equations **1**–**8** only. To cover the integer and mod2 options simultaneously we have to consider this time all four strata $A_3^{s,\sigma}A_2$ individually. The equation-cycle table for this case is Table 2 below. We have 7 linearly independent equations in 13 unknowns. The set of the discriminantal cycles suggested for an integer basis in the theorem occupies the second half of the table, and is indeed linearly independent. In the table we set

$$\begin{aligned}
\hat{I}_d &= (I_d - I^c_{+,+} - I^c_{-,+})/2,\\
\hat{I}^c_{-,+} &= (I^c_{-,+} - I^c_{+,-})/2,\\
I^c/2 &= (I^c_{+,+} + I^c_{+,-} + I^c_{-,+} + I^c_{-,-})/2,\\
\hat{I}_\ell &= (I_\ell - I^c/2 + \hat{I}^c_{+,+} + I^c_{-,+})/2.
\end{aligned}$$

The mod2 reduction reduces this time the rank of the equation matrix by 2. Therefore, two extra basic cycles should be added to obtained a $\mathbb{Z}_2$-basis, for example, $A_2^3 + A_3^{\pm,+}A_2$ and $A_3^{+,+}A_2 + A_3^{-,-}A_2$. This finishes our proofs.

Table 2 ($\mathcal{L}_1$)	1	3	3	6	6	8	8	$\hat{I}'_d$	$I^{c\,\prime}_{+,+}$	$I^{c\,\prime}_{+,-}$	$\hat{I}^{c\,\prime}_{-,+}$	$I^{c\,\prime}/2$	$\hat{I}'_\ell$
A_2^3	2	1	1	.	.	.	.	.	.	.	.	.	.
$TA_2^{2,opp}$	.	.	.	-1	-1	.	.	1	.	.	.	.	1
$TA_2^{2,dir}$	.	.	.	-1	-1	-1	-1	1	.	.	.	.	-1
$A_3^{+,+}A_2$	.	1	.	2	.	.	.	1	.	.	.	.	.
$A_3^{+,-}A_2$	.	.	1	.	2	.	.	1	.	.	.	.	.
$A_3^{-,+}A_2$	.	.	-1	.	.	.	.	1	.	.	.	.	.
$A_3^{-,-}A_2$	.	-1	.	.	.	.	.	1	.	.	.	.	.
$A_3^{+,+;e/h}$	.	.	.	.	.	-1	.	-1	2	.	.	1	1
$A_3^{+,-;e/h}$	.	.	.	.	.	.	-1	.	.	2	-1	1	.
$A_3^{-,+;e/h}$	.	.	.	.	.	.	-1	-1	.	.	1	1	1
$A_3^{-,-;e/h}$	.	.	.	.	.	-1	.	.	.	.	.	1	.
$A_4^{\pm(+,+)}$	.	.	.	.	.	2	.	.	1	.	.	1	.
$A_4^{\pm(+,-)}$	.	.	.	.	.	.	2	.	.	1	.	1	.

1.4.4 Non-oriented source or target

Assume first of all that the source surface M is not oriented while the target plane has an orientation chosen. This means gluing together discriminantal strata of codimension 1 in $\mathcal{L}(M, T^*\mathbb{R}^2, \mathbb{R}^2)$ differing only by the sign σ in their notation. The modified equations and basic cycles are collected in Table 3.

The sign σ is now gone from the notations.

Table 3	1	3	6	8	10	10	11	I'_d	$I^{c\,\prime}_+$	$I^{c\,\prime}_-$	I'_ℓ	$D^\pm_4$
A_2^3	2	1	.	.	.	.	.	.	.	.	.	.
$TA_2^{2,opp}$	.	.	-1	.	.	.	.	2	.	.	2	.
$TA_2^{2,dir}$	.	.	-1	-1	1	1	.	2	.	.	-2	.
$A_3^+A_2$	.	1	2	.	.	.	.	2	.	.	.	.
$A_3^-A_2$	.	-1	.	.	.	.	.	2	.	.	.	.
$A_3^{+;e/h}$	.	.	.	-1	.	.	2	.	2	.	1	.
$A_3^{-;e/h}$	.	.	.	-1	.	.	.	.	.	2	1	.
A_4	.	.	.	2	.	.	-2	1	1	1	.	.
$D^+_{4,2}$	.	.	.	.	.	-1	1	2	1	-1	-2	1
$D^+_{4,r/\ell}$	.	.	.	.	-1	1	.	.	1	-1	.	1
$D^+_{4,0}$	.	.	.	.	1	.	.	-2	1	-1	2	1
D^-_4	.	.	.	.	.	.	-1	.	3	-3	.	1

Analysis of Table 3 and comparison with the oriented case show that in the space $\mathcal{L}(M, E, N)$ for non-oriented source M and oriented target N,

i) a rational basis of discriminantal cycles is formed by the cycles in the second half of Table 3;

ii) for a basis over the integers one can take

$$I^{c\,\prime}/2, \quad I^{c\,\prime}_+, \quad (I'_d + I'_\ell - I^{c\,\prime}/2)/2, \quad (I'_d - I^{c\,\prime}_+ + D^\pm_4)/2, \quad D^\pm_4\,;$$

iii) to obtain a $\mathbb{Z}_2$-basis one should add $A_2^3 + A_3^+ A_2$ to the mod2 reductions of the integer basis.

We see that, depending on the triviality of the linear combinations of the I'_ℓ, $D_4^\pm$ and $A_2^3 + A_3^+ A_2$ cycles, the rational or integer local invariant spaces have ranks at least 3 and at most 5, with the upper bound goes up to 6 over $\mathbb{Z}_2$.

Switching to the space $\mathcal{L}_1(M, E, N)$ of corank at most 1 maps, we need to drop every mentioning of the $D_4^\pm$ cycle in the above items. In particular, this reduces all the rank bounds by 1. In particular, we have

Proposition 1.4.1. *The space of integer local invariants of Lagrangian maps of a non-oriented surface M to oriented $\mathbb{R}^2$ is 4-dimensional. Its basis is formed by the invariants*

$$I^c/2,\ I^c_+,\ (I_d + I_\ell - I^c/2)/2 \quad \textit{and} \quad (I_d - I^c_+)/2.$$

Assume now the target surface N non-oriented making no assumption on orientability of the source M. In addition to the loss of the local degree index σ in the notations of the strata in Section 1.3 we have had so far in the current section, this condition allows for only one type of the A_4 bifurcation and also makes no difference between the $D^+_{4,r}$ and $D^+_{4,\ell}$ transitions. However, this does not imply any further amendment to Table 3. Therefore, all our observations about the spaces of discriminantal cycles stay true if at least one of the surfaces M and N is not oriented.

1.5 Non-trivial discriminantal cycles

In this section we are showing that some of the integer discriminantal cycles we have found are non-trivial in perhaps the simplest possible situations, namely in the space of Lagrangian mappings of a 2-sphere, in its component of contractible maps (the contractibility requirement includes the contractibility of the induced map to the Lagrangian Grassmannian). The idea is to construct a loop in a space of Lagrangian maps having a non-zero intersection number with a cycle. The loop in its turn will be non-contractible.

We start with a two-parameter family of caustics formed by the bifurcations of the section of the D_4^+ caustic in $\mathbb{R}^3$ by a smooth sheet tangent to the cuspidal edge at the D_4^+ point, as illustrated in Figure 19. The corresponding generating family depending on two additional parameters λ is

$$F(x, y, u, v, \lambda) = x^2 y + \frac{1}{3}y^3 + (v + \lambda_1)y^2 + (av^2 + \lambda_2)y + ux\,,$$

where $a > 1$ is a constant. The equation $F_y = 0$ shows that the source bifurcates between a sphere in the xyv-coordinate space and the empty set. The local degrees of the Lagrangian maps at all pleat points are the same, and we are assuming them to be $+1$ at this moment.

A more complicated version of the homotopy γ of planar caustics in Figure 19 appeared in [20] (without any relation to the sections of the D_4^+ caustic) as a candidate for a non-trivial loop in $\mathcal{L}(S^2, T^*\mathbb{R}^2, \mathbb{R}^2)$ in assumption that the orientation of S^2 is ignored. We are going to show that γ is indeed a

non-trivial loop in such a setting provided the space of the Lagrangian maps is interpreted correctly.

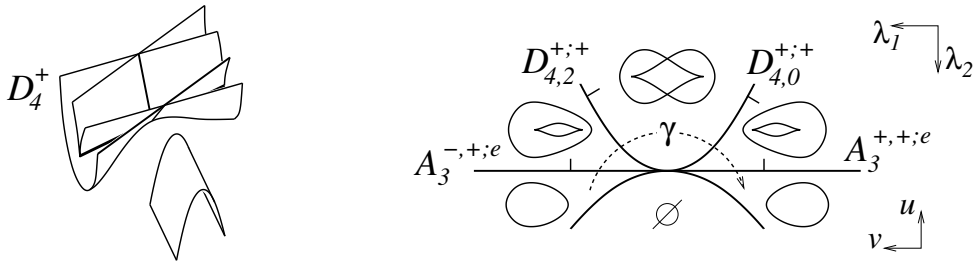

Figure 19: Sections of the D_4^+ caustic by a smooth sheet non-transversal to its cuspidal edge and generic in any other sense. In the bifurcation diagram, all the cusps in its left half are of $(-,+)$-type, while all those in the right half are $(+,+)$-cusps.

A Lagrangian map of a surface $M \to T^*\mathbb{R}^2 \to \mathbb{R}^2_{u,v}$, defined by a global generating family F of functions in the way considered for map germs in Section 1.1, lifts to a map $M \to \mathbb{R}^3_{u,v,F}$ if we use the values of the family as the third coordinate in the target. The image of such a map is called a *wave front* (see [4] or [7] for the theory of Legendrian maps and other related topics). Using this lifting, the homotopy of the Lagrangian maps in $\mathcal{L}(S^2, T^*\mathbb{R}^2, \mathbb{R}^2)$ corresponding to the path γ in Figure 19 may be understood via the homotopy of the corresponding wave fronts in $\mathbb{R}^2_{u,v,F}$. The latter is an eversion of a flying saucer front: starting γ with the saucer with the inward co-orientation, we are changing it to the outward one. See Figure 20.

From Figure 20 we see that the final Lagrangian map γ_1 of the path γ is a composition $\gamma_0 \circ j$ of the initial map with the reflection $j : (x, y, v) \mapsto (-x, y, v)$

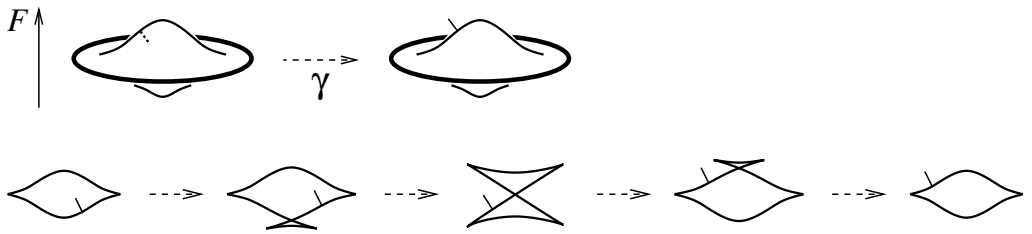

Figure 20: Eversion of a flying saucer front, and the sequence of bifurcations of its sections by the planes $v = const$ during the homotopy of the planar caustics along the path γ in Figure 19.

of the sphere. Up to a homotopy on S^2, j may be taken to be any orientation-reversing involution of the sphere.

Let $\bar{\gamma}$ be a path in $\mathcal{L}(S^2, T^*\mathbb{R}^2, \mathbb{R}^2)$ formed by all the compositions $\gamma_t \circ j$, where $\gamma = \{\gamma_t, 0 \leq t \leq 1\}$. The path $\Gamma = \bar{\gamma}\gamma$ is a loop in $\mathcal{L}(S^2, T^*\mathbb{R}^2, \mathbb{R}^2)$.

Proposition 1.5.1. (conjectured by Ohmoto) *The loop* Γ *is not contractible.*

Proof. According to Figure 19, the indices of intersection of Γ with the discriminantal cycles $D_4^{\pm,+}$ and $D_4^{\pm,-}$, contributed respectively by γ and $\bar{\gamma}$, are both $+2$. □

Corollary 1.5.2. *Consider the space of integer discriminantal cycles in the connected component of* $\mathcal{L}(S^2, T^*\mathbb{R}^2, \mathbb{R}^2)$ *containing maps for which the induced maps of* S^2 *to the Lagrangian Grassmannian of 2-planes in* $\mathbb{R}^4$ *are contractible. In its subspace spanned by the cycles* $D_4^{\pm,+}$ *and* $D_4^{\pm,-}$*, only the difference* $D_4^{\pm,+} - D_4^{\pm,-}$ *may be the derivative of an integer-valued local invariant.*

The version of the above for a non-oriented sphere is as follows. Elimination of the orientation of S^2 means that we do not distinguish between the two orientation options, that is, the space $\mathcal{L}(S^2_{nonor}, T^*\mathbb{R}^2, \mathbb{R}^2)$ is the quotient $\mathcal{L}(S^2, T^*\mathbb{R}^2, \mathbb{R}^2)/\mathbb{Z}_2$ where the $\mathbb{Z}_2$-action is by composing with any fixed orientation-reversing involution of the sphere. Within such a setting, the path γ in Figure 19 is closed in this quotient. As it was noticed in Section 1.4.4, the strata in Figure 19 lose now the second superscript in their notation, and we see that the intersection index of γ with the $D_4^{\pm}$ discriminantal cycle is 2. Hence this cycle may be the derivative of a mod2 local invariant, but not of an integer or rational one. This addresses the question from [20].

Due to the local nature of all the constructions of this section, all the claims we have done here stay valid for any Legendrian fibration $E^4 \to N^2$, not just for the cotangent bundle of $\mathbb{R}^2$.

Chapter 2

Local invariants of Lagrangian mappings between 3-manifolds

In this chapter we consider the three-dimensional analogue of the theory developed in Chapter 1 for surfaces. The only concession we are making in this substantially more complicated case is that we now do not distinguish between the A_3^+ and A_3^- singularities. As a whole, the exposition in this chapter progresses in the order similar to that of Chapter 1. Everything said in Section 1.1 specifically for two dimensions translates now in the obvious way to three dimensions.

We carry on using the abbreviation $\mathcal{L}$, but this time in the three-dimensional sense, for the space $\mathcal{L}(M, T^*N, N)$ of all Lagrangian maps $M \looparrowright T^*N \to N$ between fixed 3-manifolds M and N. Both M and N are oriented and without boundaries. Moreover, M is compact.

Some of the diagrams appearing in this Chapter are borrowed from [13] and amended for the Lagrangian setting.

2.1 Stratification and some invariants of generic caustics in three dimensions

Let f be a generic Lagrangian map between two oriented 3-manifolds, and $\mathcal{C}(f)$ its caustic. Similar to the 2-dimensional case, we co-orient the regular part A_2 of $\mathcal{C}(f)$ to the side where the number of local preimages of a point is greater. Below is the list of the strata we distinguish in the singular locus of $\mathcal{C}(f)$ following [4], page 18. The names of the strata correspond to the uni- and multi-germ function singularities whose deformations serve as local generating families for f (see [7]).

So, singularites of a generic caustic in three dimensions are:

A_2^2, transversal intersections of two smooth sheets (as shown in Figure 21);

A_2^3, transversal intersections of three smooth sheets (as shown in Figure 21);

A_3^σ, cuspidal edges, consisting of values of f at its pleat points, that is, points near which f has the generating family $F(x,u,v,w) = \pm x^4 + vx^2 + ux$. The sign $\sigma = \pm$ denotes the local degree ± 1 of the Lagrangian map. Since we have decided not to distinguish between functions x^4 and $-x^4$ in the 3-dimensional case, we now include both sign options in the generating family into the same equivalence class. Formally this means

that we are enlarging our $\mathcal{R}_+$-equivalence by allowing to multiply the functions by -1 (as shown in Figure 21);

$A_3^\sigma A_2$, transversal intersections of edges with regular sheets (as shown in Figure 21);

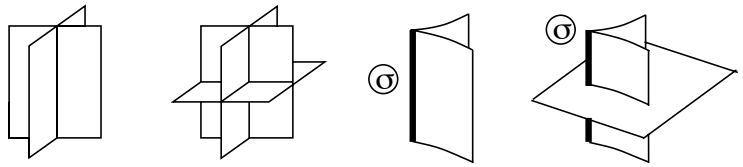

Figure 21: The A_2^2, A_2^3, A_3^σ and $A_3^\sigma A_2$ singularities of generic caustics

A_4^σ, $\sigma = \pm$ points, with the generating family $F(x,u,v,w) = x^5 + wx^3 + vx^2 + ux$. Figure 22 defines the choice of the index σ. We assume there that the target is taken with the standard right orientation which may differ from $du \wedge dv \wedge dw$;

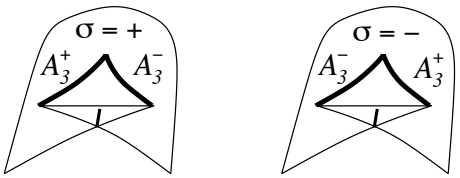

Figure 22: Positive and negative swallowtails, A_4^σ.

$D_4^{\pm,\sigma}$, the central points of the two caustics shown in Figure 23. The local generating families are the $\mathcal{R}_+$-versal deformations

$$F(x,y,u,v,w) = \pm x^2 y + y^3 + wy^2 + vy + ux \qquad (4)$$

of the $D_4^{\pm}$ function singularities. Here $\sigma = \pm$ indicates the local degree ± 1 of the map along the cuspidal edges (which is not the same as the choice of the sign of x^2y).

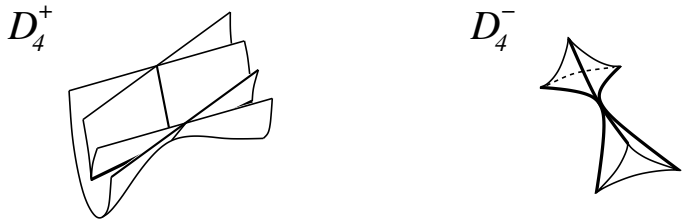

Figure 23: The $D_4^{\pm}$ caustics in $\mathbb{R}^3$ also known as the 'purse' and 'pyramid' respectively.

In the Figures $21 - 27$ the thicker line represents a cuspidal edge.

Similar to Section 1.2 the most obvious way to define an invariant of generic Lagrangian maps is to count the numbers of isolated singularities of their caustics.

Examples 2.1.1. The number of isolated singularities of $\mathcal{C}(f)$ of a particular type is, a local invariant. We have nine such invariants:

I_t, the number of triple points A_2^3;

$I_{s_\pm}$, the numbers of positive and negative swallowtails;

$I_{c_\pm}$, the numbers of $A_3^{\pm}A_2$ points;

$I_{d_\pm^-}$, the numbers of $D_4^{-,\pm}$ points;

$I_{d^+_\pm}$, the numbers of $D_4^{+,\pm}$ points.

Another obvious invariant is of a mapping.

I_χ, half of the Euler characteristic of the critical locus of a mapping.

2.2 Bifurcations in generic one-parameter families of caustics

2.2.1 Corank 1 bifurcation

The classification below is extracted from [26] and Chapter 2 of [4]. Our illustrations to the transitions define the co-orientations of the corresponding strata in $\mathcal{L}$, completely following the understanding introduced in the 2-dimesional case.

2.2.1.1 Multi-germs

Here we describe multi-germs without corank 2 points. As before we are using the letter T to denote tangency of the participating components. The letters e and h distinguish between elliptic and hyperbolic versions of bifurcations. We let r represent the number of faces of the bounded regions after the bifurcation to be co-oriented outwards. In some cases we still use r even if there is no bounded region, in this case we shall comment on what this represents. Figure 24 provides the illustrations, some of them just for particular choices of the indices.

$A_2^{4,r}$, $r = 2, 3, 4$, intersection of four smooth sheets. The pre-bifurcation tetrahedral region has $4 - r$ faces co-oriented outwards. Therefore, the $r = 2$ stratum $A_2^{4,2}$ is not co-orientable in $\mathcal{L}$ by local means.

$TA_2^{3,r}$, $r = 0, 1, 2, 3$, three smooth sheets are pairwise transversal to each other, but the line of intersection of any two of them is tangent to the third sheet at the moment of bifurcation.

$TA_2^{2,e,r}$, $r = 0, 1, 2$, elliptic tangency of two smooth sheets.

$TA_2^{2,h,r}$, $r = 0, 1$, same, but hyperbolic. We write $r = 1$ if the sheets have the same co-orientation, and $r = 0$ if the co-orientations are opposite. For $r = 1$, we fail to locally co-orient the stratum in $\mathcal{L}$.

$A_3^{\pm}A_2^{2,r}$, $r = 0, 1, 2$, cuspidal edge meets the intersection of two smooth sheets.

$A_3^{2,e,\pm,\pm}$, two cuspidal edges of given signs meet face-to-face. We will use $A_3^{2,e,+,-}$, not $A_3^{2,e,-,+}$.

$A_3^{2,h,\pm,\pm}$, one of the cuspidal edges is overtaking the other. If the signs of the edges coincide, we fail to co-orient the stratum in $\mathcal{L}$ by local means. For $A_3^{2,h,+,-}$, we set the positive side of the bifurcation to be that with two $A_3^+A_2$ points.

$A_4^{\pm}A_2^r$, $r = 0, 1$, a smooth sheet passes through a swallowtail.

$TA_3^{\pm}A_2^{e,r}$, $r = 0, 1$, cuspidal edge becomes tangent to a smooth sheet so that the two local components of the caustic do not intersect before the

bifurcation.

$TA_3^{\pm}A_2^{h,r}$, $r = 0, 1$, the hyperbolic version of the previous. For $r = 1$, the co-orientation of the A_2 sheet is towards the cuspidal edge before the bifurcation. For $r = 0$, it is opposite.

2.2.1.2 Uni-germs

For corank 1 uni-germs we have the following transformations of the caustics (see Figure 25) along with the normal forms of the generating family bifurcations.

$A_3^{\sigma,+,+}$, $\pm F = x^4 + (v^2 + w^2 - \lambda)x^2 + ux$, birth of a flying saucer. Here σ is the sign of the edge, and the two pluses in the notation are the signs of the squares in the coefficient of x^2.

$A_3^{\sigma,+,-}$, $\pm F = x^4 + (v^2 - w^2 + \lambda)x^2 + ux$, hyperbolic transformation of an edge.

$A_3^{\sigma,-,-}$, $\pm F = x^4 - (v^2 + w^2 + \lambda)x^2 + ux$, death of a compact component of an edge.

A_4^e, $F = x^5 + (w^2 - \lambda)x^3 + vx^2 + ux$, birth of cuspidal lips.

A_4^h, $F = x^5 + (\lambda - w^2)x^3 + vx^2 + ux$, beaks bifurcation on the edge.

$A_5^{\sigma,s}$, $\sigma, s = \pm : \pm F = x^6 - \lambda x^4 + vx^3 + wx^2 + ux$. Here σ is the local degree of the whole map, while s is the sign of the two swallowtails born in the bifurcation.

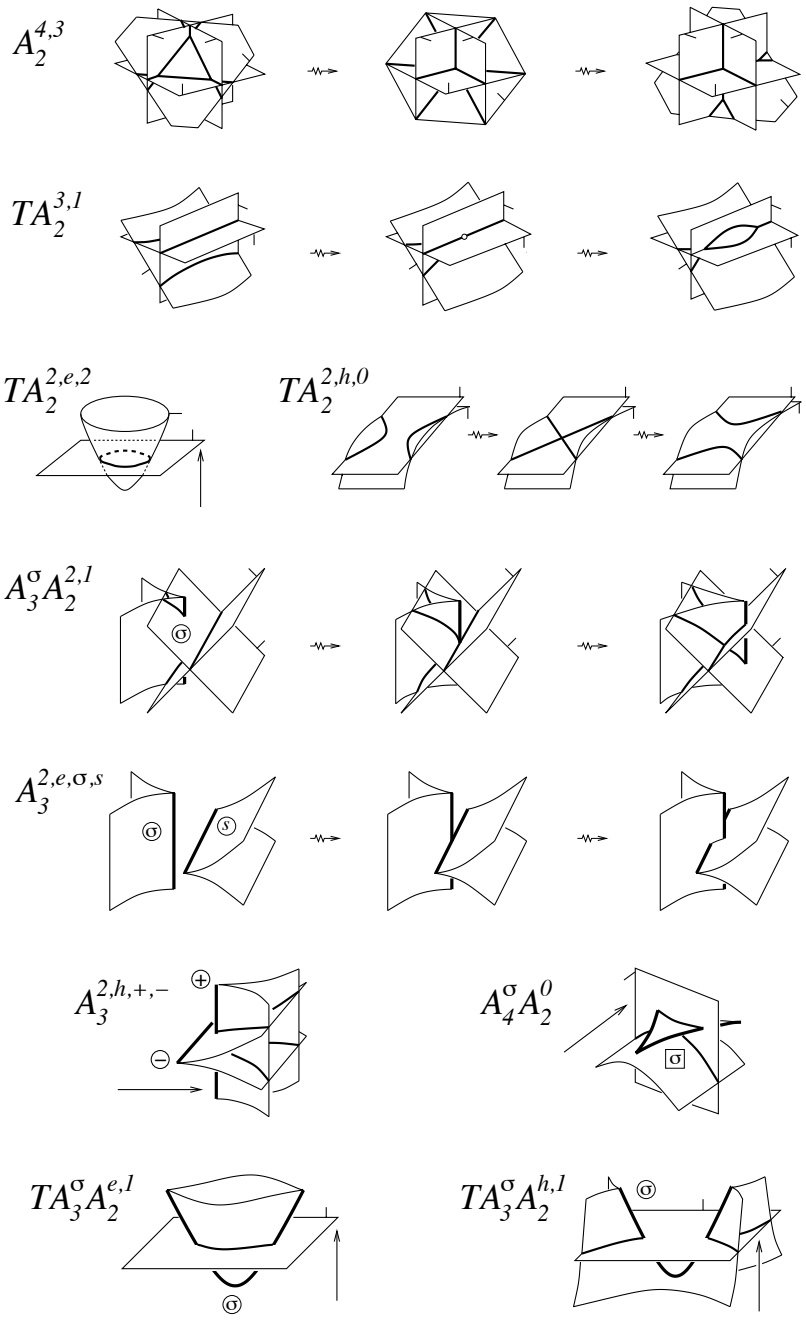

Figure 24: Generic one-parameter families of corank 1 multi-germs of caustics

2.2.2 Corank two bifurcations

This time we allow one of the critical points involved to have corank 2.

2.2.2.1 Multi-germs

Below is the list of multi-germ bifurcations in this case. The illustrations are in Figure 26. The planar families in Figure 10 are the families of sections of the purse and pyramid by the moving A_2 sheet we are seeing now.

$D_4^{-,\sigma}A_2$, a smooth sheet passing through the pyramid in the direction of its co-orientation.

$D_{4,1}^{+,\sigma}A_2^+$, a smooth sheet passing through the purse so that the number of triple points increases. The sheet is moving in the direction of its co-orientation.

$D_{4,1}^{+,\sigma}A_2^-$, a smooth sheet passing through the purse so that the number of triple points increases. The sheet is moving in the direction opposite to its co-orientation.

$D_{4,2}^{+,\sigma}A_2^+$, a smooth sheet passing through the purse so that the triple point passes from the left to the right if we are looking in the direction of the movement which in this case coincides with the co-orientation of the sheet.

$D_{4,2}^{+,\sigma}A_2^-$, a smooth sheet passing through the purse so that the triple point passes from the right to the left if we are looking in the direction of the movement which is now opposite to the co-orientation of the sheet.

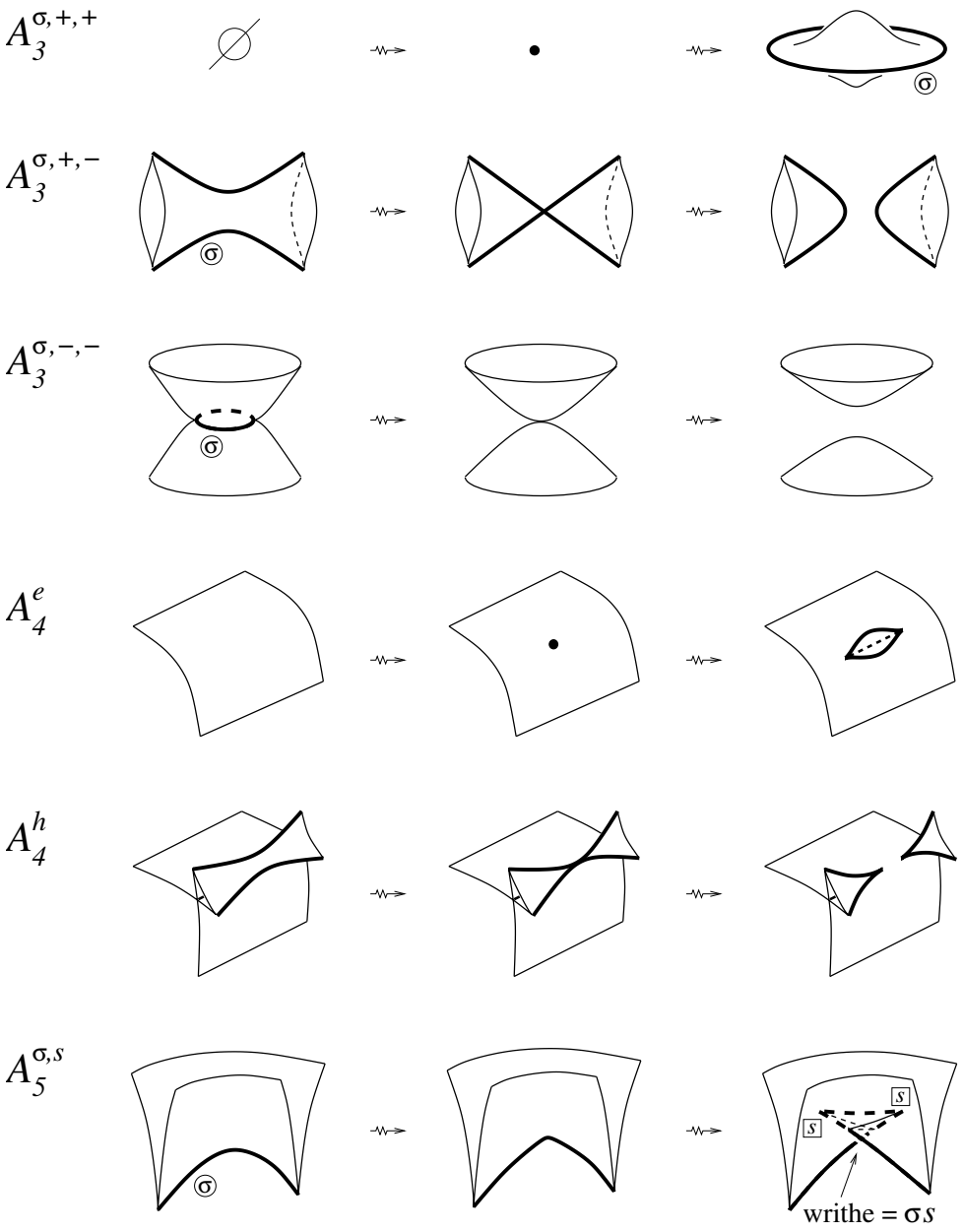

Figure 25: Generic one-parameter bifurcations of caustics of corank 1 maps.

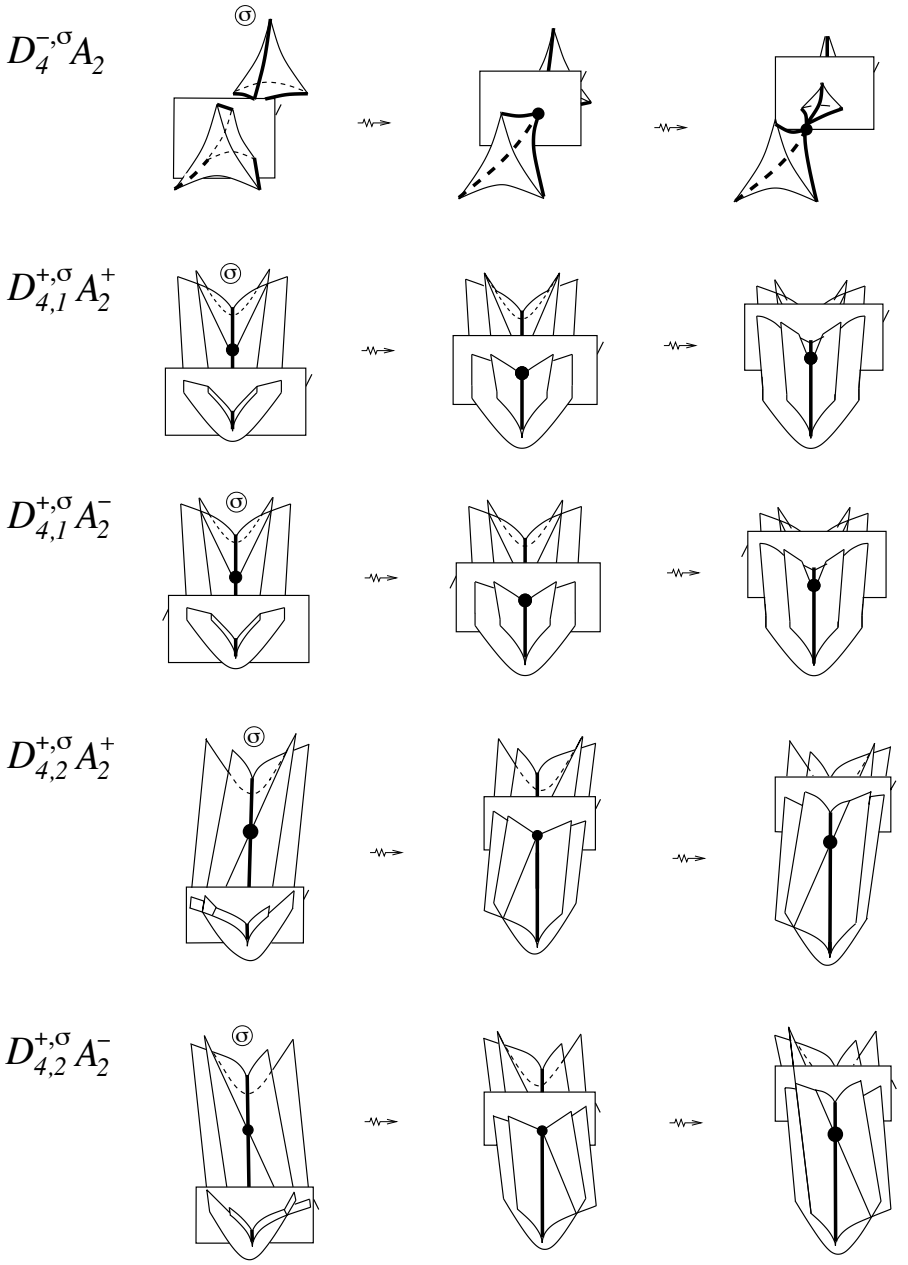

Figure 26: Generic one-parameter bifurcations of multi-germ caustics involving corank 2 points of the maps.

2.2.2.2 Uni-germs

All such bifurcations are shown in Figure 27 and taken from [4], pages 32 and 33. According to [26], the generating families for the first four transitions are induced from (4) and have the form

$$F = \pm x^2 y + \frac{1}{3}y^3 + \varphi\frac{y^2}{2} + vy + ux, \tag{5}$$

where, is in the line order, φ respectively is:

- $D^{-,\sigma}_{4,q}$: $\quad \lambda - w^2 \pm v + au$
- $D^{+,\sigma}_{4,a}$: $\quad \lambda - w^2 + v + au, \quad |a| < 1$
- $D^{+,\sigma}_{4,b}$: $\quad \lambda - w^2 \pm v + au, \quad |a| > 1$
- $D^{+,\sigma}_{4,c}$: $\quad \lambda - w^2 - v + au, \quad |a| < 1$

Here $a \in \mathbb{R}$ is a modulus. In $D^{-,\sigma}_{4,q}$, q is for 'quadratic'.

The D^{σ}_{5} generating family is

$$\pm F = x^2 y + y^4 - (\lambda \pm w + au)y^3 + wy^2 + vy + ux, \quad a \in \mathbb{R}.$$

2.2.3 Derivatives of the basic invariants

Direct analysis of the illustrations to our lists of bifurcations in generic one-parameter families yields

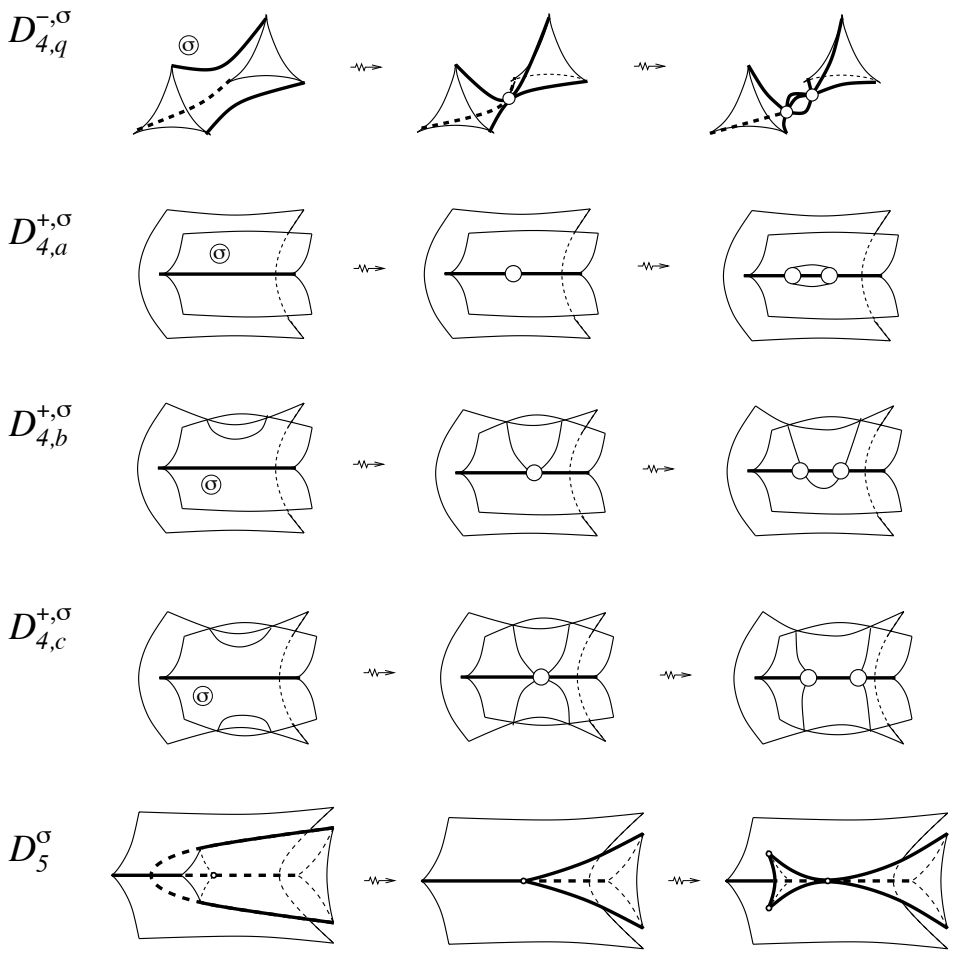

Figure 27: Generic one-parameter bifurcations of uni-germ caustics near corank 2 points of the maps.

Lemma 2.2.1. *The derivatives of the 10 invariants introduced in Example 2.1.1 are*

$$
\begin{aligned}
I'_t &: 2TA_2^3 + 2A_3A_2^2 + A_4A_2 + 2D_{4,1}^+A_2 \\
I'_{s_+} &: A_4^{e/h} + 2A_5^{+,+} + 2A_5^{-,+} + D_5 \\
I'_{s_-} &: A_4^{e/h} + 2A_5^{+,-} + 2A_5^{-,-} + D_5 \\
I'_{c_+} &: 2TA_3^+A_2 + 4A_3^{2,e,+,+} + 2A_3^{2,e,+,-} + 2A_3^{2,h,+,-} + A_4A_2 \\
&\quad +2A_5^+ - 2D_5^- \\
I'_{c_-} &: 2TA_3^-A_2 + 2A_3^{2,e,+,-} + 4A_3^{2,e,-,-} - 2A_3^{2,h,+,-} + A_4A_2 \\
&\quad +2A_5^- - 2D_5^+ \\
I'_{d_+^+} &: 2D_{4,q}^{+,+} - D_5^+ \\
I'_{d_-^+} &: 2D_{4,q}^{+,-} - D_5^- \\
I'_{d_+^-} &: 2D_{4,q}^{-,+} + D_5^+ \\
I'_{d_-^-} &: 2D_{4,q}^{-,-} + D_5^- \\
I'_\chi &: -D_{4,q}^+ + D_{4,q}^- + A_3^q
\end{aligned}
$$

Here, similar to the conventions introduced in Section 1.3.3, omission of an index means summation along all possible values of this index. Also $A_4^{e/h} = A_4^e + A_4^h$. and $D_{4,q}^+ = D_{4,a}^+ + D_{4,b}^+ + D_{4,c}^+$.

It is easy to check that the ten derivatives in the last Lemma are linearly independent over $\mathbb{R}$. Let $\mathcal{I}'$ be the linear space spanned over $\mathbb{R}$ by these 10 derivatives. We have

Corollary 2.2.2. *For an integer basis of the lattice $\mathcal{I}'_{\mathbb{Z}}$ of integer discrimi-*

nantal cycles in the space $\mathcal{I}'$ one can take the derivatives of the invariants

$$
\begin{array}{lcl}
\left(I_t - I_{c_-}\right)/2 & : & TA_2^3 + A_3A_2^2 - TA_3^-A_2 - A_3^{2,e,+,-} - 2A_3^{2,e,-,-} + A_3^{2,h,+,-} \\
 & & -A_5^- + D_{4,1}^+A_2 + D_5^+ \\
I_{s_+} & : & A_4^{e/h} + 2A_5^{+,+} + 2A_5^{-,+} + D_5 \\
\left(I_{s_+} - I_{s_-}\right)/2 & : & A_5^{+,+} - A_5^{+,-} + A_5^{-,+} - A_5^{-,-} \\
\left(I_{c_+} - I_{c_-}\right)/2 & : & TA_3^+A_2 - TA_3^-A_2 + 2A_3^{2,e,+,+} - 2A_3^{2,e,-,-} + 2A_3^{2,h,+,-} \\
 & & +A_5^+ - A_5^- + D_5^+ - D_5^- \\
I_{c_-} & : & 2TA_3^-A_2 + 2A_3^{2,e,+,-} + 4A_3^{2,e,-,-} - 2A_3^{2,h,+,-} + A_4A_2 \\
 & & +2A_5^- - 2D_5^+ \\
I_{d_+^+} & : & 2D_{4,q}^{+,+} - D_5^+ \\
I_{d_-^+} & : & 2D_{4,q}^{+,-} - D_5^- \\
\left(I_{d_+^-} + I_{d_+^+}\right)/2 & : & D_{4,q}^{+,+} + D_{4,q}^{-,+} \\
\left(I_{d_-^-} + I_{d_-^+}\right)/2 & : & D_{4,q}^{+,-} + D_{4,q}^{-,-} \\
I_\chi & : & -D_{4,q}^+ + D_{4,q}^- + A_3^q
\end{array}
$$

2.2.4 Classification of the discriminantal cycles and invariants

All statements in this section, unless specified, refer to any connected component of $\mathcal{L}(M, T^*N, N)$. The source and target 3-manifolds M and N are oriented. All invariants are considered up to a choice of additive constants on connected components of the spaces of maps.

The main result of this chapter is

Theorem 2.2.3. *The space of rational discriminantal cycles in $\mathcal{L}(M, T^*N, N)$ has rank 10.*

This Theorem immediately implies the following two corollaries.

Corollary 2.2.4. *The space of rational discriminantal cycles in $\mathcal{L}(M, T^*N, N)$ is spanned by the ten derivatives from Lemma 2.2.1.*

Corollary 2.2.5. *The space of integer discriminantal cycles in $\mathcal{L}(M, T^*N, N)$ has rank 10. It is spanned by the ten derivatives from Corollary 2.2.2.*

An immediate translation of the last two corollaries to the language of local invariants is

Corollary 2.2.6. *The dimension of the space of the integer invariants on $\mathcal{L}(M, T^*N, N)$ is 10, and it is spanned over the integers by the invariants from Corollary 2.2.2. For the 10-dimensional space of the rational invariants one can take a simpler basis consisting of the ten invariants from Example 2.1.1.*

We also prove the mod2 analogue of Theorem 2.2.3:

Theorem 2.2.7. *The space of $\mathbb{Z}_2$ discriminantal cycles in $\mathcal{L}(M, T^*N, N)$ has rank 16.*

This contains the ten dimensional space spanned by the mod2 reductions of the invariants in Corollary 2.2.2. For the case of ordinary maps between 3-manifolds with the target $\mathbb{R}^3$ or S^3, papers [13] and [2] introduced mod2

invariants I_{fe}, dc^+ and dc^-. Each of these invariants combines the number of components and the self-linking number of one of three framed links constructed from the cuspidal edge and self-intersection locus of the critical value set of a map. We have modified the three invariants to the Lagrangian setting, and the corresponding derivatives are linearly independent modulo the ten-dimensional space mentioned above. This also provides the knowledge of 13 mod2 linearly independent Lagrangian invariants for the special targets. However, we are not giving any details of the three invariants in this thesis in order not to increase its length any further. This results in three more linearly independent generators for the mod2 discriminantal cycles. This results in a 13 dimensional space inside our rank 16 space.

Theorems 2.2.3 and 2.2.7 are proved in Section 2.4.

2.3 Bifurcations in 2-parameter families

To derive equations on the increments of the invariants across the codimension 1 strata in $\mathcal{L}$ listed in the previous section, we shall now study – similar to what was done in Section 1.4 – bifurcations of codimension two singularities of Lagrangian maps between 3-manifolds.

We have 68 strata, four of which ($A_2^{4,2}$, $TA_2^{2,h,1}$, $A_3^{2,h,+,+}$, $A_3^{2,h,-,-}$) we have failed to co-orient. One of our main concerns in deriving the equations will be the reduction of the number of unknown increments.

2.3.1 Corank one bifurcations

There is basically no difference within corank 1 singularities between Lagrangian and ordinary maps of 3-manifolds, especially after our decision to put functions x^4 and $-x^4$ within the same equivalence class. Therefore, the main task of this section is to adjust the relevant considerations of [13] to the Lagrangian setting.

2.3.1.1 Extra A_2 component

Firstly we shall consider passing an extra generic A_2 sheet of $\mathcal{C}$ through a point of codimension 1 bifurcation S. Figure 28 shows three types of bifurcation diagrams. The left gives the equations **1-5** in the following table which reduces to the equation $u = v$. The middle and right are for the cases **6** and **7**. From the equations obtained from this we are able to introduce bigger strata, like we did in Section 1.4.1. In the cases when one of the summands in a big stratum is non-co-orientable, then we have the increment of any integer invariant over the big stratum be zero.

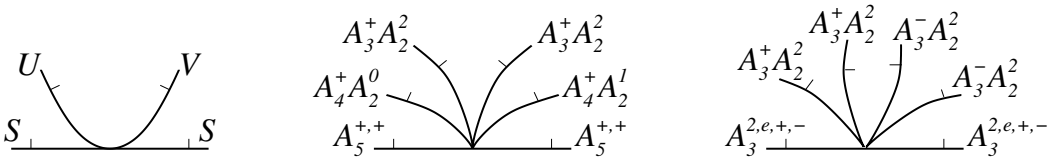

Figure 28: Discriminants of the families obtained from interaction of a generic smooth sheet with a codimension 1 bifurcation.

	S	r	Equation	Big stratum
1.	$TA_2^{3,r}$	$2,3$	$[a_2^{4,2}] = a_2^{4,3} = a_2^{4,4}$	$[A_2^4]$
2.	$TA_2^{2,e,r}$	$0,1,2$	$ta_2^{3,r+1} = ta_2^{3,r}$	TA_2^3
3.	$TA_3^\sigma A_2^{e,r}$	$0,1$	$a_3^\sigma a_2^{2,r+1} = a_3^\sigma a_2^{2,r}$	$A_3^\sigma A_2^2$
4.	$A_3^{\sigma,+,+}$		$ta_3^\sigma a_2^{e,0} = ta_3^\sigma a_2^{e,1}$	$TA_3^\sigma A_2^e$
	$A_3^{\sigma,-,-}$		$ta_3^\sigma a_2^{h,0} = ta_3^\sigma a_2^{h,1}$	$TA_3^\sigma A_2^h$
5.	A_4^e		$a_4^+ a_2^0 = a_4^- a_2^1$	
			$a_4^+ a_2^1 = a_4^- a_2^0$	
6.	$A_5^{+,+}$		$a_4^+ a_2^0 = a_4^+ a_2^1$	$A_4 A_2$
7.	$A_3^{2,e,+,-}$		$2a_3^+ a_2^2 = 2a_3^- a_2^2$	$A_3 A_2^2$ over $\mathbb{Z}$

2.3.1.2 Cubic Bifurcations

The A_3^e singularity has generating family $x^5 + w^2x^3 + vx^2 + ux$. Writing w^3 instead of w^2, we obtain a codimension 2 uni-germ, with a Lagrangian versal-deformation $x^5 + (w^3 + \lambda_1 w + \lambda_2)x^3 + vx^2 + ux$. (See [3] for the details.) Its discriminant is a semi-cubical parabola $4\lambda_1^3 + 27\lambda_2^2 = 0$, and yields coincidence of the increments across its half-branches. Similarly replacing quadratic configurations by cubic in some other codimension 1 bifurcations S, we obtain a list like in the previous subsection:

	S	Equation	Big stratum		
8.	A_4^e	$a_4^e = a_4^h$	$A_4^{e/h}$	$=$	$A_4^e + A_4^h$
9.	$A_3^{\sigma,+,\pm}$	$a_3^{\sigma,+,+} = a_3^{\sigma,+,-} = a_3^{\sigma,-,-}$	$A_3^{\sigma,q}$	$=$	$A_3^{\sigma,+,+} + A_3^{\sigma,+,-} + A_3^{\sigma,-,-}$
10.	$TA_3^\sigma A_2^e$	$ta_3^\sigma a_2^e = ta_3^\sigma a_2^h$	$TA_3^\sigma A_2$	$=$	$TA_3^\sigma A_2^e + TA_3^\sigma A_2^h$
11.	$TA_2^{2,e,r}, TA_2^{2,h,r}$	$ta_2^{2,e,2} = -ta_2^{2,e,0} = ta_2^{2,h,0}$	$TA_2^{2,opp}$	$=$	$TA_2^{2,e,2} - TA_2^{2,e,0} + TA_2^{2,h,0}$
		$ta_2^{2,e,1} = [ta_2^{2,h,1}]$	$[TA_2^{2,dir}]$	$=$	$TA_2^{2,e,1} + [TA_2^{2,h,1}]$

We do not omit the indices in the big strata here but introduce new notation. Let q stand for quadratic, dir = direct for the tangency between two sheets with coinciding co-orientations and opp = opposite for the tangency between two sheets of opposite co-orientation.

So far we have reduced the number of unknown increments to 46.

2.3.1.3 Multi-germ families: Non-transversal interactions with a cuspidal edge

Consider three codimension 2 events that occur when the plane tangent to the critical point set at its edge point is in a special position with the other local components of $\mathcal{C}$. These are when the plane coincides with the plane tangent to a smooth A_2 sheet, the plane contains the tangent direction of the line of intersection of two A_2 sheets and the plane contains the tangent direction of another cuspidal edge. These three events are shown in Figure 29.

Respectively we obtain the equations,

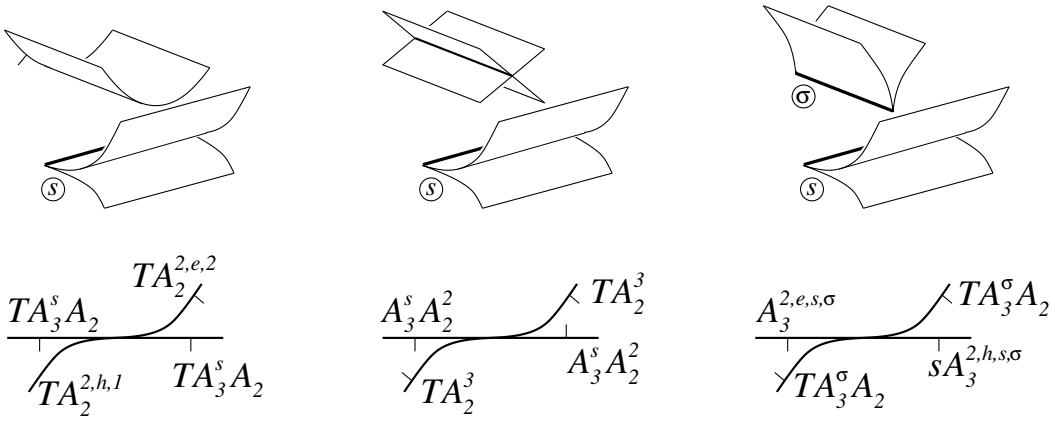

Figure 29: Codimension 2 degenerations due to special positions with respect to the tangent plane at an edge point.

$$
\begin{aligned}
\textbf{12}. \quad ta_2^{2,opp} &= [ta_2^{2,dir}] \\
\textbf{13}. \quad 2ta_2^3 &= 2a_3^+a_2^2 \\
&= 2a_3^-a_2^+ \\
\textbf{14}. \quad 2ta_3^+a_2 &= a_3^{2,e,+,+} + [a_3^{2,h,+,+}] \\
&= a_3^{2,e,+,-} + a_3^{2,h,+,-} \\
2ta_3^-a_2 &= a_3^{2,e,+,-} - a_3^{2,h,+,-} \\
&= a_3^{2,e,-,-} + [a_3^{2,h,-,-}]
\end{aligned}
$$

Equation **12** enables us to create the big stratum, $[TA_2^2] = TA_2^{2,opp} + [TA_2^{2,dir}]$ over mod2 invariants only.

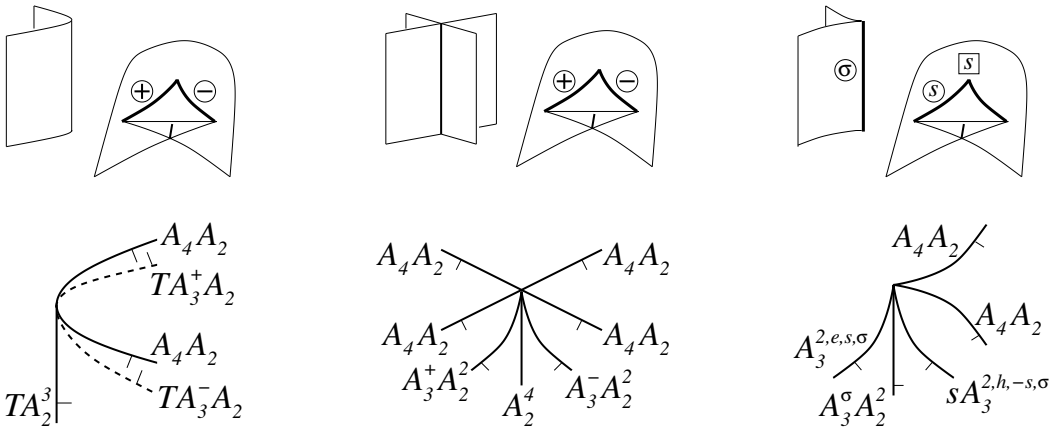

Figure 30: Codimension 2 degenerations involving swallowtails.

2.3.1.4 Multi-germ families: Interaction with a swallowtail

Similar to before we now consider how the swallowtail interacts with other local components of $\mathcal{C}$. In Figure 30 left, we have at the most degenerate moment, the incoming smooth sheet tangent to the direction of the self-intersection curve at the swallowtail point. The two remaining cases in Figure 30 are clear. These give us the equations:

$$
\begin{aligned}
\textbf{15}.\quad 2a_4a_2 &= ta_3^+a_2 + ta_3^-a_2 + ta_2^3 \\
\textbf{16}.\quad a_3^-a_2^2 &= a_3^+a_2^2 + [a_2^4] \\
\textbf{17}.\quad 2a_4a_2 &= a_3^+a_2^2 + a_3^{2,e,+,+} - a_3^{2,h,+,-} \\
&= a_3^+a_2^2 + a_3^{2,e,+,-} + [a_3^{2,h,+,+}] \\
&= a_3^-a_2^2 + a_3^{2,e,+,-} + [a_3^{2,h,-,-}] \\
&= a_3^-a_2^2 + a_3^{2,e,-,-} + a_3^{2,h,+,-}
\end{aligned}
$$

2.3.1.5 Uni-germs of codimension 2

Putting generating functions x^4 and $-x^4$ into the same class reduces classification of uni-germs of corank 1 to the classification of similar singularities of ordinary maps. Translation of the corresponding normal forms from [13] to the Lagrangian language of generating functions provides us with the normal forms given in the caption of 31 and the bifurcation diagrams shown in that Figure. The diagrams in the first and second lines there are coming from different orientation choices.

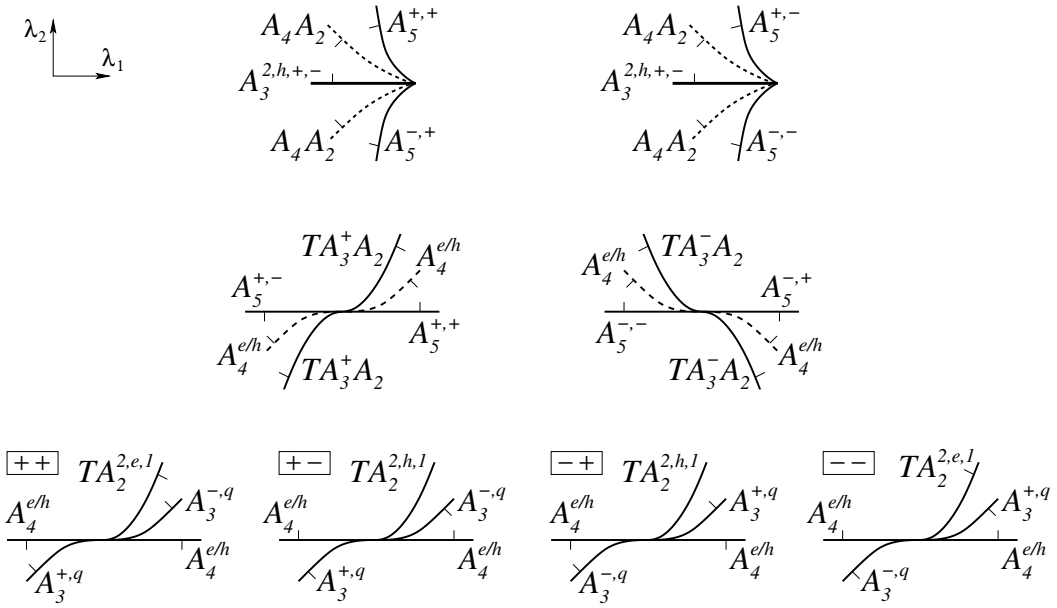

Figure 31: Discriminants of the families

$$x^7 + (\lambda_1 \pm w + \alpha v)x^5 + \lambda_2 x^4 + wx^3 + vx^2 + ux, \quad \alpha \in \mathbb{R};$$

$$(\pm x^6 + wx^4 + (\pm w^2 + \lambda_1 w + \lambda_2)x^3 + vx^2 + ux;$$

$$x^5 + vx^3 + (\pm v^2 + \lambda_1 v + \lambda_2 \pm w^2)x^2 + ux.$$

$$
\begin{array}{lllll}
\textbf{18}. & & a_3^{2,h,+-} & = & a_5^{+,+} - a_5^{-,+} \\
 & & & = & a_5^{+,-} - a_5^{-,-} \\
\textbf{19}. & & 2a_4^{e/h} & = & a_5^{+,+} + a_5^{+,-} - 2ta_3^{+}a_2 \\
 & & & = & a_5^{-,+} + a_5^{-,-} - 2ta_3^{-}a_2 \\
\textbf{20}. & a_3^{+,q} & - \; a_3^{-,q} & = & [ta_2^2]
\end{array}
$$

Equation **20** gives us the big stratum $A_3^q = A_3^{+,q} + A_3^{-,q}$ over $\mathbb{Z}$.

2.3.2 Corank two bifurcations

So far we have decreased the number of unknown increments to 42 out of which five may be non-trivial only in the mod2 case. We shall now consider the corank two bifurcations to reduce this number further and to add to our system of equations on the increments.

2.3.2.1 Uni-germs: D_4

We start with the cubic version of the one-parameter quadratic bifurcation of the $D_4^{\pm}$ singularities introduced in Section 2.2.2.2. Namely, in the $D_4^{\pm}$ $\mathcal{R}_+$-miniversal family

$$F = \pm x^2 y + \frac{1}{3}y^3 + \frac{\varphi}{2}y^2 + \beta y + \delta x$$

we now set

$$\varphi = \alpha^3 + s\alpha + t \pm \beta + a\delta, \quad a \in \mathbb{R}, a \neq \pm 1. \tag{6}$$

This gives us an st-family of caustics in $\mathbb{R}^3_{\alpha,\beta,\delta}$ with the big caustic in the 5-space being a direct product of either purse or pyramid with $\mathbb{R}^2$.

What follows is equally valid for deforming with $s\alpha + t$ of any function $\varphi|_{s=t=0}$ in α, β, δ with the same terms $\alpha^3 \pm \beta + a\delta$ of the two lowest quasi-homogenous weights. The bifurcation diagrams in the parameter st-plane are shown in Figure 32.

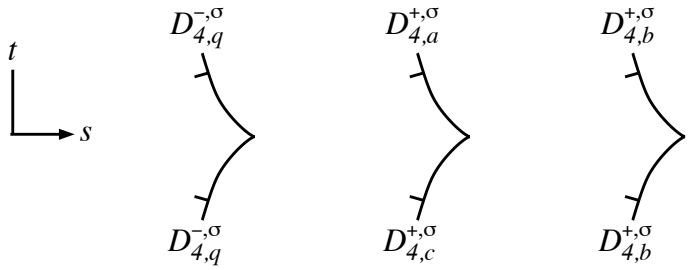

Figure 32: The bifurcations diagrams in the st-plane for the (6) settings: the left is for D_4^-, the final two are for D_4^+ with the middle when $|a| < 1$ and the right when $|a| > 1$.

In Figure 32, the left and right diagrams produce the trivial roundabout equation whereas the middle yields

	Equation	Big stratum
21.	$d^{+,\sigma}_{4,a} = d^{+,\sigma}_{4,c}$	$D^{+,\sigma}_{4,a/c}$

We shall now inspect a reason for the constraint $a \neq \pm 1$ in Section 2.2.2.2.

So, for D_4^+, set in (5) (same as in F at the start of this section)

$$\varphi = \pm\alpha^2 \pm \beta \pm \delta + q(\beta, \delta) + t + s\ell(\beta, \delta) + \text{ higher quasi-homogeneous terms.}$$

Here q is a quadratic form not divisible by $\pm\beta \pm \delta$ (with the signs chosen in a particular φ), and ℓ is a linear form which is not a multiple of $\pm\beta \pm \delta$.

Function φ, as described is such that for $t = s = 0$ its restriction to one of the lines $\delta = \pm\beta$ in $\alpha = 0$ has a Morse point at the origin and this point moves along this line off the origin if $s \neq 0$.

For example, set

$$\varphi = \alpha^2 + \beta + \delta \pm \beta^2 + 2s\beta + t. \tag{7}$$

Restriction of φ onto $\beta = -\delta < 0 = \alpha$ is $\pm\beta^2 + 2s\beta + t$. It has critical point on its zero level (that is, a double root in β) iff $s^2 = \pm t$. Since we want it to be only on $\beta < 0$, we take just half of this parabola: $\beta = \mp s < 0$. Such a critical point on one of the arms of the 'V' self-intersection locus of the purse corresponds to a TA_2^2 degeneration (it may be checked that it is $TA_2^{2,dir}$). The bifurcation diagrams for the sign choices in (7) are shown in Figure 33.

The TA_2^2 stratum in both diagrams contributes mod2 only, due to the equations **11** and **12**. In both of the diagrams here, one of the q_i's is b and

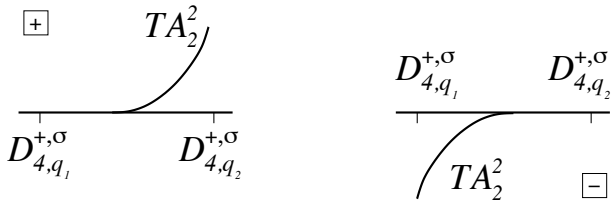

Figure 33: Bifurcation diagrams for the settings (7)

the other is a/c. Here the roundabout equations in both cases are,

$$\textbf{22}. \qquad \begin{aligned} d^{+,+}_{4,a/c} - d^{+,+}_{4,b} + [ta_2^2] = 0 \\ d^{+,-}_{4,a/c} - d^{+,-}_{4,b} + [ta_2^2] = 0 \end{aligned}$$

All other sign choices in φ (for α^2, β, δ) yield the same equations.

2.3.2.2 Uni-germs: D_5

Following [26], we have only one codimension 2 singularity induced from the $\mathcal{R}_+$-miniversal deformation of the D_5 function. The corresponding generating family is

$$\pm G = x^2 y + \frac{1}{4}y^4 + \frac{1}{3}\alpha y^3 + \frac{1}{2}\psi y^2 + \beta y + \delta x,$$

assuming our 3-dimensional caustics are in $\mathbb{R}^3_{\alpha,\beta,\delta}$, s and t are the parameters, and $\psi|_{s=t=0} := \psi_0(\alpha, \beta, \delta)$ is $k\alpha^2$, $k = const \neq 0$, modulo terms of higher quasi-homogeneous order. We take $\psi = k\alpha^2 + s\alpha + t$ which is sufficient for our considerations.

Similar to what we will be doing later in Chapters 3 and 4 (all the ideas for

our current considerations are detailed there) for $D_6^{\pm}$ caustics, it is convenient to introduce the function,

$$\Psi = y^2(y^3 + \alpha y^2 + \psi y + \beta) + \frac{\delta^2}{4}$$

and describe all degenerations in G in terms of those in Ψ. Our approach will be as follows. Take a stratum $X \subset \mathbb{R}^4_{\alpha,\psi,\beta,\delta}$ parametrized in terms of Ψ. Consider its preimage $\tilde{X} \subset \mathbb{R}^5_{\alpha,\beta,\delta,s,t}$ under the map

$$(\alpha, \beta, \delta, s, t) \mapsto (\alpha, \psi(\alpha, \beta, \delta, s, t), \beta, \delta),$$

where $\dim\tilde{X} = \dim\ X + 1$. The critical value set $Y \subset \mathbb{R}^2_{s,t}$ of the restriction of the projection $\pi : \mathbb{R}^5_{\alpha,\beta,\delta,s,t} \to \mathbb{R}^2_{s,t}$ to $\tilde{X}$ is one of 1-dimensional strata in the bifurcation diagram we need.

The correspondence $X \sim Y$ is:

$\dim X = 0$: $D_5 \sim D_5$

$\dim X = 1$: $D_4^{\pm} \sim D_{4,q}^{\pm}$ $A_4 \sim A_4^{e/h}$ $A_3A_2 \sim TA_3A_2$ $D_3A_2 \sim TD_3A_2$

$\dim X = 2$: $A_2^2 \sim TA_2^2$ $A_3 \sim A_3^q$

$\dim X = 3$: A_2, the regular part of the caustic, cannot have any critical values under π as long as we assume our Lagrangian submanifold $G_x|_{s=t=0} = G_y|_{s=t=0} = 0$ smooth (and this is so for the family we are considering).

We will mostly be working with closures $\overline{X}$ of the strata. Therefore, we will be getting $-$ along with the strata Y $-$ also the critical value sets for the strata of $\overline{X}\backslash X$.

The D_5^σ stratum in $\mathbb{R}^5_{\alpha,\beta,\delta,s,t}$ is $\alpha = \psi = \beta = \delta = 0$, that is, the s-axis. Hence the D_5^σ stratum in the parameter plane $\mathbb{R}^2_{s,t}$ is $t = 0$.

The D_4^σ stratum in $\mathbb{R}^5$ is $\beta = \delta = \psi = 0 \Rightarrow k\alpha^2 + s\alpha + t = 0$. This surface projects to $\mathbb{R}^2_{s,t}$ with a fold. The critical value set is the discriminant of the polynomial in α: $s^2 - 4kt = 0$. This is the $D^{\pm,\sigma}_{4,q}$ stratum, which is co-oriented towards the positivity of the discriminant.

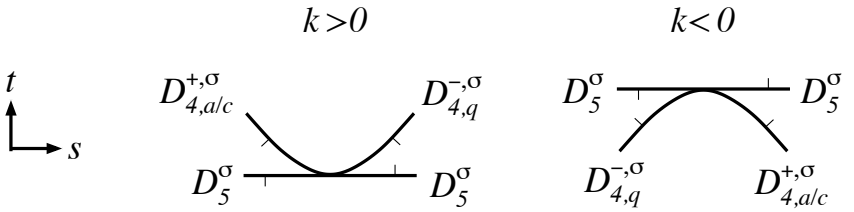

Figure 34: The D_5 and $D_{4,q}$ strata of the bifurcation diagram

The mutual position of the bifurcational strata found so far is shown in Figure 34. The co-orientations of the D_5^σ half-branches here will be explained in the A_4 part below. The $+/-$ choice in the $D^{\pm,\sigma}_{4,q}$ coincides with the sign of the double root α of the equations $k\alpha^2 + s\alpha + t = 0$ for the (s,t) taken on the half-branch. For D_4^+, only the a/c option occurs.

The A_4 stratum. Take $\Psi = (y-u)^4(y + \frac{u}{4})$. This is a parametrization of

the A_4 curve in the ordinary D_5 caustic in $\mathbb{R}^4 = \mathbb{R}^4_{\alpha,\psi,\beta,\delta}$. This gives us,

$$\begin{aligned}
\alpha &= -\frac{15}{4}u \quad \Longrightarrow \quad u = -\frac{4}{15}\alpha \\
\beta &= -\frac{5}{2}u^3 \\
\delta^2 &= u^5 \quad \Longrightarrow \quad u > 0 \quad \Longrightarrow \quad \alpha < 0 \\
\psi &= 5u^2 \quad \Longrightarrow \quad k\alpha^2 + s\alpha + t = \frac{16}{45}\alpha^2, \quad \alpha < 0, \quad \delta^2 \sim -\alpha^5.
\end{aligned}$$

Projection of the surface $\left\{k\alpha^2 + s\alpha + t = \frac{16}{45}\alpha^2\right\}$ to $\mathbb{R}^2_{s,t}$ has critical locus $\left\{s = -2(k - \frac{16}{45})\alpha, \alpha < 0\right\}$ doubled in the δ-direction. The critical value set is the stratum $2A_4^{e/h}$ defined by the vanishing of the discriminant of the quadratics and co-oriented towards positivity of the discriminant: $s^2 - 4t(k - \frac{16}{45}) = 0$ (only the $\alpha < 0$ half is needed). See Figure 35.

A reason behind our co-orientations of the D_5 half-branches in Figure 35 is as follows. At the $A_4^{e/h}$ strata we create two A_4 points. Same happens when we cross a D_5 stratum in the positive direction. These are the only strata at which the number of A_4 points changes. Since we know the co-orientation of $A_4^{e/h}$, and the total roundabout increment of the number of A_4 points must be zero, this gives us the co-orientations of the D_5^σ half-branches.

The A_3A_2 stratum of the D_5 caustic in $\mathbb{R}^4$ is parametrised using

$$\Psi = \left(y - \frac{u}{2}\right)^3 \left(y + \frac{u}{3}\right)^2.$$

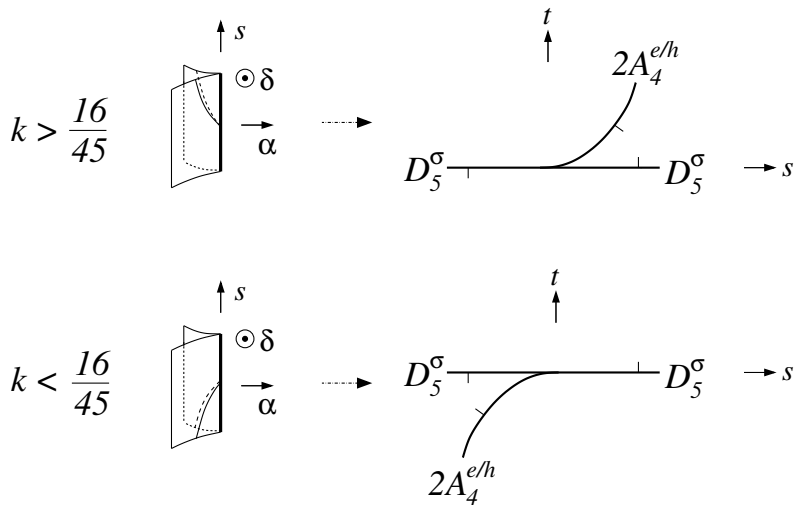

Figure 35: The A_4 surface in $\mathbb{R}^5_{\alpha,\beta,\delta,s,t}$ with the fold locus on it. Its edge is the D_5 stratum. Projection to $\mathbb{R}^2_{s,t}$ provides the bifurcational strata.

Hence,

$$\begin{aligned}
\alpha &= -\frac{5}{6}u \\
\psi &= -\frac{5}{36}u^2 \Rightarrow \psi = -\frac{\alpha^2}{5} \Rightarrow \alpha^2\left(k+\frac{1}{5}\right)+s\alpha+t=0 \\
\beta &= \frac{5}{24}u^3 \\
\delta^2 &= -\frac{1}{18}u^5 \Rightarrow u<0 \Rightarrow \alpha>0.
\end{aligned}$$

The critical locus of projecting the surface $\left\{\alpha^2\left(k+\frac{1}{5}\right)+s\alpha+t=0\right\}$ to $\mathbb{R}^2_{s,t}$ is $s=-2\left(k+\frac{1}{5}\right)\alpha$ (doubled by δ). The critical value set is $2TA_3^{-\sigma}A_2$: $s^2-4\left(k+\frac{1}{5}\right)t=0$ co-oriented to the positivity of the left hand side. Similar to the A_4 case we obtain the bifurcation curves in Figure 36.

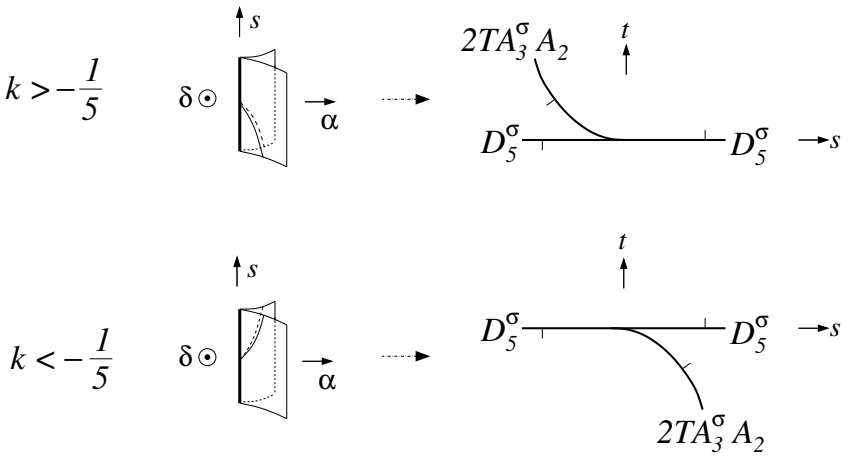

Figure 36: Obtaining the TA_3A_2 strata of the bifurcation diagram

The D_3A_2 stratum of the D_5 caustic is parametrised by

$$\Psi = y^3(y-u)^2.$$

Hence we have,

$$\begin{aligned}
\delta &= \beta = 0 \\
\alpha &= -2u \Rightarrow \psi - \frac{\alpha^2}{4} = 0 \Rightarrow \left(k - \frac{1}{4}\right)\alpha^2 + s\alpha + t = 0 \\
\psi &= u^2
\end{aligned}$$

This time we are mapping the whole surface,

$$\left(k - \frac{1}{4}\right)\alpha^2 + s\alpha + t = 0, \tag{8}$$

without any constraint on α to $\mathbb{R}^2_{s,t}$. The critical value set is $TD^{\sigma}_3 A_2$ given by the discriminant of (8) is $s^2 - 4\left(k - \frac{1}{4}\right) t = 0$. It is co-oriented in $\mathbb{R}^2_{s,t}$ by the positivity of the left hand side of the equation. See Figure 37.

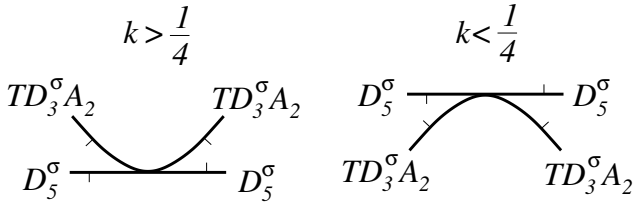

Figure 37: The $TD_3 A_2$ strata

Consider now the A_2^2 stratum of the D_5 caustic, with the parametrization,

$$\Psi = (y^2 + uy + v)^2 (y + w). \tag{9}$$

The vanishing of the coefficient of y in the expansion gives,

$$v^2 = -2uw. \tag{10}$$

Positivity of the constant term $\frac{\delta^2}{4}$ implies $v^2 w = 4u^2 w^3 > 0 \Rightarrow w > 0$. For the quadratic factor in (9) to have two real roots: $u^2 - 4v > 0$. One can show that the 3-dimensional variety in $\mathbb{R}^5_{\alpha,\beta,\delta,s,t}$ which is the preimage of the parametrized 2-dimensional surface (9,10) from $\mathbb{R}^4_{\alpha,\psi,\beta,\delta}$ projects to $\mathbb{R}^2_{s,t}$ with the critical value set being the discriminant of the quadratic equation $\left(k + \frac{1}{5}\right) \alpha^2 + s\alpha + t = 0$, that is, exactly the $2A_3 A_2$ stratum. Hence the stratum

TA_2^2 for our 2-parameter deformation is empty.

The A_3 stratum. This time we are searching for A_3^q points which correspond (along with $D_{4,q}^{\pm}$ points) to the transformations of the critical point set. The critical point set of the map $(x, y, \alpha) \mapsto (\alpha, \beta, \delta)$ is given by

$$\text{Hessian}(G)_{x,y} = \begin{vmatrix} 2y & 2x \\ 2x & 3y^2 + 2\alpha y + \psi \end{vmatrix} = 0,$$

that is, it doubly covers the set $y(3y^2 + 2\alpha y + \psi) \geq 0$ in $\mathbb{R}^2_{y,\alpha}$, that is, the set

$$y\left(3\left(y + \frac{\alpha}{3}\right)^2 + \left(k - \frac{1}{3}\right)\left(\alpha + \frac{s}{2\left(k - \frac{1}{3}\right)}\right)^2 + t - \frac{s^2}{4\left(k - \frac{1}{3}\right)}\right) \geq 0.$$

Therefore the A_3^q stratum in $\mathbb{R}^2_{s,t}$ is $s^2 = 4\left(k - \frac{1}{3}\right)t$, while the $D_{4,q}^{\pm}$ is $s^2 = 4kt$. The mutual position of these strata in $\mathbb{R}^2_{s,t}$ is shown in Figure 38.

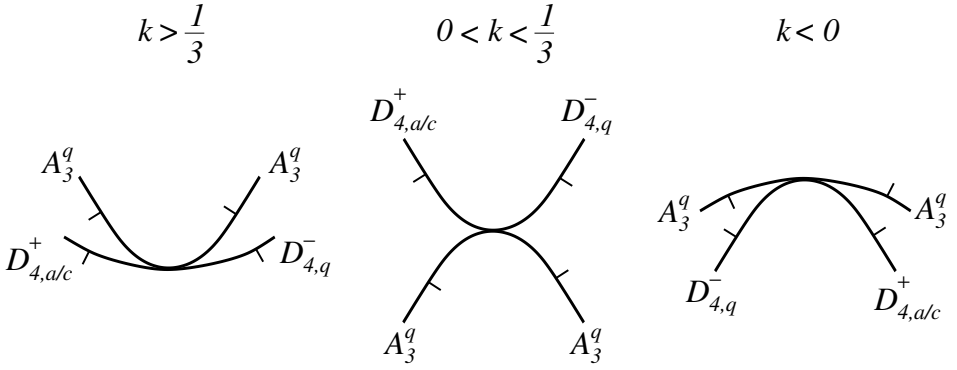

Figure 38: The A_3^q and $D_{4,q}^{\pm}$ strata

The Euler characteristic of the critical point set jumps at a positive cross-

ing by 2 on $D^-_{4,q}$, by -2 on $D^+_{4,a/c}$ and by 2 on A^q_3. Due to that, our earlier knowledge of the $D^\pm_{4,q}$ co-orientations gives us now the co-orientation of the A^q_3 half-branches. It may also be easily checked that one of these half-branches is $A^{+,q}_3$ and the other $A^{-,q}_3$.

Collecting all the information obtained in this section, we obtain

Lemma 2.3.1. *The two-parameter bifurcations with the big caustic D_5 yield the following roundabout equations:*

$$\textbf{23}. \qquad \begin{aligned} &2d^+_5 + d^{+,+}_{4,a/c} - d^{-,+}_{4,q} - 2a^{e/h}_4 + 2ta^+_3 a_2 + a^{+,q}_3 + a^{-,q}_3 = 0 \\ &2d^-_5 + d^{+,-}_{4,a/c} - d^{-,-}_{4,q} - 2a^{e/h}_4 + 2ta^-_3 a_2 + a^{+,q}_3 + a^{-,q}_3 = 0 \end{aligned}$$

2.3.2.3 Extra A_2 component

We now consider passing a generic smooth sheet through the codimension one bifurcations S listed in Figure 27. Sending an A_2 sheet through the D_4 sigularities of Figure 27 gives us the bifurcation diagrams shown in Figure 39 (cf Figure 28, left), and the equation and big strata in the table below.

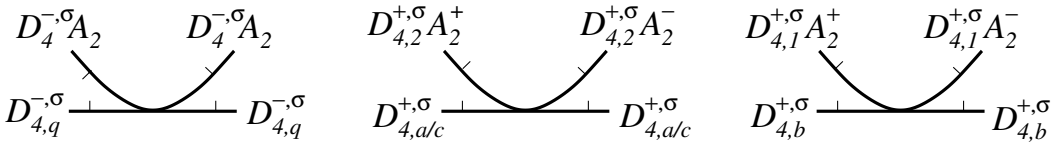

Figure 39: The bifurcation diagrams for a generic A_2 sheet passing through the D_4 caustics in Figure 27.

	S	Equations	Big stratum
24.	$D^{-,\sigma}_{4,q}$	$2d^{-,\sigma}_4 a_2 = 0$	$[D^{-,\sigma}_4 A_2]$
25.	$D^{+,+}_{4,a}$ or $D^{+,+}_{4,c}$	$d^{+,+}_{4,1} a^+_2 = d^{+,+}_{4,1} a^-_2$	$D^{+,+}_{4,1} A_2$
	$D^{+,-}_{4,a}$ or $D^{+,-}_{4,c}$	$d^{+,-}_{4,1} a^+_2 = d^{+,-}_{4,1} a^-_2$	$D^{+,-}_{4,1} A_2$
26.	$D^{+,+}_{4,b}$	$d^{+,+}_{4,2} a^-_2 = d^{+,+}_{4,2} a^+_2$	$D^{+,+}_{4,2} A_2$
	$D^{+,-}_{4,b}$	$d^{+,-}_{4,2} a^-_2 = d^{+,-}_{4,2} a^+_2$	$D^{+,-}_{4,2} A_2$

Due to equation **24**, we are considering from this moment the strata $D^{-,\sigma}_4$ as non-co-orientable.

Consider now $S = D^{\sigma}_5$. Restrict our attention to the sections by the smooth A_2 sheets of the caustics in the last line of Figure 27. This way the 2-parameter bifurcation of the 3-dimensional caustics we are considering now induces a generic 2-parameter bifurcation of planar caustics whose diagram we had in Figure 18. Forgetting the difference between x^4 and $-x^4$ function singularities and adding the D^{σ}_5 stratum to that earlier bifurcation diagram, we obtain Figure 40. This gives us the equations,

$$\textbf{27}. \qquad \begin{aligned} &2a_4 a_2 - t a^-_3 a_2 - t a^+_3 a_2 - d^{+,+}_{4,1} a_2 + [d^{-,+}_4 a_2] = 0 \\ &2a_4 a_2 - t a^+_3 a_2 - t a^-_3 a_2 - d^{+,-}_{4,1} a_2 + [d^{-,-}_4 a_2] = 0 \end{aligned}$$

2.3.2.4 Extra A_3 component

This and the next two subsections are in a sense similar to Section 2.3.1.4 where the interaction of a swallowtail with other local components of a caustic

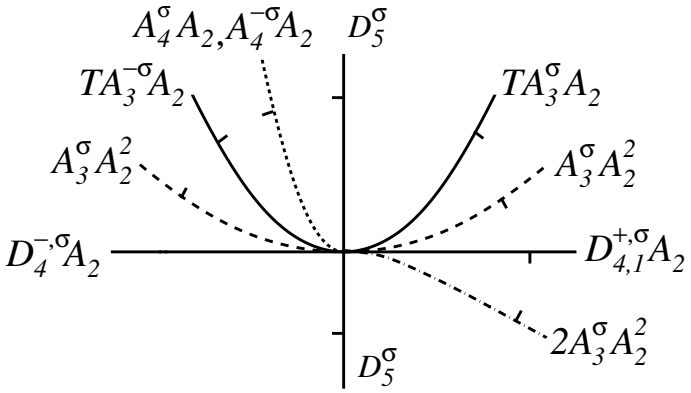

Figure 40: Bifurcation diagram of passing a smooth sheet through D_5.

was studied. We now replace the swallowtail with either purse or pyramid.

All through these three subsections we are taking the pyramid as it is shown in Figure 23 and assume that its 'top' edge is a flat curve. Let Π be the plane of this edge. Every additional component C of the caustic will be a cylinder with its generators assumed to be perpendicular to Π. All our two-parameter bifurcations will be obtained by parallel translations of C. In each case C will have a distinguished generator ℓ. The bifurcation diagram of the family will be drawn in Π and will be the set of the meeting points of ℓ with Π at the moments of bifurcations.

Similar approach will be taken to the bifurcations involving a purse: the role of Π will be taken by a plane containing its only cuspidal edge and dividing the purse in Figure 23 into two diffeomorphic (but not necessarily symmetric) halves.

So, we start with a cuspidal surface as a component C in this section, and

look first at its bifurcations with a pyramid. The distinguished generator of C this time is the cuspidal edge line.

There are two ways to place the cuspidal surface relative to the pyramid. One is shown in Figure 41 which gives the left bifurcation diagram in the same figure. The second is obtained by rotating the cuspidal surface by 180° about its edge which gives the right bifurcation diagram.

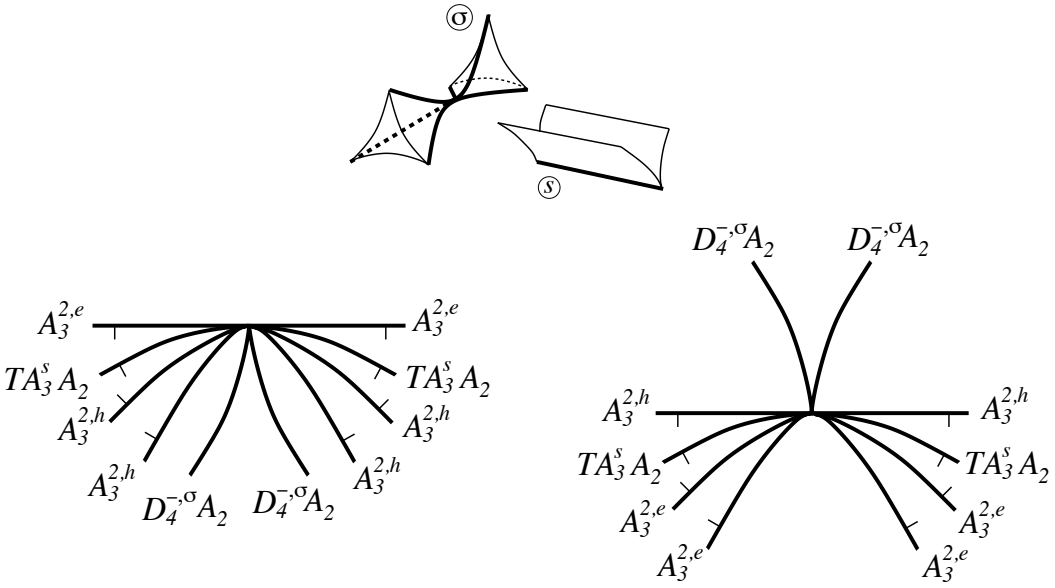

Figure 41: A cuspidal edge surface passing through a pyramid along with the corresponding bifurcation diagram (left) and the bifurcation diagram when the surface is rotated by 180° about its edge (right).

We are not specifying all the indices in the notations of the strata in the diagrams of Figure 41, but it is clear that the symmetric pairs of half-branches in each case have the same names and are co-oriented in opposite ways (in

the clock-wise sense) if they are co-orientable. This yields trivial roundabout equations for the pyramid.

Consider now a cuspidal surface and a purse, in a relative position as in Figure 42, and also with the cuspidal surface upside down. We have two subcases in each situation: at the most degenerate moment, the two self-intersection rays of the purse may be either to the same side or to different sides of the plane tangent to the cuspidal surface at its edge. As we can see from the diagrams in Figure 42, the one-side option gives us the equations

$$\textbf{28}. \qquad \begin{aligned} -2d_{4,1}^{+,+}a_2 + 2a_3^+a_2^2 &= 0 \\ -2d_{4,1}^{+,-}a_2 + 2a_3^-a_2^2 &= 0 \end{aligned}$$

Figure 42 also shows that the different-sides option gives the trivial equations, due to the symmetry of the bifurcation diagrams.

2.3.2.5 Extra A_2^2 component

We now replace the cuspidal surface of the previous subsection with two transversal smooth sheets. Assuming that their self-intersection line passes through the vertex of a pyramid at the most degenerate moment, we obtain the bifurcation diagram shown in Figure 43. Since we are now treating the $D_4^{-,\sigma}A_2$ strata as non-co-orientable, the diagram yields the trivial roundabout equation.

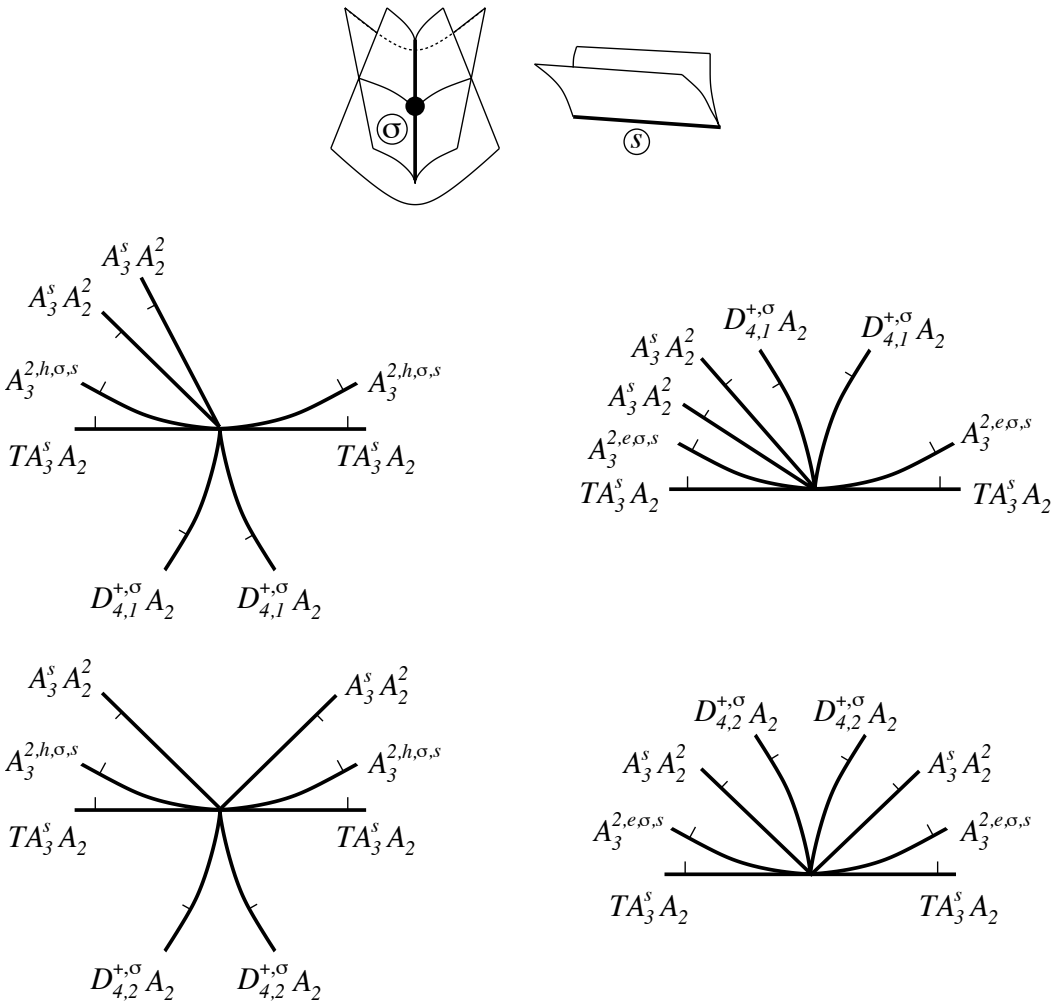

Figure 42: Bifurcations of a cuspidal surface around a purse. The left pair of the diagrams corresponds to the relative position of the surface as shown at the top of the figure, and the right pair is for the cuspidal surface rotated by 180 degrees about its edge. The top pair of the diagrams is for the self-intersection rays of the purse being to the same side of the plane tangent to the cuspidal surface at its edge at the most critical moment, and the bottom pair is for the two rays being on its different sides.

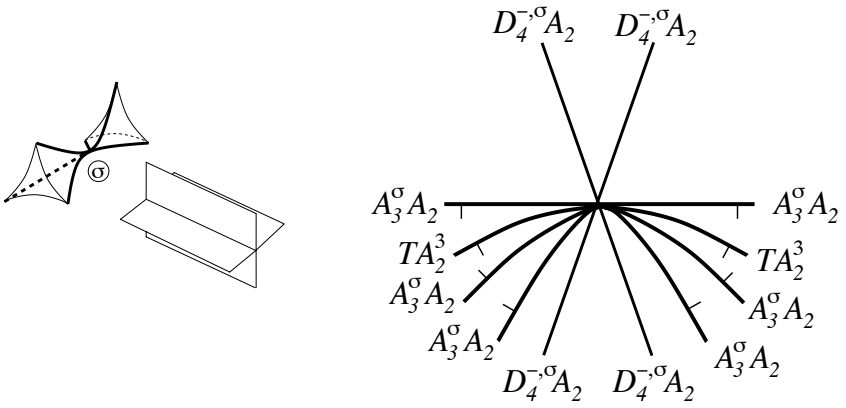

Figure 43: Bifurcations of a pair of transversal A_2 sheets with a pyramid.

Consider now similar bifurcations of a pair of transversal A_2 sheets with a purse.

There are quite a few possible configurations due to the relative positions of the purse and the sheets at the most degenerate moment. Assume that at such a moment one of the four connected components into which the two sheets cut the ambient space contains both self-intersection rays of the purse and one of its cuspidal half-branches. Figure 44 shows the bifurcation diagram we have in this case. It clearly gives us the trivial equation.

In each of other combinatorially possible situations, we will also have similar components in the bifurcation diagram

- two $[A_2^4]$ half-branches;
- symmetric pair of TA_2^3 half-branches contributing zero to the roundabout equation;

- similar $A_3^\sigma A_2^2$ pair;
- two lines of $D_4^{+\sigma} A_2$ strata each contributing zero to the equation.

Hence the equation is always trivial.

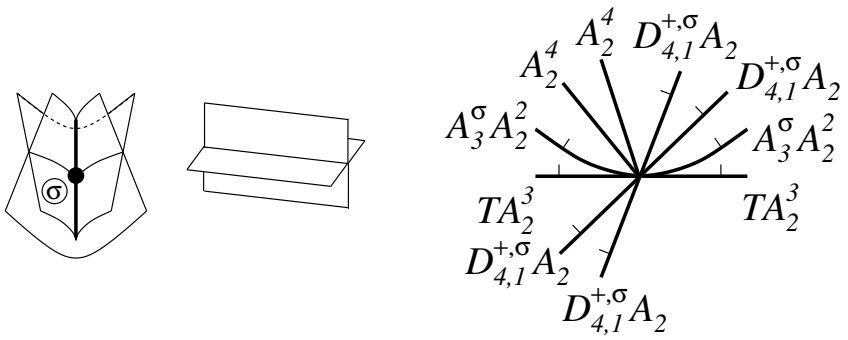

Figure 44: Bifurcations of a pair of transversal sheets with a purse.

2.3.2.6 Tangent A_2 component

There remains only one set of generic two-parameter multi-germ bifurcations to consider: tangencies of smooth sheets to the one-dimensional strata of a purse and a pyramid at the D_4 points.

We start with the tangencies to the cuspidal edges and treat them in the spirit of the previous two subsections. For a model A_2 sheet we take a parabolic cylinder.

The bifurcation diagram for a rather steep A_2 sheet and a pyramid is shown in Figure 45. Due to its symmetry about the vertical axis, the equation it provides is trivial.

Reducing the steepness of our parabolic A_2 sheet and continuing this process for the sheet in the upside-down position, we get a series of bifurcation diagrams with the $D_4^{-,\sigma}A_2$ curve situated successively in pairs of the sectors between the other strata in Figure 45. In each case the diagram is symmetric and yields the trivial equation. Switching the co-orientation of the A_2 sheet to the opposite does not affect the result.

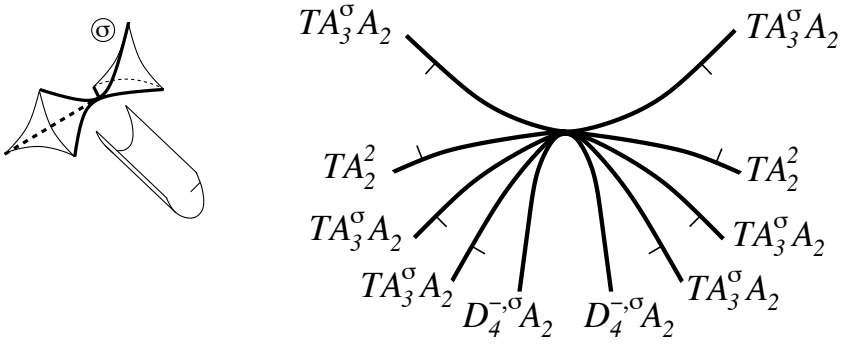

Figure 45: Bifurcations of an A_2 sheet tangent to a cuspidal edge of a pyramid

Now consider similar interaction of a steep parabolic A_2 sheet with a purse, as in Figure 46. The corresponding bifurcation diagram shown there implies the trivial equation again. Changing the coefficient of the parabola in the A_2 sheet (like it was done in presence of a purse) and of its co-orientation does not change the equation.

We remark that TA_2^3 bifurcations do not appear in Figure 46 since the A_2 sheet in its most degenerate position is not tangent to the self-intersection rays of the purse.

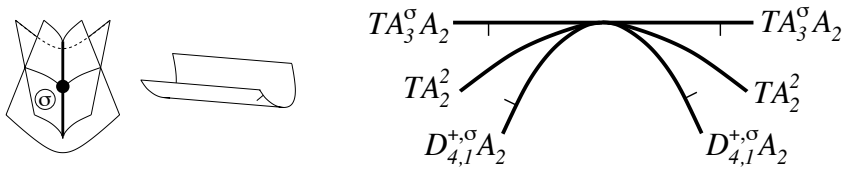

Figure 46: Bifurcations of a purse and a smooth A_2 sheet of a caustic tangent to the cuspidal edge of the purse at the D_4^+ point

Finally, consider a codimension 2 degeneration of tangency of a smooth A_2 sheet to one of self-intersection rays at a D_4^+ point. Recall that in Section 1.4.2 we considered two-parameter bifurcations of a section of a purse by a surface which was in the same relative position to the purse at the distinguished moment. We can now assume that the diagrams in Figure 17 there are actually sections of the purse by an A_2 sheet co-oriented away from us. This gives us the bifurcation diagrams shown in Figure 47 and the equations

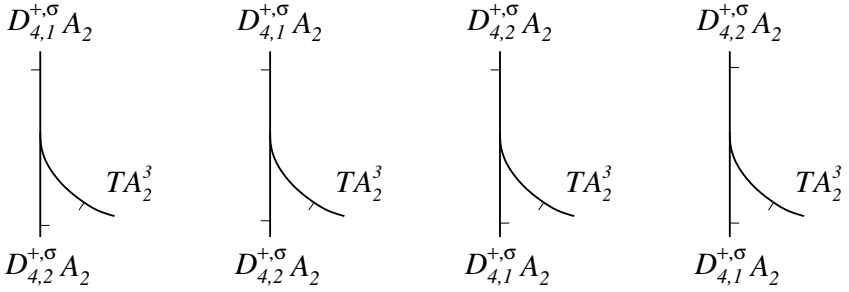

Figure 47: Bifurcation diagrams an A_2 sheet of a caustic tangent to a self-intersection ray of a purse at its D_4^+ point

$$\textbf{29}. \qquad d^{+,+}_{4,1}a_2 + d^{+,+}_{4,2}a_2 - ta_2^3 = 0$$

$$d^{+,-}_{4,1}a_2 + d^{+,-}_{4,2}a_2 - ta_2^3 = 0$$

$$\textbf{30}. \qquad d^{+,+}_{4,1}a_2 - d^{+,+}_{4,2}a_2 - ta_2^3 = 0$$

$$d^{+,-}_{4,1}a_2 - d^{+,-}_{4,2}a_2 - ta_2^3 = 0$$

If we consider the opposite co-orientation of the smooth sheet it gives us the same equations.

Remark 2.3.2. The last four equations imply that the strata $D^{+,\sigma}_{4,2}A_2$ should be treated as non-co-orientable.

2.3.2.7 D_6 and E_6 bifurcations

The three remaining possible big caustics of generic two-parameter families are D_6^+, D_6^- and E_6. About them we claim

Theorem 2.3.3. *Generic two-parameter families of three-dimensional caustics with big caustics D_6^+ and E_6 add to the system of equations* **1**–**30** *equations* **31** *and* **32** *respectively:*

$$\textbf{31}. \qquad -2d^{+,+}_{4,1}a_2 + 4a_4a_2 - 2ta_3^+a_2 - 2ta_3^-a_2 = 0$$

$$-2d^{+,-}_{4,1}a_2 + 4a_4a_2 - 2ta_3^+a_2 - 2ta_3^-a_2 = 0$$

$$\textbf{32}. \qquad -2a_3^{2,h,+,-} + 2ta_3^+a_2 - 2ta_3^-a_2 = 0$$

Generic families with big caustics D_6^- add nothing.

Our proof of this theorem is lengthy, and we devote to it the next three chapters while using the statement in the rest of the current chapter.

2.4 Proofs of Theorems 2.2.3 and 2.2.7

The proofs are now reduced to the analysis of the system of equations **1**–**32** obtained in Section 2.3.

We initially had 68 elementary discriminantal strata. In Section 2.3 we have been able to join them, both over $\mathbb{Z}$ and $\mathbb{Z}_2$, into respectively 23 and 30 bigger strata. Equations on the increments of the invariants across these select strata obtained during the bifurcation analysis, over $\mathbb{Z}$, are collected in columns in Table 4e below. Similar to Section 1.4.3, the equations which are integer linear combinations of the others are not included there. We are using dots instead of zeros.

Table 4e	13	14	14	14	14	15	17	18	18	23	23	27	27
TA_2^3	2	.	.	.	.	1	.	.	.	.	.	.	.
$A_3A_2^2$	−2	.	.	.	.	.	1	.	.	.	.	.	.
$TA_3^+A_2$	.	−2	−2	.	.	1	.	.	.	.	2	−1	−1
$TA_3^-A_2$	.	.	.	−2	−2	1	.	.	.	2	.	−1	−1
$A_3^{2,e,+,+}$	.	1	.	.	.	.	1	.	.	.	.	.	.
$A_3^{2,e,+,-}$	.	.	1	1	.	.	.	.	.	.	.	.	.
$A_3^{2,e,-,-}$	.	.	.	.	1	.	.	.	.	.	.	.	.
$A_3^{2,h,+,-}$	.	.	1	−1	.	.	−1	−1	−1	.	.	.	.
A_4A_2	.	.	.	.	.	−2	−2	.	.	.	.	2	2
$A_4^{e/h}$	.	.	.	.	.	.	.	.	.	−2	−2	.	.
$A_5^{+,+}$	.	.	.	.	.	.	.	1	.	.	.	.	.
$A_5^{+,-}$	.	.	.	.	.	.	.	.	1	.	.	.	.
$A_5^{-,+}$	.	.	.	.	.	.	.	−1	.	.	.	.	.
$A_5^{-,-}$	.	.	.	.	.	.	.	.	−1	.	.	.	.
$D_{4,1}^{+,+}A_2$	.	.	.	.	.	.	.	.	.	.	.	−1	.
$D_{4,1}^{+,-}A_2$	.	.	.	.	.	.	.	.	.	.	.	.	−1
$D_{4,abc}^{+,+}$	.	.	.	.	.	.	.	.	.	1	.	.	.
$D_{4,abc}^{+,-}$	.	.	.	.	.	.	.	.	.	.	1	.	.
$D_{4,q}^{+,+}$	.	.	.	.	.	.	.	.	.	−1	.	.	.
$D_{4,q}^{+,-}$	.	.	.	.	.	.	.	.	.	.	−1	.	.
D_5^+	.	.	.	.	.	.	.	.	.	2	.	.	.
D_5^-	.	.	.	.	.	.	.	.	.	.	2	.	.
A_3^q	.	.	.	.	.	.	.	.	.	2	2	.	.

With 13 linearly independent equations in 23 unknowns, we have a ten-dimensional solution space. This finishes our proof of Theorem 2.2.3.

For completeness of the picture and to allow an easier verification that the derivatives of the invariants from Example 2.1.1 indeed satisfy all the equations obtained in Section 2.3, we have collected in Table 4s the coefficients of these derivatives. The table also helps to spot the linear independence of

the derivatives.

Table 4s	t	s_+	s_-	c_+	c_-	d^+_+	d^+_-	d^-_+	d^-_-	χ
TA_2^3	2	.	.	.	.	.	.	.	.	.
$A_3A_2^2$	2	.	.	.	.	.	.	.	.	.
$TA_3^+A_2$	.	.	.	2	.	.	.	.	.	.
$TA_3^-A_2$	.	.	.	.	2	.	.	.	.	.
$A_3^{2,e,+,+}$	.	.	.	4	.	.	.	.	.	.
$A_3^{2,e,+,-}$	.	.	.	2	2	.	.	.	.	.
$A_3^{2,e,-,-}$	.	.	.	.	4	.	.	.	.	.
$A_3^{2,h,+,-}$	.	.	.	2	-2	.	.	.	.	.
A_4A_2	1	.	.	1	1	.	.	.	.	.
$A_4^{e/h}$	.	1	1	.	.	.	.	.	.	.
$A_5^{+,+}$	.	2	.	2	.	.	.	.	.	.
$A_5^{+,-}$	.	.	2	2	.	.	.	.	.	.
$A_5^{-,+}$	.	2	.	.	2	.	.	.	.	.
$A_5^{-,-}$	.	.	2	.	2	.	.	.	.	.
$D_{4,1}^{+,+}A_2$	2	.	.	.	.	.	.	.	.	.
$D_{4,1}^{+,-}A_2$	2	.	.	.	.	.	.	.	.	.
$D_{4,abc}^{+,+}$	.	.	.	.	.	2	.	.	.	-1
$D_{4,abc}^{+,-}$	.	.	.	.	.	.	2	.	.	-1
$D_{4,q}^{+,+}$	.	.	.	.	.	.	.	2	.	1
$D_{4,q}^{+,-}$	.	.	.	.	.	.	.	.	2	1
D_5^+	.	1	1	.	-2	-1	.	1	.	.
D_5^-	.	1	1	-2	.	.	-1	.	1	.
A_3^q	.	.	.	.	.	.	.	.	.	1

We now similarly collect in Table 5e $\mathbb{Z}_2$ linearly independent mod2 reductions of the equations on the increments of the invariants across the select obtained during the bifurcation analysis.

With 14 linearly independent equations in 30 unknowns, we have a rank 16 solution space. This completes our proof of Theorem 2.2.7.

Table 5s contains the coefficients of the mod2 reductions of the derivatives mentioned in Corollary 2.2.2. Comparison of this table with Table 5e allows one to easily check that the derivatives indeed satisfy the mod2 equations.

Table 5e	15	16	17	17	18	20	22	22	23	23	27	27	29	29
A_2^4	.	1	.	.	.	.	.	.	.	.	.	.	.	.
TA_2^3	1	.	.	.	.	.	.	.	.	.	.	.	1	1
$A_3^+A_2^2$	.	1	1	.	.	.	.	.	.	.	.	.	.	.
$A_3^-A_2^2$	.	1	.	1	.	.	.	.	.	.	.	.	.	.
$TA_3^+A_2$	1	.	.	.	.	.	.	.	.	.	1	1	.	.
$TA_3^-A_2$	1	.	.	.	.	.	.	.	.	.	1	1	.	.
$A_3^{2,e/h,+,+}$	.	.	1	.	.	.	.	.	.	.	.	.	.	.
$A_3^{2,e/h,+,-}$	.	.	1	1	1	.	.	.	.	.	.	.	.	.
$A_3^{2,e/h,-,-}$	.	.	.	1	.	.	.	.	.	.	.	.	.	.
A_4A_2	.	.	.	.	.	.	.	.	.	.	.	.	.	.
$A_4^{e/h}$	.	.	.	.	.	.	.	.	.	.	.	.	.	.
$A_5^{+,\pm}$	.	.	.	.	1	.	.	.	.	.	.	.	.	.
$A_5^{-,\pm}$	.	.	.	.	1	.	.	.	.	.	.	.	.	.
$A_3^{+,q}$	.	.	.	.	.	1	.	.	.	.	.	.	.	.
$A_3^{-,q}$	.	.	.	.	.	1	.	.	.	.	.	.	.	.
TA_2^2	.	.	.	.	.	1	1	1	.	.	.	.	.	.
$D_{4,1}^{+,+}A_2$	.	.	.	.	.	.	.	.	.	.	1	.	1	.
$D_{4,1}^{+,-}A_2$	.	.	.	.	.	.	.	.	.	.	.	1	.	1
$D_{4,2}^{+,+}A_2$	.	.	.	.	.	.	.	.	.	.	.	.	1	.
$D_{4,2}^{+,-}A_2$	.	.	.	.	.	.	.	.	.	.	.	.	.	1
$D_4^{-,+}A_2$	.	.	.	.	.	.	.	.	.	.	1	.	.	.
$D_4^{-,-}A_2$	.	.	.	.	.	.	.	.	.	.	.	1	.	.
$D_{4,a/c}^{+,+}$	.	.	.	.	.	.	1	.	1	.	.	.	.	.
$D_{4,a/c}^{+,-}$	.	.	.	.	.	.	.	1	.	1	.	.	.	.
$D_{4,b}^{+,+}$	.	.	.	.	.	.	1	.	.	.	.	.	.	.
$D_{4,b}^{+,-}$	.	.	.	.	.	.	.	1	.	.	.	.	.	.
$D_{4,q}^{+,+}$	.	.	.	.	.	.	.	.	1	.	.	.	.	.
$D_{4,q}^{+,-}$	.	.	.	.	.	.	.	.	.	1	.	.	.	.
D_5^+	.	.	.	.	.	.	.	.	.	.	.	.	.	.
D_5^-	.	.	.	.	.	.	.	.	.	.	.	.	.	.

Table 5s	$(t-c_-)/2$	s_+	$(s_- - s_+)/2$	$(c_+ - c_-)/2$	c
A_2^4	.	.	.	.	.
TA_2^3	1	.	.	.	.
$A_3^+ A_2^2$	1	.	.	.	.
$A_3^- A_2^2$	1	.	.	.	.
$TA_3^+ A_2$	.	.	.	1	.
$TA_3^- A_2$	1	.	.	1	.
$A_3^{2,e/h,+,+}$	.	.	.	.	.
$A_3^{2,e/h,+,-}$	1	.	.	.	.
$A_3^{2,e/h,-,-}$	.	.	.	.	.
$A_4 A_2$	.	.	.	.	1
$A_4^{e/h}$	.	1	.	.	.
$A_5^{+,\pm}$	.	.	1	1	.
$A_5^{-,\pm}$	1	.	1	1	.
$A_3^{+,q}$	.	.	.	.	.
$A_3^{-,q}$	.	.	.	.	.
TA_2^2	.	.	.	.	.
$D_{4,1}^{+,+} A_2$	1	.	.	.	.
$D_{4,1}^{+,-} A_2$	1	.	.	.	.
$D_{4,2}^{+,+} A_2$	.	.	.	.	.
$D_{4,2}^{+,-} A_2$	.	.	.	.	.
$D_4^{-,+} A_2$	.	.	.	.	.
$D_4^{-,-} A_2$	.	.	.	.	.
$D_{4,a/c}^{+,+}$	.	.	.	.	.
$D_{4,a/c}^{+,-}$	.	.	.	.	.
$D_{4,b}^{+,+}$	.	.	.	.	.
$D_{4,b}^{+,-}$	.	.	.	.	.
$D_{4,q}^{+,+}$	.	.	.	.	.
$D_{4,q}^{+,-}$	.	.	.	.	.
D_5^+	1	1	.	1	.
D_5^-	.	1	.	1	.

Table 5s (continued)	d_+^+	d_-^+	$\left(d_+^- + d_+^+\right)/2$	$\left(d_+^- + d_-^+\right)/2$	χ
A_2^4	.	.	.	.	.
TA_2^3	.	.	.	.	.
$A_3^+ A_2^2$	.	.	.	.	.
$A_3^- A_2^2$	.	.	.	.	.
$TA_3^+ A_2$	.	.	.	.	.
$TA_3^- A_2$	.	.	.	.	.
$A_3^{2,e/h,+,+}$	.	.	.	.	.
$A_3^{2,e/h,+,-}$	.	.	.	.	.
$A_3^{2,e/h,-,-}$	.	.	.	.	.
$A_4 A_2$	.	.	.	.	.
$A_4^{e/h}$	.	.	.	.	.
$A_5^{+,\pm}$	.	.	.	.	.
$A_5^{-,\pm}$	.	.	.	.	.
$A_3^{+,q}$	.	.	.	.	1
$A_3^{-,q}$	.	.	.	.	1
TA_2^2	.	.	.	.	.
$D_{4,1}^{+,+} A_2$	.	.	.	.	.
$D_{4,1}^{+,-} A_2$	.	.	.	.	.
$D_{4,2}^{+,+} A_2$	.	.	.	.	.
$D_{4,2}^{+,-} A_2$	.	.	.	.	.
$D_4^{-,+} A_2$	.	.	.	.	.
$D_4^{-,-} A_2$	.	.	.	.	.
$D_{4,a/c}^{+,+}$	.	.	1	.	1
$D_{4,a/c}^{+,-}$	.	.	.	1	1
$D_{4,b}^{+,+}$	.	.	1	.	1
$D_{4,b}^{+,-}$	.	.	.	1	1
$D_{4,q}^{+,+}$	.	.	1	.	1
$D_{4,q}^{+,-}$	.	.	.	1	1
D_5^+	1	.	.	.	.
D_5^-	.	1	.	.	.

Chapter 3

D_6^+ bifurcations

The aim of this chapter is to prove the D_6^+ part of Theorem 2.3.3 from Section 2.3.2.7. We will derive the equations **31** claimed there. This result will require the list of adjacencies of the most generic 3-dimensional section of the 'big' caustic $C(D_6^+) \subset \mathbb{R}^5$ to the codimension 1 degenerations of caustics we had in Section 2.2. Our calculations below show that such codimension 1 degenerations are

$$D_5,\ D_4A_2,\ A_3^2,\ A_4A_2,\ TA_3A_2,\ A_4^e$$

(see Figures 53 and 55).

3.1 Reduction to a polynomial in one variable

We will be working with a $\mathcal{R}_+$-miniversal deformation of the D_6^+ function singularity in the form

$$\begin{aligned} F &= x^2y + \frac{1}{5}y^5 + \frac{1}{4}\alpha y^4 + \frac{1}{3}\beta y^3 + \frac{1}{2}\gamma y^2 + \delta y + \epsilon x \\ &= x^2y + \epsilon x + p(y). \end{aligned} \tag{11}$$

One of its helpful features is the quasi-homogeneity. We fix the weights of the variables as

$$x \sim 2 \quad y \sim 1 \quad \alpha \sim 1 \quad \beta \sim 2 \quad \gamma \sim 3 \quad \delta \sim 4 \quad \epsilon \sim 3.$$

The D_6^+ caustic, $\mathcal{C}(D_6^+)$, in $\mathbb{R}^5$ is the set of all parameters $(\alpha, \beta, \gamma, \delta, \epsilon)$ for which the equations

$$F_x = F_y = \begin{vmatrix} F_{xx} & F_{xy} \\ F_{yx} & F_{yy} \end{vmatrix} = 0$$

have common solutions in x, y. Eliminating x from the equations

$$\begin{aligned} F_x &= 2xy + \epsilon = 0 \\ F_y &= x^2 + y^4 + \alpha y^3 + \beta y^2 + \gamma y + \delta \\ &= x^2 + p'(y) = 0 \end{aligned}$$

gives us a polynomial equation in just one variable, y:

$$Q := y^2 p'(y) + \frac{\epsilon^2}{4} = 0. \tag{12}$$

The determinant of the Hessian matrix of F is

$$H := \begin{vmatrix} F_{xx} & F_{xy} \\ F_{yx} & F_{yy} \end{vmatrix} = \begin{vmatrix} 2y & 2x \\ 2x & p''(y) \end{vmatrix} = 2yp''(y) - 4x^2 = 0.$$

Using F_y to eliminate x from this yields

$$0 = yp''(y) + 2p'(y) = \frac{(y^2 p'(y))'}{y}.$$

That is,

$$\frac{Q'}{y} = 0 \text{ or simply } Q' = 0.$$

Here $y = 0$ may be considered as is a special root of Q and Q', when $Q = y^2 p'(y)$.

The big D_6^+ caustic $\mathcal{C}(D_6^+)$ in the 5-dimensional parameter space corresponds to those polynomials Q which have either root $y \neq 0$ of multiplicity $r > 1$ or root $y = 0$ of multiplicity $k > 2$. These two options mean that the big caustic and its transversal sections have singularities A_r or D_k (see [26] for the details). It is convenient here to consider the D_3 singularity of a function in this particular 5-parameter family as the A_3 singularity at the origin $x = y = 0$.

In the following subsections we analyse how $\mathcal{C}(D_6^+)$ may be represented as a collection of a generic 2-parameter family of 3-dimensional caustics. For this we study generic projections π of the pair $(\mathbb{R}^5, \mathcal{C}(D_6^+))$ onto a plane. The problem is highly modular in the C^∞ setting (see [26]), but we need only know the planar bifurcation diagram $\mathcal{B}(D_6^+)$, and even in that we more or less need only the order of the branches of the curves corresponding to the codimension 1 degenerations.

Our approach to this task is via consideration of successive approximations to a generic projection. The approximations will be done in the weighted-homogeneous sense. Namely, the lowest weight part of a generic mapping π, $\mathbb{R}^5_{\alpha,\beta,\gamma,\delta,\epsilon} \to \mathbb{R}^2_{A,B}$ reduces to $(A, B) = (\alpha, \beta)$, and we will refer to this as *the straight projection*, and denote it π_s. The next order approximation is addition of the terms $C\gamma + E\epsilon$, with arbitrary real coefficients C and E, to the second component of the straight projection. We call this approximation *a tilted projection* and denote π_t. It turns out – see the rest of this chapter – that these two approximations give us all the information about $\mathcal{B}(D_6^+)$ for the roundabout equations. The helping observation here is that if two strata in the bifurcation diagram of π_s (respectively π_t) are distinct then they stay distinct and have the same order of tangency in the bifurcation diagram of π_t (respectively π): consideration of projection terms of higher quasihomogeneous degree affects only those terms in the parametrizations of the strata which do not affect the tangency orders.

The bifurcation curves in $\mathbb{R}^2$ are the images of all possible 1-dimensional

strata of $\mathcal{C}(D_6^+)$ and the critical value sets of the restriction of the projection to its higher-dimensional strata. We will show that only 2-dimensional strata provide non-trivial contributions in the latter case, see Section 3.6.

So, in the following subsections we analyse the contributions of the one and two dimensional strata of the big caustic to the planar bifurcation diagrams for the straight and (if need) tilted projections. These two diagrams will be denoted $\mathcal{B}_s(D_6^+)$ and $\mathcal{B}_t(D_6^+)$.

3.2 One-dimensional strata

According to the multiplicity options for the roots of Q mentioned above, we have the following parametrizations of one-dimensional strata in $\mathcal{C}(D_6^+)$:

- D_5 where $Q = y^5(y-t)$
- D_4A_2 where $Q = y^4(y-t)^2$
- D_3A_3 where $Q = y^3(y-t)^3$
- A_5 where $Q = (y-t)^5(y-s)$
- A_4A_2 where $Q = (y-t)^4(y-s)^2$
- A_3^2 where $Q = (y-t)^3(y-s)^3$

In the first three cases $t \in \mathbb{R}$, $t \neq 0$, and in the last three, the real parameters t, s are subject to the constraint of the coefficient of y in Q being zero. Recall

that

$$Q := y^2 p'(y) + \frac{\epsilon^2}{4} = y^2(y^4 + \alpha y^3 + \beta y^2 + \gamma y + \delta) + \frac{\epsilon^2}{4} \tag{13}$$

Firstly we shall consider the D strata. The D_5 parametrization

$$Q = y^5(y - t)$$

gives us

$$\alpha = -t \quad \beta = \gamma = \delta = \epsilon = 0.$$

Therefore, the D_5 stratum in $\mathcal{B}_s(D_6^+) \subset \mathbb{R}^2_{A,B}$ is

$$B = 0.$$

Next we take D_4A_2, with the parametrization

$$Q = y^4(y - t)^2 = y^2(y^4 - 2ty^3 + t^2y^2).$$

Similar to above we obtain,

$$\alpha = -2t \text{ and } \beta = t^2.$$

This gives the equation

$$A^2 = 4B$$

of the D_4A_2 stratum in $\mathcal{B}_s(D_6^+)$.

Finally consider D_3A_3, with the parametrization

$$Q = y^3(y-t)^3 = y^2(y^4 - 3ty^3 + 3t^2y^2 - t^3y).$$

Similarly we compare this with (13) to obtain

$$\alpha = -3t \text{ and } \beta = 3t^2.$$

This results in the equation

$$A^2 = 3B.$$

Now we deal with the possible A_k strata. Firstly take A_5, with the parametrization (where $t \neq 0$)

$$\begin{aligned}(y-t)^5(y-s) &= y^6 + (-s-5t)\,y^5 + (10t^2+5ts)\,y^4 \\ &\quad +(-10t^2s - 10t^3)\,y^3 + (5t^4 + 10t^3s)\,y^2 \\ &\quad +(-5t^4s - t^5)\,y + t^5s.\end{aligned}$$

Comparing the constant terms with (13),

$$\frac{\epsilon^2}{4} = t^5s. \tag{14}$$

Since (13) does not have a y term we set our y coefficient to zero

$$-5t^4s - t^5 = 0 \Leftrightarrow -t^4(5s + t) = 0 \Rightarrow s = -\frac{t}{5}.$$

Due to (14) we have

$$\frac{\epsilon^2}{4} = -\frac{t^6}{5}.$$

Since it is not possible to have a real value of ϵ, the A_5 stratum is empty in $\mathcal{C}(D_6^+)$ and hence in $\mathcal{B}(D_6^+)$.

Consider the A_4A_2 parametrization (where $s, t \neq 0$)

$$\begin{aligned}(y-t)^4(y-s)^2 &= y^6 + (-4t-2s)\,y^5 + (s^2+6t^2+8ts)\,y^4 \\ &\quad +(-4ts^2-12t^2s-4t^3)\,y^3 + (8t^3s+6t^2s^2+t^4)\,y^2 \\ &\quad +(-2t^4s-4t^3s^2)\,y + t^4s^2.\end{aligned}$$

Comparing the constant terms with (13) we see that $\frac{\epsilon^2}{4} = t^4s^2$ is satisfied for any values of t, s. Now setting the coefficient of y to be zero we have

$$-2t^4s - 4t^3s^2 = 0 \Leftrightarrow -2t^3s(t + 2s) = 0 \Rightarrow s = -\frac{t}{2}.$$

We substitute this value into

$$\alpha = -4t - 2s \text{ and } \beta = s^2 + 6t^2 + 8ts.$$

Elimination of t yields

$$4\beta = \alpha^2.$$

Therefore the equation of the A_4A_2 stratum in $\mathcal{B}_s(D_6^+)$ is $4B = A^2$.

Finally we consider A_3^2 with the parametrization (where $s, t \neq 0$)

$$\begin{aligned}(y-t)^3(y-s)^3 &= y^6 + (-3t-3s)\,y^5 + (3t^2+9ts+3s^2)\,y^4 \\ &\quad +(-t^3-9t^2s-9ts^2-s^3)\,y^3 \\ &\quad +(3t^3s+9t^2s^2+3ts^3)\,y^2 + (-3t^3s^2-3t^2s^3)\,y \\ &\quad +t^3s^3.\end{aligned}$$

Comparison of the constant term shows that

$$\frac{\epsilon^2}{4} = t^3s^3.$$

Considering the y coefficient we have

$$-3t^3s^2 - 3t^2s^3 = 0 \Leftrightarrow -3t^2s^2(t+s) = 0 \Leftrightarrow s = -t.$$

Thus from the previous display

$$\frac{\epsilon^2}{4} = -t^6.$$

Due to the minus sign here, the A_3^2 stratum is empty in $\mathcal{C}(D_6^+)$ and hence in $\mathcal{B}(D_6^+)$.

In conclusion we so far have the following co-dimension one strata in $\mathcal{B}(D_6^+)$ (shown in Figure 48):

- D_4A_2: $A^2 = 4B$
- D_3A_3: $A^2 = 3B$
- D_5: $B = 0$
- A_4A_2: $A^2 = 4B$

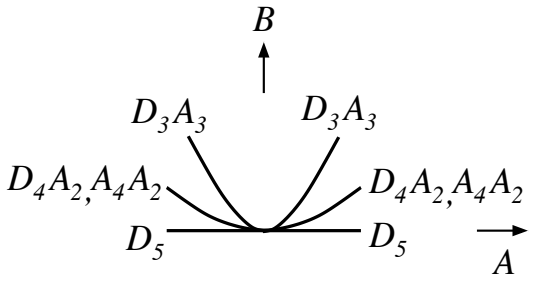

Figure 48: The part of $\mathcal{B}_s(D_6^+)$ coming from the one-dimensional strata of $\mathcal{C}(D_6^+)$

3.3 Contribution of the one-dimensional strata of $\mathcal{B}_s(D_6^+)$ to the roundabout equations

Lemma 3.3.1. *Contributions of the strata D_5 and D_3A_3 to the D_6^+ roundabout equations are trivial.*

Proof. The family F in (11) defines an (α, β)-family of Lagrangian maps

$$(x, y, \gamma) \mapsto (\gamma, \delta, \epsilon) = (\gamma, -x^2 - y^4 - \alpha y^3 - \beta y^2, -2xy) \tag{15}$$

The symmetry $(\alpha, \beta) \mapsto (-\alpha, \beta)$ of the parameter plane lifts to the symmetry $(x, y, \gamma, \delta, \epsilon) \mapsto (x, -y, -\gamma, \delta, -\epsilon)$ that defines orientation-preserving diffeomorphisms of the source and target 3-spaces in (15) under which the family of maps is equivariant. Therefore, 1-parameter families of Lagrangian maps induced from F along pairs of oriented curves in the (α, β)-plane symmetric about the β-axis are orientation-preserving diffeomorphic. Hence the pair of half-branches of the D_5 stratum in Figure 48 are either both co-oriented upwards or both downwards. (One should notice at this point that a germ of a path in $\mathbb{R}^2_{\alpha,\beta}$ in the β-direction across the D_5 stratum provides a generic D_5 transition as listed in Section 2.2.2.2. This is due to the D_5 stratum of $\mathcal{C}(D_5^+) \subset \mathbb{R}^5_{\alpha,\beta,\gamma,\delta,\epsilon}$ being transversal to the corresponding 4-plane $\alpha = const$). Hence the contributions of the two D_5 half-branches of the planar bifurcation diagram to the roundabout equations cancel. Same is true for D_3A_3. □

3.4 Two-dimensional strata of the D_6^+ caustic and their straight projection

Our aim now is to construct parametrizations of the closures of two-dimensional strata of $\mathcal{C}(D_6^+)$ and check if the projection π_s has any critical points on the open two-dimensional strata.

There are several 2-dimensional strata in $\mathcal{C}(D_6^+)$ to consider, these include:

- A_4 where $Q = (y-t)^4(y^2+uy+v)$
- D_4 where $Q = y^4(y^2+uy+v)$
- D_3A_2 where $Q = y^3(y-c)^2(y-d)$
- A_2^3 where $Q = (y^3+ay^2+b)^2$
- A_3A_2 where $Q = (y-t)^3(y-s)^2(y-r)$

Similar to the previous subsection, three parameters in the A_4 and A_3A_2 cases are subject to the constraint of the coefficient of y in Q being zero.

The first stratum we will consider is A_4 where

$$\begin{aligned} Q &= (y-t)^4(y^2+uy+v) \\ &= y^6+y^5(u-4t)+y^4(v-4tu+6t^2)+y^3(-4tv+6t^2u-4t^3) \\ &\quad +y^2(6t^2v-4t^3u+t^4)+y(-4t^3v+t^4u)+t^4v. \end{aligned}$$

Similar to what we did earlier, we shall compare this with the equation (13). Setting the y coefficient to zero we find v in terms of u, t:

$$-4t^3v + t^4u = 0 \Leftrightarrow t^3(-4v + tu) = 0 \Rightarrow v = \frac{ut}{4}.$$

We then substitute this v into the Q for A_4:

$$y^6 + y^5(u - 4t) + y^4(-\frac{15}{4}tu + 6t^2) + y^3(5t^2u - 4t^3) + y^2(-\frac{5}{2}t^3u + t^4) + \frac{t^5u}{4}.$$

Comparing the coefficients we get

$$\alpha = u - 4t \text{ and } \beta = -\frac{15}{4}tu + 6t^2.$$

Consider this as a map $(t, u) \mapsto (\alpha, \beta)$ associated with π_s and find its critical points, and critical values which are a part of $\mathcal{B}_s(D_6^+)$. The Jacobian of this map is

$$\begin{vmatrix} \alpha_t & \alpha_u \\ \beta_t & \beta_u \end{vmatrix} = \begin{vmatrix} -4 & 1 \\ -\frac{15}{4}u + 12t & -\frac{15}{4}t \end{vmatrix} = 3t + \frac{15}{4}u.$$

Hence the critical points of π_s are on the line

$$u = -\frac{4}{5}t. \tag{16}$$

Comparing the constant terms

$$\frac{\epsilon^2}{4} = \frac{t^5 u}{4} \Leftrightarrow \epsilon^2 = t^5 u \Rightarrow u \text{ and } t \text{ must be of the same sign.}$$

However (16) states that the signs of u and t must be opposite to each other, therefore the critical value set of the map (which would form the A_4^e and A_4^h strata) in $\mathcal{B}(D_6^+)$ is empty.

The next stratum to consider is D_4:

$$Q = y^4(y^2 + uy + v) = y^6 + uy^5 + vy^4$$

Thus $\alpha = u, \beta = v$ and $\epsilon = \delta = \gamma = 0$. Hence a generic mapping π maps the closure of the D_4 stratum of $\mathcal{C}(D_6^+)$ isomorphically onto $\mathbb{R}^2_{A,B}$. Therefore the $D_{4,q}^{-,\sigma}, D_{4,a}^{+,\sigma}, D_{4,b}^{+,\sigma}$ and $D_{4,c}^{+,\sigma}$ strata of $\mathcal{B}(D_6^+)$ are empty.

Consider the stratum D_3A_2 in $\mathcal{C}(D_6^+)$:

$$\begin{aligned} Q &= y^3(y-c)^2(y-d) \\ &= y^6 + y^5(-d-2c) + y^4(2cd+c^2) - y^3c^2d. \end{aligned}$$

Compare the coefficients

$$\begin{aligned} \alpha &= -d - 2c \\ \beta &= 2cd + c^2 \\ \gamma &= -c^2 d \\ \delta &= \epsilon = 0 \end{aligned}$$

The Jacobi matrix of α, β, γ with respect to c, d has rank 1 exactly on the line $c = d$. Substituting $c = d$ into Q we obtain

$$y^3(y - c)^3.$$

Thus the D_3A_2 stratum of $\mathcal{C}(D_6^+)$ in $\mathbb{R}^5$ is a curved cuspidal edge surface in the coordinate space $\mathbb{R}^3_{\alpha,\beta,\gamma}$, which is 1-to-1 parametrized by the (c, d)-plane so that the $c = d$ line is sent to the cuspidal edge curve D_3A_3. Since the Jacobian of the map π_s, $(A, B) = (\alpha, \beta)$ composed with this parametrization is $-2(c - d)$ we see that the D_3A_2 stratum of the D_6^+ caustic is mapped by π_s onto the AB-plane so that 'half' of the plane is covered twice, the other half not at all. These halves are separated by the image of the cuspidal curve D_3A_3 (see Figure 48).

Next we look at A_2^3:

$$\begin{aligned} Q &= (y^3 + ay^2 + b)^2 \\ &= y^6 + 2ay^5 + a^2y^4 + 2by^3 + 2aby^2 + b^2. \end{aligned}$$

Comparing the coefficients we have

$$\begin{aligned} \alpha &= 2a \\ \beta &= a^2 \\ \epsilon^2 &= 4b^2 \end{aligned}$$

Thus the whole two-dimensional stratum A_2^3 of $\mathcal{C}(D_6^+)$ sent by the straight projection $\pi_s : \mathbb{R}^5 \to \mathbb{R}^2_{A,B}$ just to the curve $4B = A^2$, that is, to the stratum D_4A_2 (same as A_4A_2 under this projection) of the bifurcation diagram $\mathcal{B}(D_6^+)$.

Finally we consider A_3A_2:

$$\begin{aligned} Q &= (y-t)^3(y-s)^2(y-r) \\ &= y^6 + y^5(-r-2s-3t) + y^4(2sr + s^2 + 3tr + 6ts + 3t^2) \\ &\quad + y^3(-s^2r - 6tsr - 3ts^2 - 3t^2r - 6t^2s - t^3) \\ &\quad + y^2(3ts^2r + 6t^2sr + 3t^2s^2 + t^3r + 2t^3s) \\ &\quad + y(-3t^2s^2r - 2t^3sr - t^3s^2) + t^3s^2r. \end{aligned}$$

Since the coefficient of y must be zero, we have,

$$-3t^2s^2r - 2t^3sr - t^3s^2 = -t^2s(3sr + 2tr + ts) = 0. \tag{17}$$

We introduce the notation

$$q_1(t, s, r) := 3sr + 2tr + ts.$$

The meanings of the factors in (17) are as follows:

- $t = 0$ corresponds to the D_3A_2 stratum of the big caustic;
- $s = 0$ corresponds to the members of the family F (equation (11)) which in general have an A_3 point at $(x, y) = (0, t)$, a Morse point at $(0, r)$, and two further Morse points at $(\pm\sqrt{-t^3r}, 0)$. The vanishing of s reflects the vanishing of the y-coordinates of the last two points;
- $q_1 = 0$ is directly related to the description of the A_3A_2.

Comparing the coefficients,

$$\begin{aligned} 0 &= \epsilon^2 - 4t^3s^2r \;:=\; q_2 \\ \alpha &= -r - 2s - 3t \\ \beta &= 2sr + s^2 + 3tr + 6ts + 3t^2 \end{aligned}$$

Thus the A_3A_2 stratum of $\mathcal{C}(D_6^+) \subset \mathbb{R}^5_{\alpha,\beta,\gamma,\delta,\epsilon}$ is parametrised by the surface $\{q_1 = q_2 = 0\} \subset \mathbb{R}^4_{r,s,t,\epsilon}$.

Critical points of π_s on the open A_3A_2 stratum of $\mathcal{C}(D_6^+)$ are contained in the set of zeros on $q_1 = q_2 = 0$ of the determinant of Jacobi matrix of q_1, q_2, α, β with respect to r, s, t, ϵ. This determinantal equation is

$$\epsilon(5r^2 + 2rs - 6rt - 16s^2 + 6st + 9t^2) = 0\,.$$

The expression in the brackets here will be denoted by q_3.

Vanishing of the factor ϵ in the last equation implies (via $q_2 = 0$) that at least one of the r, s, t must be zero, which then implies (via $q_1 = 0$) that actually at least two of the r, s, t are zero. Such points are in the union of the strata D_5, D_4A_2 and D_3A_3 of the $\mathcal{C}(D_6^+)$, not in the open stratum A_3A_2.

Further, the intersection of two quadratics $q_1 = 0$ and $q_2 = 0$ in $\mathcal{R}^3_{r,s,t}$ consists of the double line $A_4A_2 : r = t = -2s$, and simple lines $A_3^2 : r = s = -t$ and $A_5 : s = t = -5r$.

So, we see that π_s has no critical points on the open A_3A_2 stratum of the D_6^+ caustic.

We summarise our observations of this section about the two-dimensional strata of the D_6^+ caustic as

Lemma 3.4.1. *The behaviour of the two-dimensional strata of* $\mathcal{C}(D_6^+) \subset \mathbb{R}^5_{\alpha,\beta,\gamma,\delta,\epsilon}$ *under the mappings* π *or* π_s *is as follows*

- π *is a diffeomorphism on the closure of the* D_4 *stratum;*
- π *has no critical points on the open* A_4 *and* D_3A_2 *strata;*

- *the π_s-image of the A_2^3 stratum is just a curve, that is, it coincides with the strata A_4A_2 and D_4A_2 of $\mathcal{B}_s(D_6^+)$;*

- *π_s is a local diffeomorphism on the open stratum A_3A_2.*

Therefore we surely must consider tilted projections of the A_2^3 stratum. Having a double curve in the critical point set of π_s in the regular part of the closure of the A_3A_2 stratum calls for similar considerations too. We are addressing these two issues in the next section.

3.5 Tilting the two-dimensional strata

3.5.1 The A_2^3 stratum

So, we take

$$\begin{aligned} Q &= (y^3 + ay^2 + b)^2 \\ &= y^6 + 2ay^5 + a^2y^4 + 2by^3 + 2aby^2 + b^2. \end{aligned}$$

We have

$$\alpha = 2a, \quad \beta = a^2, \quad \gamma = 2b, \quad \delta = 2ab, \quad \epsilon = \pm 2b. \tag{18}$$

Only those regions of the ab-plane in which the polynomial $q = y^3 + ay^2 + b$ has three real roots correspond to real A_2^3 points. To determine them, we

notice that q has a multiple root on their boundaries:

$$\begin{aligned} q &= y^3 + ay^2 + b = 0 \\ q_y &= y(3y + 2a) = 0 \end{aligned}$$

From $q_y = 0$ we have two options:

$$y = 0 \qquad \text{and} \qquad y = -\frac{2}{3}a,$$

for which $q = 0$ yields respectively

$$b = 0 \qquad \text{and} \qquad b = -\frac{4}{27}a^3,$$

and therefore

$$Q = y^4(y + a)^2 \qquad \text{and} \qquad Q = \left(y + \frac{2a}{3}\right)^4 \left(y - \frac{a}{3}\right)^2$$

which belong to respectively the D_4A_2 and A_4A_2 strata of $\mathcal{C}(D_6^+)$. From the parametrization (18), this gives us Figure 49 in 3-dimensions with $\epsilon = \pm 2b = \pm\gamma$. Here the α-axis is the $D_4^+A_2$ stratum (not the $D_4^-A_2$ stratum since the D_6^+ caustic has A_2^3 points next to it) and the two cubic curves are A_4A_2.

Now consider the possible images of the A_2^3 stratum to the plane under the map

$$\pi_t : (\alpha, \beta, \gamma, \delta, \epsilon) \mapsto (A, B) = (\alpha, \beta + C\gamma + E\epsilon).$$

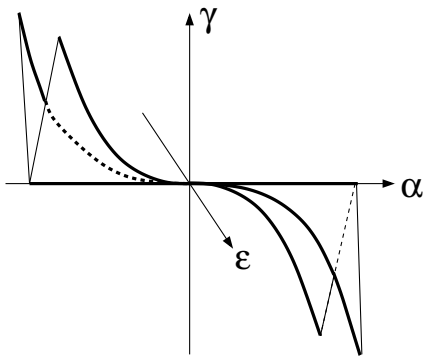

Figure 49: Projection of the A_2^3 stratum of $\mathcal{C}(D_6^+) \subset \mathbb{R}^5_{\alpha,\beta,\gamma,\delta,\epsilon}$ to the $\alpha\gamma\epsilon$-space. The image of the A_2^3 consists of the regions of the planes $\epsilon = \pm\gamma$ between the D_4A_2 line $\gamma = 0$ and the A_4A_2 curves $\gamma = -\frac{4}{27}a^3$.

In the ab-charts, this is

$$(a,b) \mapsto (\alpha,\beta,\gamma,\delta,\epsilon) = (2a, a^2, 2b, 2ab, \pm 2b) \mapsto (A,B) = (2a, a^2 + 2Cb \pm 2Eb).$$

Thus π_t has no critical points on the open stratum A_2^3 in $C \neq \mp E$.

For any choice of the coefficients C and E, the D_4A_2 stratum $b = 0$ is mapped by π_t to the same parabola

$$B = \frac{A^4}{4}.$$

This is the D_4A_2 stratum of $\mathcal{B}_t(D_6^+)$.

The π_t-images of the cubic curves A_4A_2 from Figure 39 give us the A_4A_2

strata of $\mathcal{B}_t(D_6^+)$:

$$B = \frac{A^2}{4} - \frac{A^3}{27}(C \pm E).$$

Now we must consider what happens at specific values for (C, E) for the A_4A_2 strata. The idea here is that topologically there are two different ways of looking at the surface in Figure 49: either from roughly (but not exactly) the ϵ-direction or from the γ-direction. We do these options in this order.

Firstly consider the case $(C, E) = (2, 1)$, this gives the two A_4A_2 curves in $\mathcal{B}_t(D_6^+)$:

$$B = \frac{A^2}{4} - \frac{A^3}{9} \qquad \text{and} \qquad B = \frac{A^2}{4} - \frac{A^3}{27}.$$

Therefore we obtain the bifurcation diagram shown in Figure 50. The co-orientation of the $D_{4,1}^{+,\sigma}A_2$ stratum is to the right. The co-orientation of the A_4A_2 strata is towards the $D_{4,1}^{+,\sigma}A_2$ strata. This is due to where the two triple points exist, as shown on Figure 49. Since the regions are bounded by the strata $D_{4,1}^{+,\sigma}A_2$ on one side and A_4A_2 on the other hence the co-orientation of these are inside these regions.

Next we consider the case when $(C, E) = (0, 1)$ with the A_4A_2 strata in $\mathcal{B}_t(D_6^+)$:

$$B = \frac{A^2}{4} \pm \frac{A^3}{27}.$$

This gives us the bifurcation diagram shown in Figure 51. We know that the $D_4^+A_2$ half-branches are actually $D_{4,2}^{+,\sigma}A_2$ since there are triple points on either side. We cannot co-orient this stratum due to equations **29** and **30** (see page 98). The co-orientation of the A_4A_2 strata is towards the $D_{4,2}^{+,\sigma}A_2$ stratum.

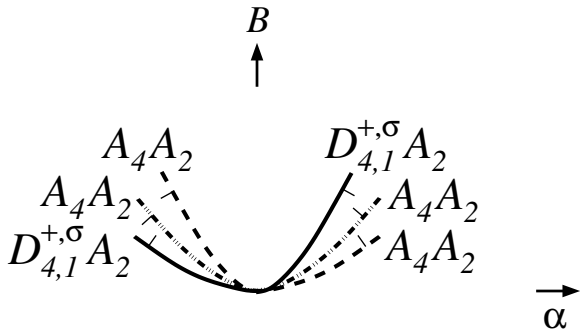

Figure 50: The bifurcation diagram coming from the tilted projection of the stratum A_2^3 for $(C, E) = (2, 1)$. The D_4A_2 and A_4A_2 strata here split those in Figure 48.

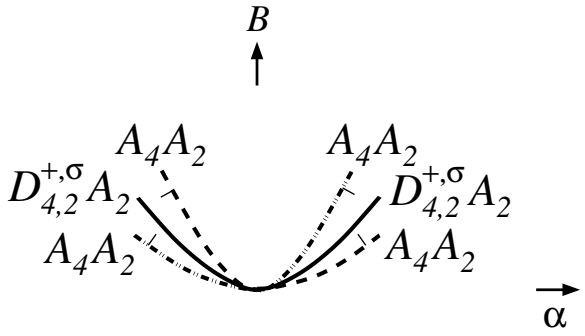

Figure 51: The bifurcation diagram coming from the tilted projection of A_2^3 for $(C, E) = (0, 1)$.

3.5.2 The A_3A_2 stratum

We now have

$$Q = (y-t)^3(y-s)^2(y-r),$$

with r, s, t subject to the relations

$$q_1 = 3sr + 2tr + ts = 0 \qquad \text{and} \qquad q_2 = \epsilon^2 - 4t^3s^2r = 0,$$

and with the expressions for the coefficients of Q

$$\begin{aligned} \alpha &= -r - 2s - 3t \\ \beta &= 2sr + s^2 + 3tr + 6ts + 3t^2 \\ \gamma &= -s^2r - 6tsr - 3ts^2 - 3t^2r - 6t^2s - t^3 \\ \delta &= 3ts^2r + 6t^2sr + 3t^2s^2 + t^3r + 2t^3s \end{aligned} \tag{19}$$

In particular, $q_2 = 0$ tell us that r and t must be of the same sign.

We consider the A_3A_2 stratum of $\mathcal{C}(D_6^+) \subset \mathbb{R}^5_{\alpha,\beta,\gamma,\delta,\epsilon}$ as parametrized by the surface $S = \{q_1 = q_2 = 0\} \subset \mathbb{R}^4_{r,s,t,\epsilon}$, and look for critical points of $\pi_t|_{A_3A_2}$ as critical points on S of π_t composed with the parametrization map, that is, of

$$(r, s, t, \epsilon) \mapsto (\alpha, \beta, \gamma, \delta, \epsilon) \mapsto (A, B) = (\alpha, \beta + C\gamma + E\epsilon),$$

where C and E are arbitrary real constants so far. Similar to what we had in Sections 3.4, vanishing of the determinant of the Jacobi matrix of q_1, q_2, α, B with respect to r, s, t, ϵ gives on the surface S an equation for the critical point set of the projection of the closure of the A_3A_2 stratum to the AB-plane (its fold locus values form the stratum TA_3A_2 of the bifurcation diagram, and the critical value set as a whole contains also some other strata). However, it turns out that replacing q_1 in this determinant by the total coefficient $q = -t^2sq_1$ of y in Q simplifies the calculations. So, we take this root and obtain the determinant of thus modified Jacobi matrix:

$$-3t(-t+s)(r-t)(r-s)(2s^2Et^3 + 2\epsilon Cs^2 + 4\epsilon Cts - 2\epsilon s + 2\epsilon Ct^2 - \epsilon t).$$

The last factor in this expression will be denoted by D. Similar to our earlier observations about the straight projection of the closed A_3A_2 stratum, we see that vanishing of all the other factors here singles out the curves on S which correspond to the following strata of the D_6^+ caustic contained in the closure of the A_3A_2 stratum:

$t = 0$, union of D_5 and D_4A_2;

$s = t$, A_5;

$t = r$, A_4A_2;

$r = s$, A_3^2

None of these is currently of interest for us.

Our aim at the moment is to understand the curve $D = 0$ on the surface $S = \{q_1 = q_2 = 0\}$ and its π_t-image.

We now eliminate ϵ from the system $q_1 = q_2 = D = 0$ by replacing q_2 and D with their resultant in ϵ:

$$t^3 s^2 \left(4C^2 r s^4 + 16C^2 r s^3 t + 24C^2 r s^2 t^2 + 16C^2 r s t^3 + 4C^2 r t^4 \right. \tag{20}$$
$$\left. -E^2 s^2 t^3 - 8Crs^3 - 20Crs^2 t - 16Crst^2 - 4Crt^3 + 4rs^2 + 4rst + rt^2\right) = 0.$$

Similar to the previous, the factors t and s here have no relation to the open A_3A_2 stratum. We denote the long factor in (20) by R_1.

Now take the resultant of R_1 and q_1 with respect to s:

$$r^2 t^{12} \left(2Ct - 1\right)^2 \left(4C^2 r^4 t^2 + 16C^2 r^3 t^3 + 24C^2 r^2 t^4 + 16C^2 r t^5 \right. \tag{21}$$
$$+4C^2 t^6 - 36E^2 r^3 t^3 - 24E^2 r^2 t^4 - 4E^2 r t^5 + 12Cr^4 t + 16Cr^3 t^2 - 8Cr^2 t^3$$
$$\left. -16Crt^4 - 4Ct^5 + 9r^4 - 12r^3 t - 2r^2 t^2 + 4rt^3 + t^4\right) = 0.$$

We can dismiss all the factors here except for the longest one which we denote R_2.

The quartic (lowest degree) part of R_2 factorises as $(t - r)^2(t + 3r)^2$. Therefore, the equation $D = 0$ defines on the surface S four curves: for two of them their projections to the rt-plane have tangent line $t = r$ at the origin, and for two others the tangent line is $t = -3r$. The equation $q_2 = 0$ tell us that the second pair of curves is complex, and we can forget about them

here.

From $R_2 = 0$ we find the quadratic parts of the Taylor expansions $t = t(r)$ of the first pair of curves:

$$t = r + 2(C \pm E)r^2 + \cdots \tag{22}$$

We substitute this back into $q_1 = 0$ to obtain s in terms of r:

$$s = -\frac{1}{2}r - \frac{3}{4}(C \pm E)r^2 + \cdots .$$

Substituting these into $D = 0$ to obtain ϵ yields

$$\epsilon = \pm r^3 + \cdots$$

Thus the parametrisations of the π_t-images of the two critical curves are

$$\begin{aligned} A &= \alpha = -3r - \frac{9}{2}(C \pm E)\, r^2 + \cdots , \\ B &= \frac{9}{4}r^2 + \frac{31}{4}(C \pm E)r^3 + \cdots . \end{aligned}$$

Eliminating r from the the last two expansions, we obtain the expansions for the TA_3A_2 strata in $\mathcal{B}_t(D_6^+)$:

$$B = \frac{1}{4}A^2 - \frac{1}{27}(C \pm E)A^3 + \cdots$$

Let us now compare the TA_3A_2 strata obtained with the A_4A_2 strata of the $\mathcal{B}_t(D_6^+)$ coming from the curves $t = r$ on our surface $S \subset \mathbb{R}^4_{r,s,t,\epsilon}$. For $t = r$, the equation $q_1 = 0$ gives $s = -r/2$. after which $q_2 = 0$ yields $\epsilon = \pm r^3$. So, we have two A_4A_2 curves on S, whose π_t-images are given by

$$A = -3r \qquad B = \frac{9}{4}r^2 + (C \pm E)r^3.$$

Hence the A_4A_2 strata in $\mathcal{B}(D_6^+)$ are

$$B = \frac{1}{4}A^2 - \frac{1}{27}(C \pm E)A^3.$$

Thus we see that, in the π_t-bifurcation diagram, the TA_3A_2 and A_4A_2 strata have at least order 4 tangency. This stays true for a generic mapping π.

We now want to try and visualise the bifurcation diagram for D_6^+. To do this we start with the projection $S' \subset \mathbb{R}^3_{t,r,\epsilon}$ of our surface S parametrizing the closure of the A_3A_2 stratum in $\mathcal{C}(D_6^+)$. From $q_1 = 0$, $s = -\frac{2tr}{3r+t}$ on S, and the condition $0 = q_2 = -\frac{\epsilon^2}{4} + t^3s^2r$ guarantees that the denominator $3r + t$ vanishes on S just at its vertex $0 = r = t = s = \epsilon$. Therefore, S projects onto S' bijectively. From $0 = p = -\frac{\epsilon^2}{4} + t^3s^2r$, we see that S' has no points with $tr < 0$, covers the $tr > 0$ region twice and contains the r- and t-axes. See Figure 52.

According to our earlier calculations, the following strata of $\mathcal{C}(D_6^+)$ and critical curves show up on S' in Figure 52:

- D_5, $t = s = 0 = \epsilon$, the r-axis;
- D_3A_3, $r = s = 0 = \epsilon$, the t-axis;
- A_4A_2, $t = r$;
- TA_3A_2, the pre-images of the TA_3A_2 strata of $\mathcal{B}_t(D_6^+)$.

As we have seen previously the TA_3A_2 strata coincide with the A_4A_2 strata for π_s, in the 0-order approximation to a generic mapping π. In the next order approximation π_t, the TA_3A_2 have quadratic tangency on S' with A_4A_2 (the sides depend on the signs of $(C \pm E)$).

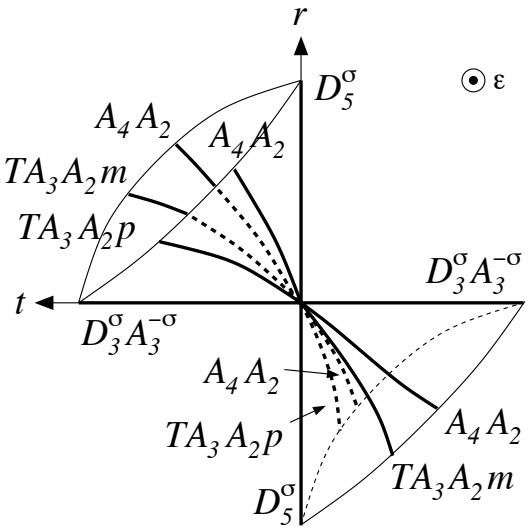

Figure 52: The strata on the surface $S' \subset \mathbb{R}^3_{r,t,\epsilon}$ parametrizing the closure of the stratum A_3A_2 in $\mathcal{B}(D_6^+)$ when $C = 2$ and $E = 1$

In consistency with our particular case studies of the previous subsection, Figure 52 illustrates the TA_3A_2 situation for the first of those cases, when

$C = 2$ and $E = 1$. In the diagram, the p in the notation of the TA_3A_2 strata is for the component with $(C + E)$ in the parametrization (22) whereas m is for the $(C - E)$ component.

Let us now figure out how the surface S' is mapped, via the stratum A_3A_2 of $\mathcal{C}(D_6^+)$ by π_t to the AB-plane. Consider, for example, its quarter S'_+ within the octant where all the r, t, ϵ are non-negative. According to (19) the boundary of S'_+ formed by the positive r- and t-rays is mapped to respectively the negative A-ray and the left half of the dashed parabola D_3A_3 in Figure 53. The image of S'_+ covers the small sector of the AB-plane between these two branches, and the only singularities this covering has are folds along the A_4A_2 and TA_3A_2p curves on S'_+. These folds give us the two strata of $\mathcal{B}_t(D_6^+)$ shown in the top of the left insert in Figure 53. Similar considerations for the other quarters of S' explain the rest of the inserts in Figure 53. The strata there are co-oriented to the sides on which the folding of S' has more pre-images. The co-orientations of the A_4A_2 strata (towards the nearest D_4A_2 branches) are already known from the A_3A_2 work done in Section 3.5.1.

We will assume now and till the end of this section that open strata of our D_6^+ caustic of dimension higher than 2 do not contribute to the bifurcation diagrams. In such case, Figure 53 and Lemma 3.3.1 yield the equation that has appeared as equation **31** in Theorem 2.3.3:

$$-2d_{4,1}^{+,\sigma}a_2 + 4a_4a_2 - 2ta_3^+a_2 - 2ta_3^-a_2 = 0.$$

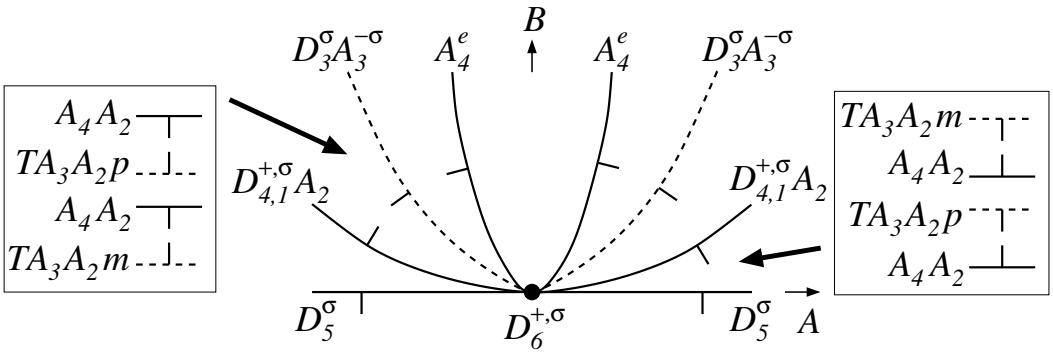

Figure 53: Part of the bifurcation diagram $\mathcal{B}(D_6^+)$ when $C = 2$ and $E = 1$. Positions of the A_4A_2 and D_4A_2 curves follow Figure 50

The reason that out of the four half-branches of TA_3A_2 in Figure 53, two must involve A_3^+ and two A_3^-, is to keep the total roundabout increments of the $A_3^+A_2$ and $A_3^-A_2$ points zero.

The only other topologically different option for the TA_3A_2 curves on S' may be achieved by taking $C = 1$ and $E = 2$. It is illustrated in Figure 54. In this case S' is mapped via π_t down to the AB-plane creating $\mathcal{B}_t(D_6^+)$ shown in Figure 55. The last figure gives us the roundabout equation $2d_{4,2}^{+,\sigma}a_2 = 0$ which we actually have already obtained from Figure 47. Hence no new equations are coming from this type of $\mathcal{B}_t(D_6^+)$.

The outcome of this section is

Lemma 3.5.1. *Assume that generic mappings π are submersive on all open strata of the D_6^+ caustic of dimension higher than 2. Then the D_6^+ part of Theorem 2.3.3 is true.*

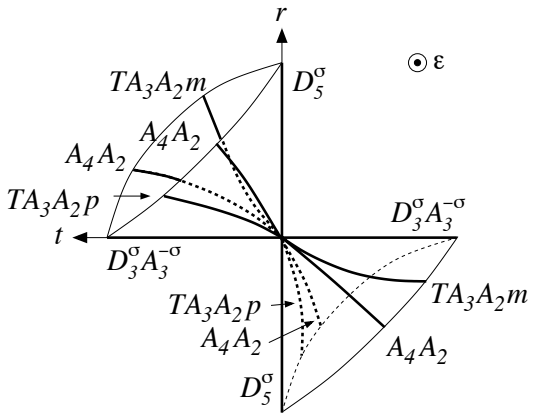

Figure 54: The surface S' for $C = 1$ and $E = 2$.

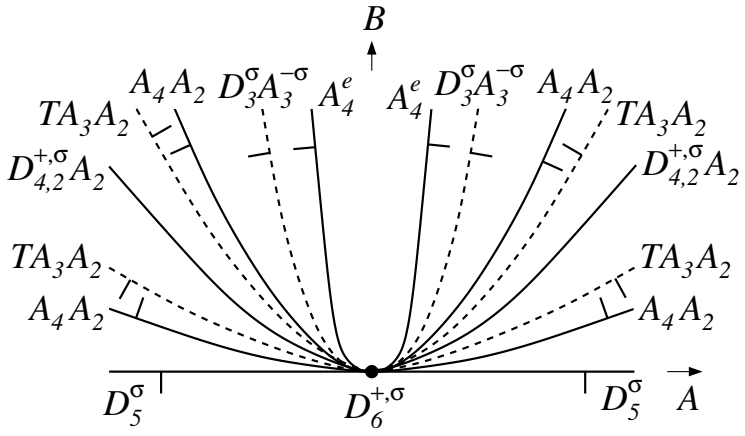

Figure 55: The bifurcation diagram $\mathcal{B}_t(D_6^+)$ when $C = 1$ and $E = 2$, with the contribution from Figure 51.

3.6 Higher dimensional strata

In this section we prove

Lemma 3.6.1. *The submersion assumption made in Lemma 3.5.1 is correct.*

Proof. The strata to consider are A_3, D_3, A_2^2 and the regular part A_2 of the whole D_6^+ caustic. We consider them in this order.

We start with the stratum A_3 and the corresponding polynomials

$$\begin{aligned} Q &= (y-t)^3\left(y^3+uy^2+vy+\frac{vt}{3}\right) \qquad (23)\\ &= y^6+(-3t+u)\,y^5+(3t^2-3tu+v)\,y^4\\ &\quad +\left(-t^3+3t^2u-\frac{8}{3}tv\right)\,y^3+(-t^3u+2t^2v)\,y^2-\frac{1}{3}t^4v \end{aligned}$$

We have the constant-term relation

$$R_{A_3} := \frac{\epsilon^2}{4}+\frac{t^4v}{3}=0.$$

Thus the A_3 stratum of $\mathcal{C}(D_6^+)$ is parametrised by the hypersurface $R_{A_3}=0$ in $\mathbb{R}^4_{u,v,t,\epsilon}$. Consider the straight projection π_0, $(A,B)=(\alpha,\beta)$ composed with this parametrisation, that is, the restriction on $R_{A_3}=0$ of the map

$$(A,B)=\big(-3t+u,3t^2-3tu+v\big)$$

Its critical point set on $R_{A_3} = 0$ is the set of common zeros of all order 3 minors of the Jacobi matrix of α, β, R_{A_3} with respect to t, u, v, ϵ. In particular, consider

$$J = \begin{vmatrix} \alpha_t & \alpha_u & \alpha_v \\ \beta_t & \beta_u & \beta_v \\ (R_{A_3})_t & (R_{A_3})_u & (R_{A_3})_v \end{vmatrix} = -\frac{1}{3}t^3(3t^2 + 3tu + 4v)$$

Let us check the vanishing of the factors in J. If $t = 0$, then the polynomial Q in (23) is general of the D_4 type. Vanishing of the long factor can be easily seen to be equivalent to t being a root of the cubic factor in (23) meaning that Q is of type A_4. Hence π_0 does not have any critical points on the open A_3 stratum of the D_6^+ caustic.

MAPLE calculations easily verify that, replacing α and β in the determinantal expression of J by any pair of functions out of $\alpha, \beta, \gamma, \delta, \epsilon$ we obtain polynomial multiples of J with the coefficients vanishing at the origin. Therefore, not just π_s but any mapping π with the principal quasihomogeneous part π_s is submersive on the open stratum A_3.

Consider now the stratum D_3: $\epsilon = \delta = 0$. It is clear that a generic mapping π of the $\alpha\beta\gamma$-coordinate plane from $\mathbb{R}^5$ to $\mathbb{R}^2$ is a submersion (the genericity condition is that the linear part of π must have rank 2). In particular, the D_3 stratum of any 3-dimensional caustic in this case is a smooth one-component curve.

It is turn of the A_2^2 stratum of $\mathcal{C}(D_6^+)$ now. So, we have

$$\begin{aligned} Q &= (y^2+ry+s)^2(y^2+ty+u) \qquad (24)\\ &= y^6+(2r+t)\,y^5+(2s+r^2+2rt+u)\,y^4+(2sr+(2s+r^2)t+2ru)\,y^3\\ &\quad +(s^2+2srt+(2s+r^2)u)\,y^2+(s^2t+2sru)\,y+s^2u \end{aligned}$$

One of the options for the coefficient of y here to vanish is $s=0$. However, such polynomials Q correspond in general to functions of family (11) with an A_2 point and two Morse points on the y-axis of the xy-plane, and two Morse points on the x-axis. This is a subset of the regular locus of the D_6^+ caustic. Therefore, the closure of the A_2^2 stratum is actually parametrised by the 3-dimensional variety $V\subset\mathbb{R}^5_{r,s,t,u,\epsilon}$ defined by the equations

$$R^y := st+2ru=0 \qquad \text{and} \qquad R^c := \epsilon^2-4s^2u=0.$$

Our treatment of the current case will now follow the approach used for the A_3 stratum. Namely, we start with the straight projection π_s, $(A,B)=(\alpha,\beta)$ composed with the parametrising map that sends V to the closure of A_2^2.

Looking for critical points of this composition, we notice that the determinant of the Jacobi matrix of α,β,R^y,R^c with respect to r,s,t,u is

$$J=-2s(4r^2u-rst-4rtu+st^2+2s^2-4su+2u^2).$$

The long factor in J here differs from the resultant of the quadratic factors

in (24) by a multiple of R^y. Therefore its zeros on V correspond to the stratum A_3A_2, and are not sent by the parametrisation map to the open stratum A_2^2.

On the other hand, $s = 0$ implies (via $R^y = 0$) that either $r = 0$ or $u = 0$, which provide in (24) polynomials Q of types D_4 or D_3A_2 respectively.

From this we conclude that π_s is submersive on the open stratum A_2^2.

Consider now the matrix of partial derivatives of $\alpha, \beta, \gamma, \delta, \epsilon$ (all defined via (24)) and R^y, R^c with respect to r, s, t, u. Consider all its order 4 minors containing the derivatives of R^y and R^c. It turns out that all such minors are sums of polynomial multiples of J and Q^y, with the coefficients vanishing at the origin. This observation implies that any mapping π with the principal quasihomogeneous part π_s is submersive on the open A_2^2 stratum of the D_6^+ caustic.

The final case to consider is A_2, the set of all regular points of $\mathcal{C}(D_6^+)$. This time

$$\begin{aligned} Q &= (y-t)^2\left(y^4 + uy^3 + vy^2 + wy + \frac{tw}{2}\right) \\ &= y^6 + (-2t+u)\,y^5 + (t^2 - 2tu + v)\,y^4 + (t^2u - 2tv + w)\,y^3 \\ &\quad + \left(t^2v - \frac{3tw}{2}\right)y^2 + \frac{t^3w}{2}, \end{aligned}$$

and we have the constant-term equation

$$R_{A_2} := \frac{\epsilon^2}{4} - \frac{t^3w}{2} = 0.$$

Repeating the consideration for π_s done in the A_3 case, we now notice that the Jacobi minor of α, β, R_{A_2} with respect to u, v, w is $-t^3/6$. Its vanishing implies that in general the polynomial Q above is of the A_3 type. Therefore, π_s is a submersion on the open stratum A_2.

Similar to the A_3 case again, we notice that replacing α and β in the minor by any two functions out of $\alpha, \beta, \gamma, \delta, \epsilon$ yields minors that are polynomial multiples of t^4. We conclude from this that any mapping π with the principal part π_s is submersive on the regular part of the D_6^+ caustic.

This finishes our proof of the Lemma and thus of the D_6^+ part of Theorem 2.2.3. $\square$

Chapter 4

D_6^- bifurcations

In this chapter we study generic mappings to a 2-dimensional plane of the D_6^- caustic, that is, of the caustic of the generating family

$$\begin{aligned} F &= -x^2y + \frac{1}{5}y^5 + \frac{1}{4}\alpha y^4 + \frac{1}{3}\beta y^3 + \frac{1}{2}\gamma y^2 + \delta y + \epsilon x \\ &= -x^2y + \epsilon x + p(y) \end{aligned} \tag{25}$$

This family differs just by the sign of the x^2y term from the D_6^+ family considered thoroughly in the previous chapter. This similarity allows us to omit many details and only highlight the differences which are due to some strata being previously real going now complex and vice versa. In particular, we show that the most generic 3-dimensional section of $C(D_6^-) \subset \mathbb{R}^5$ is adjacent

to the codimension 1 degenerations

$$D_5,\ D_4A_2,\ A_5,\ A_3^2,\ A_4^{e/h}$$

(see Figure 56 and Section 4.2).

Repeating the argument used for D_6^+, we relate our analysis of the family (25) to a slightly modified version of the one-variable polynomial used in Chapter 3:

$$Q := y^2p'(y) - \frac{\epsilon^2}{4} = y^2(y^4 + \alpha y^3 + \beta y^2 + \gamma y + \delta) - \frac{\epsilon^2}{4} \tag{26}$$

From this expression we can, for example, immediately see that all our observations done in Chapter 4 about strata containing $D_{\geq 3}$ in their notation stay true for D_6^-.

4.1 One-dimensional strata in $\mathcal{C}(D_6^-)$

These strata are

- D_5 with $Q = y^5(y - t)$
- D_4A_2 with $Q = y^4(y - t)^2$
- D_3A_3 with $Q = y^3(y - t)^3$
- A_5 with $Q = (y - t)^5(y + t/5)$ is not empty now, due to the negative

sign of $\epsilon^2/4$ in (26)

- A_4A_2 with $Q = (y-t)^4(y-t/2)^2$ is empty this time for the same reason
- A_3^2 with $Q = (y-t)^3(y+t)^3$ is not empty this time, also for the same reason

The images of these strata under the mapping π_s, $(A, B) = (\alpha, \beta)$ (the one already used in Chapter 3) are shown in Figure 56:

- D_4A_2: $A^2 = 4B$
- D_3A_3: $A^2 = 3B$
- D_5: $B = 0$
- A_5: $64B = 25A^2$
- $2A_3^2$: $A = 0,\ B \leq 0$

Similar to Lemma 3.3.1 we now have:

Lemma 4.1.1. *Contributions of the strata D_3A_3, D_5, A_5 and A_3^2 to the D_6^- roundabout equations are trivial.*

Proof. The symmetry used in the proof of Lemma 4.1.1 yields the claim for the first 3 strata immediately. For the $2A_3^2$ stratum consider a short path crossing it in the positive α-direction. Then the same symmetry shows that if one of the A_3^2 moves along it is positive, the other A_3^2 move is exactly of the same type but going in its negative way. □

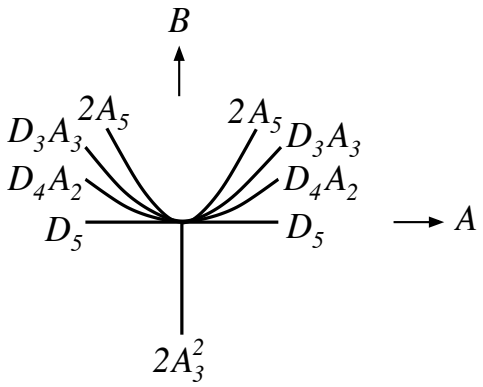

Figure 56: The part of $\mathcal{B}_s(D_6^-)$ coming from the one-dimensional strata of $\mathcal{C}(D_6^-)$

4.2 Two-dimensional strata

These strata are:

- A_4, with $Q = (y-t)^4(y^2+uy+\frac{ut}{4})$ and $\epsilon^2 + ut^4 = 0$
- D_4, with $Q = y^4(y^2+uy+v)$
- D_3A_2, with $Q = y^3(y-c)^2(y-d)$
- A_2^3, with $Q = (y^3+ay^2+b)^2$, is empty now due to the requirement $b^2 = -\epsilon^2/4$
- A_3A_2, with $Q = (y-t)^3(y-s)^2(y-r)$, where $q_1 = 3sr+2tr+ts = 0$ and $q_2 = \epsilon^2 + 4t^3s^2r = 0$

$\underline{A_4}$. Consider the A_4 stratum in $\mathcal{C}(D_6^-)$, parametrized by the surface $V = \{\epsilon^2 + ut^5 = 0\}$ in $\mathbb{R}^3_{u,t,\epsilon}$ which is then projected by π_s onto the parameter

plane $\mathbb{R}^2_{A,B}$. The complete map is

$$(A, B) = \left(u - 4t, -\frac{15}{4}tu + 6t^2\right).$$

The 3×3 determinant formed by the Jacobi matrix of the composite map and the gradient of the equation of V is a non-zero constant multiple of $\epsilon\left(u + \frac{4t}{5}\right)$. Hence the map of V to $\mathbb{R}^2_{\alpha,\beta}$ has ordinary folds along the lines $u = -\frac{4t}{5}$ and $\epsilon = 0$ on V.

On $u = -\frac{4t}{5}$ we have

$$Q = (y-t)^4\left(y^2 - \frac{4t}{5}y - \frac{t^2}{5}\right) = (y-t)^5\left(y + \frac{t}{5}\right),$$

that is, this corresponds to the A_5 stratum of $\mathcal{C}(D_6^-)$ and does not contribute to the critical points of π_s on the open A_4 stratum.

Now $\epsilon = 0$ means $ut = 0$. For $t = 0$, we get $Q = y^5(y + u)$ which is in the D_5 stratum of the caustic, not A_4. And for $u = 0$, we have $Q = (y-t)^4y^2$ which at last is in the open A_4 stratum. In this case $\alpha = -4t$, $\beta = 6t^2$. Hence $\beta = \frac{3}{8}\alpha^2$ is the $A_4^{e/h}$ stratum in $\mathcal{B}_s(D_6^-)$.

$\underline{D_4 \text{ and } D_3A_2}$. Since since $\epsilon = 0$ here and therefore there is no difference with the D_6^+ situation, we have exactly the same as we found for D_6^+: the open strata D_4 and D_3A_2 of $\mathcal{C}(D_6^-)$ contribute nothing to $\mathcal{B}(D_6^-)$.

$\underline{A_3A_2}$. The closure of the stratum in $\mathcal{C}(D_6^-)$ is parametrized by the surface $S = \{q_1 = q_2 = 0\} \subset \mathbb{R}^4_{r,s,t,\epsilon}$.

The critical points of the projection π_s of the closure are zeros of the determinant of the Jacobi matrix of α, β, q_1, q_2 with respect to r, s, t, ϵ. This determinant is a non-zero constant multiple of ϵq_c, where $q_c = 5r^2 + 2rs - 6rt - 16s^2 + 6st + 9t^2$. Let us show that zeros of this product are all in the closure of the A_3A_2 stratum of $\mathcal{C}(D_6^-)$, not in the open stratum itself.

So we have:

a) $\epsilon = 0$ implies, via $q_2 = 0$, that at least one of the r, s, t is zero, from which $q_1 = 0$ implies that at least two of them are zeros. This gives us points of the D_5 ($r \neq 0$), D_4A_2 ($s \neq 0$) and D_3A_3 ($t \neq 0$) strata.

b) The intersection of the two quadrics $q_1 = 0$ and $q_c = 0$ in $\mathbb{R}^3_{r,s,t}$ consists of three lines, two ordinary ($s = t = -5r$ and $s = -t = r$) and one double ($t = -2s = r$). The double line lifts to an empty set in S, due to $R = 0$ becoming $\frac{\epsilon^2}{4} + 16s^6 = 0$ on it. The line $s = t = -5r$ provides two curves in S that are mapped to two A_5 curves in $\mathcal{C}(D_6^-)$, and then both sent to the same curve in $\mathcal{B}_s(D_6^-)$ which is therefore the $2A_5$ stratum in the bifurcation diagram. The line $s = -t = r$ gives us just one A_3^2 curve in $\mathcal{C}(D_6^-)$ which is then folded in two to the $2A_3^2$ ray by π_s (see Figure 56),

Thus, indeed the projection π_s has no critical points on the open stratum A_3A_2 of $\mathcal{C}(D_6^-)$.

4.3 The D_6^- roundabout equation

Repeating what was done in Section 3.6 about the higher dimensional strata of $\mathcal{C}(D_6^+)$ (with the change of the sign of ϵ^2 in the Q) one shows that such strata do not contribute to $\mathcal{B}(D_6^-)$. We have already shown in Lemma 4.1.1 that the π_s-images of one-dimensional strata of $\mathcal{C}(D_6^-)$ do not contribute to the D_6^- equation. The only other stratum in $\mathcal{B}_s(D_6^-)$ is $A_4^{e/h}$ (see page 147). The symmetry argument used in the proof of Lemma 4.1.1 shows that this stratum also does not contribute to the equation. Hence the equation is trivial: $0 = 0$.

Our proof of the D_6^- part of Theorem 2.2.3 is now finished.

Chapter 5

E_6 bifurcations

The last caustic that may appear as a big caustic of a generic two-parameter family of Lagrangian maps between 3-manifolds is the caustic $\mathcal{C}(E_6)$ of the E_6 isolated function singularity, that is, the caustic of the $\mathcal{R}_+$-miniversal deformation

$$\mathcal{F} := \frac{1}{3}x^3 + \alpha xy^2 + \beta xy + \gamma x + \frac{1}{4}y^4 + \frac{1}{2}\delta y^2 + \epsilon y \tag{27}$$

of the E_6 function. The aim of this chapter is to show that the most generic 3-dimensional section of $C(E_6)$ is adjacent to the codimension one singularities

$$D_5,\ D_4,\ D_4A_2,\ A_5,\ A_3^2,\ A_4^{e/h},\ A_4A_2,\ TA_2^3,\ TA_3A_2$$

of Section 2.2 (see Table 6 in Section 5.1). This will help us to obtain equations **32** of Section 2.3.2.7.

We notice that the family (27) is quasi-homogeneous, with the weights

$$x \sim 4, \quad y \sim 3, \quad \alpha \sim 2, \quad \beta \sim 5, \quad \gamma \sim 8, \quad \delta \sim 6, \quad \epsilon \sim 9.$$

In particular, this means that the straight projection π_0 is $(\alpha, \beta, \gamma, \delta, \epsilon) \mapsto (\alpha, \beta)$. The tilted projections are denoted by π_k where k is how much higher the weights of the additional monomials participating in the maps may be comparing with the weights of the components of the principal part π_0. For instance the projections $\pi_1 : (\alpha, \beta, \gamma, \delta, \epsilon) \mapsto (\alpha, \beta + d\delta)$ depend on one extra real parameter $d \neq 0$.

5.1 Stratification of the big caustic

In the previous two chapters, the $D_6^{\pm}$ caustics were conveniently described in terms of not very complicated polynomials Q in just one variable, and various strata of the caustics corresponded to real roots of Q of appropriate multiplicities. This is no longer the case for E_6, and we will be constructing parametrizations of the strata in $\mathcal{C}(E_6)$ using the general singularity theory approach to finding adjacencies of a uni-germ of an isolated function singularity Z to various (multi-)singularities Y. Namely, assume the most degenerate singularity X of a multi-singularity Y we want to obtain is at the origin. Then such a function has zero linear terms, but may contain a bit more monomials than those appearing in the $\mathcal{R}_+$-miniversal family $\mathcal{G}$ of Z. We may try and

bring the singularity X to its normal form, which would on one hand reduce the number of the monomials we have been using in $\mathcal{G}$, but on the other hand may introduce some new. After such modifications and taking care of the other elementary singularities in Y, we should be able to obtain a family of functions that have the multi-singularity desired. A mapping of this family into the initial $\mathcal{R}_+$-miniversal deformation of Z, gives us a parametrization of the stratum Y of the caustic of Z.

Let us see how this works in the E_6 case.

We will be operating with families of polynomials in x and y. To visualize them we will be showing their *supports,* that is, the sets of the monomials $x^a y^b$ participating in the families with non-zero coefficients, on the grid of the exponents (a, b) which we will call the *Newton lattice.* For example, Figure 57 shows the support of the family (27). When we want to emphasize the value of a coefficient we write it next to the node.

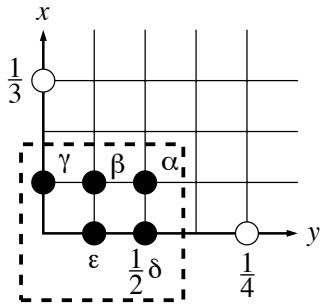

Figure 57: Newton diagram of the E_6 $\mathcal{R}_+$-miniversal deformation

Moving a critical point (x_0, y_0) to the origin, we are replacing each existing

monomial $x^a y^b$ by $(x+x_0)^a(y+y_0)^b$ which results in amending the coefficients of all the $x^{\leq a}y^{\leq b}$. The result of this procedure for a member of the family (27) is shown in Figure 58. Due to the nature of the $\mathcal{R}_+$-equivalence that considers functions up to an additive constant, we will be always assuming that the constant term is zero.

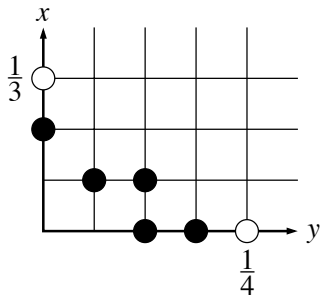

Figure 58: Members of the E_6 family (27) with a critical point shifted to the origin

5.1.1 The D strata of $\mathcal{C}(E_6)$

We start our parametrizations of strata of the E_6 caustic with the functions having at least one D_k point.

Firstly consider deforming E_6 to D_4. Under the assumption of the D_4 point being at the origin, we must have the 2-jet of the function at origin zero. Therefore the diagram of Figure 58 simplifies to that of Figure 59, where u and v are real parameters.

If the zero set of the cubic terms in Figure 59 is three distinct lines in the

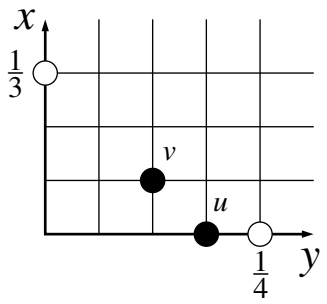

Figure 59: The Newton diagram of the deformation from E_6 to D_4

complex plane, that is $4v^3 + 9u^2 \neq 0$, we have exactly a D_4 singularity at the origin. Therefore, the closure of the D_4 stratum in the E_6 caustic may be parametrised by $\mathbb{R}^2_{u,v}$. To obtain this parametrization, we 'inscribe' the family of Figure 59 back into that of Figure 57. For this we must eliminate the y^3 term, which is done via the setting $y := y - u$. The result is in Figure 60.

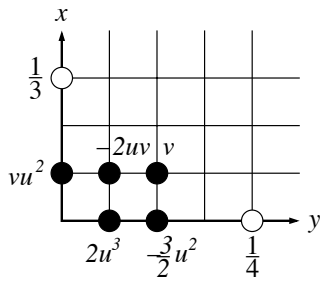

Figure 60: Parametrization of the D_4 stratum of the E_6 caustic.

Comparing Figures 57 and 60, we have

$$\alpha = v, \qquad \beta = -2uv, \qquad \gamma = vu^2, \qquad \delta = -3u^2, \qquad \epsilon = 2u^3. \tag{28}$$

In particular, the D_4 stratum projects to $\mathbb{R}^3_{\alpha,\beta,\delta}$ as the Whitney umbrella.

$$3\beta^2 + 4\alpha^2\delta = 0.$$

We notice that the self-intersection ray of the umbrella splits into a cuspidal curve if the ϵ coordinate is restored.

Another observation to make here is about the regions on the uv-parameter plane. Namely, the region $4v^3 + 9u^2 < 0$, where the zero set of the cubic form consists of three different real lines, corresponds to functions with one D_4^- point. On the other hand, the region $4v^3 + 9u^2 > 0$, where the zero set of the cubic terms contains two different non-real lines, corresponds to functions with one D_4^+ point.

The cuspidal curve $4v^3 + 9u^2 = 0$ itself corresponds to cubic terms that factorize as $\frac{1}{3}(x-cy)^2(x+2cy)$, $c \in \mathbb{R}$. Setting $x := x - cy$, brings our function to the form shown in Figure 61. This is a D_5 singularity at the origin.

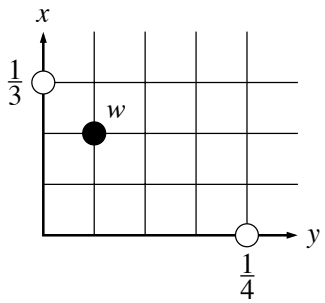

Figure 61: Deforming E_6 to D_5

To get a parametrization of the D_5 stratum in our big caustic, we set

$x := x - w$ in Figure 61, which gives Figure 62, that is, Figure 59 with $u = \frac{2}{3}w^3$, $v = -w^2$. Therefore, the formulas (28) give us a parametrization of the D_5 stratum in the E_6 caustic:

$$\alpha = -w^2, \quad \beta = \frac{4}{3}w^5, \quad \gamma = -\frac{4}{9}w^8, \quad \delta = -\frac{4}{3}w^6, \quad \epsilon = \frac{16}{27}w^9. \tag{29}$$

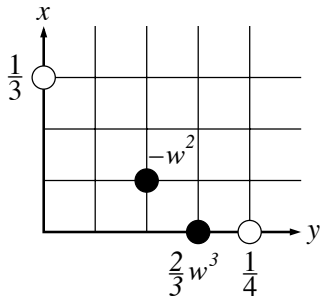

Figure 62: Result of elimination of the x^2y term in Figure 61

Another stratum to look for within the uv-plane of Figure 59 (parametrizing the closure of the D_4 stratum of the big caustic) is D_4A_2. For this, we must find out a condition on (u, v) for the functions, as in Figure 59, to have a non-Morse critical point off the origin. Thus we need the three equations

$$\begin{aligned} F_x &= x^2 + vy^2 = 0 \\ F_y &= 2vxy + 3uy^2 + y^3 = 0 \\ H &= \begin{vmatrix} F_{xx} & F_{xy} \\ F_{yx} & F_{yy} \end{vmatrix} = 4vx^2 + 12uxy + 6xy^2 - 4v^2y^2 = 0 \end{aligned}$$

to have a common solution different from $x = y = 0$.

Elimination of x and y from this system of three equations (for example, by calculating appropriate resultants in MAPLE), and taking care of avoiding the $x = y = 0$ solution, we see that the D_4A_2 stratum corresponds to $v = 0$. So, we obtain a parametrisation of the stratum in the E_6 caustic by setting $v = 0$ either in (28) or Figure 66:

$$\alpha = \beta = \gamma = 0, \quad \delta = -3u^2, \quad \epsilon = 2u^3. \tag{30}$$

5.1.2 The A-only strata of $\mathcal{C}(E_6)$

Next we are going to consider A_k singularities in E_6, assuming that A_k with the highest k is at the origin. We are interested in functions in the family in Figure 58 with singularities more complicated than A_1. Then the quadratic part of a function at the origin must be a rank 1 quadratic form. That is, $\pm(ax + by)^2$ where either $a \neq 0$ or $b \neq 0$.

5.1.2.1 Special quadratic part

We will first consider the short $a = 0$ case, the Newton diagram of which is shown in Figure 63, and $v \neq 0$ there. Therefore we have an A_2 point at the origin. The subfamilies we are looking for within this family are A_2^2 and A_2^3.

In particular, it is easy to see that the plane $u = 0$ corresponds to A_2^3 functions, with the two off-origin critical points either both real (if $8v < 9w^2$) or both complex. The members of the subfamily are of the D_4A_2 type if either

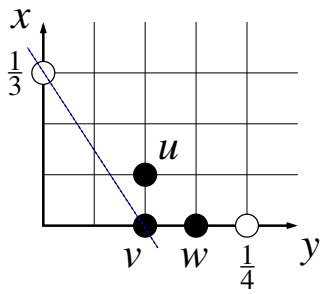

Figure 63: Functions with the special quadratic part.

$v = 0$ or $8v = 9w^2$. The setting $y := y - w$ maps the $8v < 9w^2$ region 3-to-1 onto (one of the components of) the A_2^3 stratum of the big caustic:

$$\alpha = \beta = \gamma = 0, \quad \delta = 2v - 3w^2, \quad \epsilon = 2w^3 - 2vw.$$

The boundary $4\delta^3 + 27\epsilon^2 = 0$ of the image is covered once by each of the D_4A_2 curves $v = 0$ and $8v = 9w^2$. We notice that this boundary is exactly the D_4A_2 stratum obtained in (30). The corresponding A_2^3 stratum of the E_6 caustic is the $4\delta^3 + 27\epsilon^2 < 0$ region of the $\delta\epsilon$-coordinate plane in $\mathbb{R}^5$.

In our search for the A_2^2 functions in Figure 63, we equate to zeros the gradient and Hessian in x and y of this family, and eliminating x and y with the help of MAPLE obtain the equation

$$(8v - 9w^2 + 4u^3)^2 + 144w^2u^3 = 0. \tag{31}$$

This surface is what is called the *folded Whitney umbrella*. Its singularities

are the transversal self-intersection along the A_2^3 branch $w = 2v+u^3 = 0 > u$, and the cuspidal edge along the D_4A_2 curve $u = 8v-9w^2 = 0$ (we are already familiar with the latter). The dimensions of the A_2^2 and A_2^3 strata here are respectively 2 and 1, that is, 1 less than anticipated. This means our strata are in the closures of similar strata (of the correct dimensions 3 and 2) existing in the $a \neq 0$ case of Section 5.1.2.2. The A_2^3 stratum of $\mathcal{C}(E_6)$ is considered in detail in Section 5.3.1.

5.1.2.2 General quadratic part

We can now start rather long considerations of functions with the quadratic part in Figure 58 being $\pm(ax+by)^2$, where $a \neq 0$. To collect the square in the quadratic part, we set

$$x_{new} := x + \frac{b}{a}y \qquad \text{and} \qquad y_{new} := y.$$

This 'kills' our xy and y^2 terms, but introduces xy^2 as shown in Figure 64.

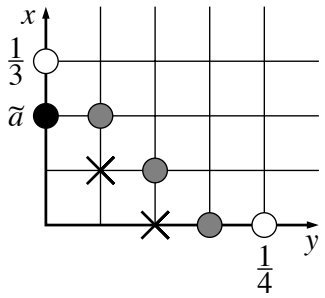

Figure 64: Singularity $A_{>1}$ at the origin, $\tilde{a} = 0$

If the coefficient of y^3 is non-zero in Figure 64, then we have the A_2 singularity at the origin. However if the coefficient of y^3 is zero then we have $A_{\geq 3}$ at the origin. In this case we rotate our 'ruler' (currently positioned through x^2, xy, y^2) about x^2 until we meet another node of the grid participating in the support of our function. First of all this may happen at xy^2 and y^4, see Figure 65.

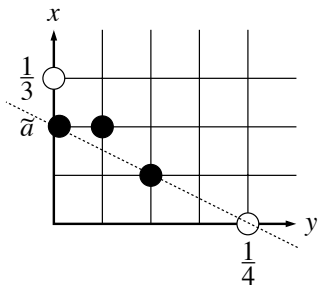

Figure 65: The Newton diagram that shows if we do not have a perfect square along the ruler then we have an A_3 point at the origin, otherwise we have $A_{\geq 4}$

If the ruler terms in Figure 65 do not form a perfect square, then the origin is an A_3 point. If they form a perfect square the we collect the ruler terms at x^2 using the substitution

$$x_{new} := x + cy^2 \qquad \text{and} \qquad y_{new} := y,$$

where c is large. This substitution is shown on Figure 66 where the terms xy^2 and y^4 have been 'killed'. Several new terms have been introduced due to this substitution.

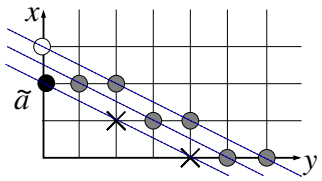

Figure 66: The Newton diagram that gives us A_4 at the origin if the coefficient of x^2y in Figure 65 is non-zero since then the coefficient of y^5 here is also non-zero

If the coefficient of x^2y in Figure 65 was non-zero then we have in Figure 66 a non-zero coefficient at y^5, and hence singularity A_4 at the origin. If the coefficient of x^2y was zero, then the terms xy^3 and y^5 in Figure 66 are absent, and we rotate the ruler about x^2 further until it hits y^6 whose coefficient cannot be zero (see Figure 67). This means an A_5 point at the origin.

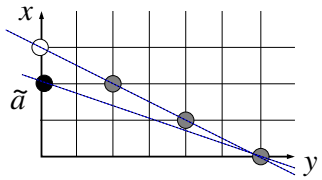

Figure 67: The Newton diagram of A_5 provided the coefficient of x^2y in Figure 65 was zero

The result of our ruler rotation exercise is that (the closures of) the A_3, A_4 and A_5 strata in the E_6 caustic may be parametrized by respectively the three families of functions shown in Figure 68.

The mapping of the first family 'packing it into the box' of Figure 57 and

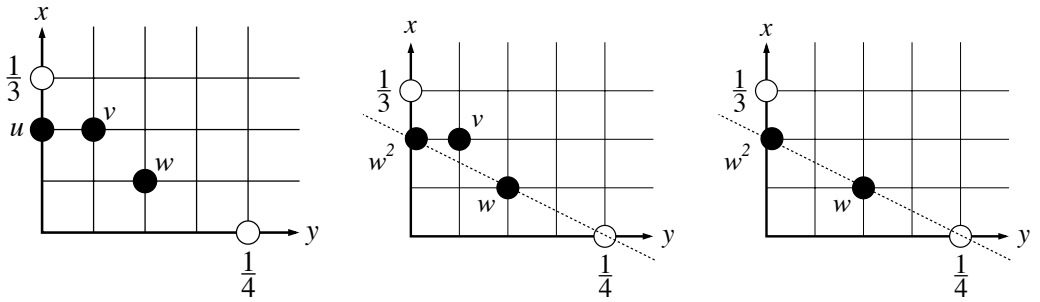

Figure 68: Families parametrising the A_3, A_4 and A_5 strata of the E_6 caustic

thus giving an A_3 parametrization is

$$
\begin{aligned}
A_3: \qquad \alpha &= -v^2 + w \qquad (32)\\
\beta &= \frac{4}{3}v^5 - 2uv + 2w^2v - \frac{10}{3}v^3w\\
\gamma &= -u^2 + v^2w^3 - 2uv^2w - \frac{7}{3}v^4w^2 + \frac{4}{3}uv^4 + \frac{16}{9}v^6w - \frac{4}{9}v^8\\
\delta &= -2uw - 3w^2v^2 + 4v^4w - \frac{4}{3}v^6 + 4uv^2\\
\epsilon &= -\frac{8}{3}v^7w - 2w^2uv + \frac{16}{27}v^9 + 2u^2v - 2w^3v^3 + \frac{16}{3}uv^3w\\
&\quad -\frac{8}{3}uv^5 + 4v^5w^2
\end{aligned}
$$

Restrictions of these formulas to the other two families parametrize the other

two strata:

$$
\begin{aligned}
A_4: \qquad \alpha &= -v^2 + w \\
\beta &= \frac{4}{3}v^5 - \frac{10}{3}v^3 w \\
\gamma &= -w^3 v^2 - w^4 + \frac{16}{9}v^6 w - v^4 w^2 - \frac{4}{9}v^8 \\
\delta &= -\frac{4}{3}v^6 + 4v^4 w + v^2 w^2 - 2w^3 \\
\epsilon &= \frac{2}{27}v(8v^8 - 36v^6 w + 18v^4 w^2 + 45v^2 w^3)
\end{aligned}
$$

$$
\begin{aligned}
A_5: \qquad \alpha &= w \\
\beta &= 0 \\
\gamma &= -w^4 \\
\delta &= -2w^3 \\
\epsilon &= 0
\end{aligned}
\tag{33}
$$

In the A_3 parametrization on the left of Figure 68, we recognize the $u = 0$ plane as the one we have used earlier for the D_4 parametrization. Let us now find some other strata within this A_3 family.

In particular, we can carry out a search for A_3A_2. Repeating the approach used in the D_4A_2 case by the end of Section 5.1.1 and for obtaining equation (31) for a part of the A_2^2 stratum, as well as ignoring certain factors

corresponding to the strata we already know, we arrive at the A_3A_2 equation

$$-12w^2uv^2 - 16v^6u - 40v^2w^4 - 9v^6w^2 - 16uw^3 + 33v^4w^3 \qquad (34)$$
$$+27v^2u^2 + 42v^4wu + 16w^5 = 0$$

This surface is shown in Figure 69.

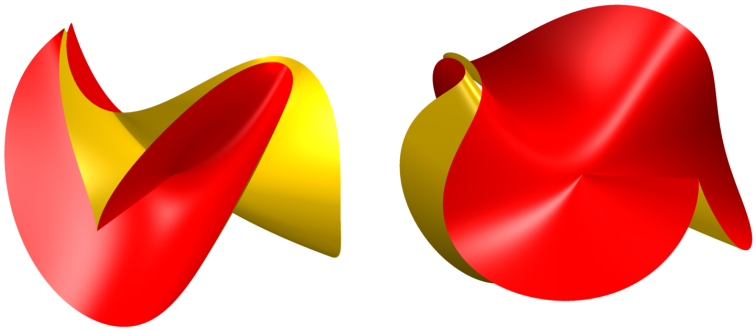

Figure 69: The 3D picture of the A_3A_2 surface given by the equation (34)

The A_4A_2 strata in $R^3_{u,v,w}$ are of course the intersections of the A_3A_2 and A_4, that is, are common zeros of the equations (34) and $u - w^2 = 0$ from Figure 68. Substitution of the second into the first gives us

$$v^2w^2(v^4 - 3v^2w + w^2) = 0. \qquad (35)$$

As we already know, the $v = 0$ here is the A_5 and $w = 0 = u$ is D_5. The quadratic's solutions $w = (3 \pm \sqrt{5})v^2/2, u = w^2$ are the A_4A_2 curves we are looking for and are shown in Figure 70 by the black dots. The parametriza-

tions of the A_4A_2 strata in $\mathcal{C}(E_6)$ are is given by

$$\begin{aligned}
\alpha &= \frac{1}{2}\left(1 \pm \sqrt{5}\right) v^2 \\
\beta &= -\frac{1}{3}\left(11 \pm 5\sqrt{5}\right) v^5 \\
\gamma &= -\frac{8}{9}\left(38 \pm 17\sqrt{5}\right) v^8 \\
\delta &= -\frac{1}{6}\left(59 \pm 27\sqrt{5}\right) v^6 \\
\epsilon &= \frac{2}{27}\left(422 \pm 189\sqrt{5}\right) v^2
\end{aligned}$$

The last stratum to consider in the uvw-space is A_3^2 which is the cuspidal edge of the A_3A_2 surface. Therefore we have to find singular points of the surface (34). Denote its left hand side by Q and equate to zero all components of its gradient:

$$\begin{aligned}
Q_u &= -16v^6 + 42v^4w - 12v^2w^2 + 54uv^2 - 16w^3 = 0 \\
Q_v &= 2v(-27v^4w^2 - 48uv^4 + 66v^2w^3 + 84uv^2w - 40w^4 - 12uw^2 + 27u^2) = 0 \\
Q_w &= -18v^6w + 99v^4w^2 + 42uv^4 - 160v^2w^3 - 24uv^2w + 80w^4 - 48uw^2 = 0
\end{aligned}$$

Taking $v = 0$ from Q_v, we obtain $w = 0$ from Q_u, which gives zero in Q_w. Therefore, the u-axis is in the singular locus of $Q = 0$. On the other hand $v = w = 0$ in Figure 68, left, gives us a one-parameter family of functions with two real A_3^2 points.

Now we want to see if we can find anything further. The pair-wise resultants of the above three derivatives of Q (however dividing Q_v through by $2v$)

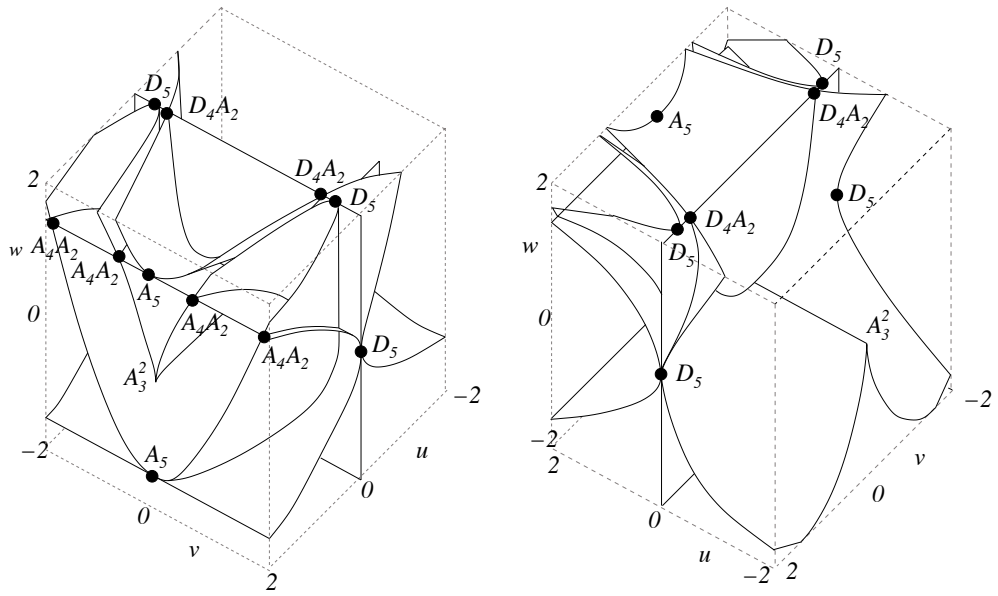

Figure 70: The $\mathbb{R}^3_{u,v,w}$ parametrizing the A_3 stratum of the big E_6 caustic. The components D_4 when $u = 0$, A_4 when $u = w^2$ and A_3A_2 when $-12w^2uv^2 - 16v^6u - 40v^2w^4 - 9v^6w^2 - 16uw^3 + 33v^4w^3 + 27v^2u^2 + 42v^4wu + 16w^5 = 0$ (cf. Figure 59). To make the diagram less busy, some of the one-dimensional strata are not shown as curves but are represented by their endpoints on the boundary of the cube.

with respect to u contain only one common factor,

$$4w^2 - 7v^2w + 4v^4.$$

Its zero set is two complex parabolas,

$$w = \frac{1}{8}v^2\left(7 \pm i\sqrt{15}\right).$$

From $Q_u = 0$ this yields

$$u = \frac{1}{36}v^4\left(-9 \pm i\sqrt{15}\right).$$

Now 'boxing' back into our $\mathcal{R}_+$-miniversal deformation of E_6 we obtain the coefficients,

$$\begin{aligned}
\alpha &= \frac{1}{8}\left(-1 \pm i\sqrt{15}\right)v^2 \\
\beta &= -\frac{1}{144}\left(3 + 5i\sqrt{15}\right)v^5 \\
\gamma &= \frac{17}{3456}\left(17 \pm 7i\sqrt{15}\right)v^8 \\
\delta &= \frac{1}{96}\left(11 \mp 3i\sqrt{15}\right)v^6 \\
\epsilon &= \frac{1}{576}\left(27 \mp 19i\sqrt{15}\right)v^9
\end{aligned}$$

These are complex expressions, and therefore do not contribute to the stratification of the real E_6 caustic.

The only curve in Figure 70 not described so far is non-straight D_5 com-

ponent. It is a part of the intersection of the A_3A_2 and D_4 surfaces. The whole intersection is obtained by setting $u = 0$ in (34), which yields $4w = 3v^2$ as an equation for this D_5 curve.

We have collected in Table 6 all the information obtained in this section about all one-dimensional strata of Figure 70. We should notice that the two D_5 curves of Figure 70 provide two different parametrizations of the same D_5 curve in the E_6 caustic: setting $v := -v/2$ in the first D_5 case in Table 6 we get the second D_5 there.

Table 6	Strata in Figure 70	Parametrizations of the strata in $\mathcal{C}(E_6)$
	A_5	$\alpha = w$ $\beta = 0$ $\gamma = -w^4$ $\delta = -2w^3$ $\epsilon = 0$
	D_5 $(u = w = 0)$	$\alpha = -v^2$ $\beta = \frac{4}{3}v^5$ $\gamma = -\frac{4}{9}v^8$ $\delta = -\frac{4}{3}v^6$ $\epsilon = \frac{16}{27}v^6$

Table 6 (continued)	Strata in Figure 70	Parametrizations of the strata in $\mathcal{C}(E_6)$
	D_5 $\left(u=0,\, w=\frac{3}{4}v^2\right)$	$\alpha=-\frac{1}{4}v^2$ $\beta=-\frac{1}{24}v^5$ $\gamma=-\frac{1}{576}v^8$ $\delta=-\frac{1}{48}v^6$ $\epsilon=-\frac{1}{864}v^6$
	D_4A_2 $(w=v^2,\, u=0)$	$\alpha=0$ $\beta=0$ $\gamma=0$ $\delta=-\frac{1}{3}v^6$ $\epsilon=-\frac{2}{27}v^9$
	A_4A_2 $\left(u=w^2,\, w=\frac{1}{2}v^2\left(3+\sqrt{5}\right)\right)$	$\alpha=\frac{1}{2}\left(1+\sqrt{5}\right)v^2$ $\beta=-\frac{1}{3}\left(11+5\sqrt{5}\right)v^5$ $\gamma=-\frac{8}{9}\left(38+17\sqrt{5}\right)v^8$ $\delta=-\frac{1}{6}\left(59+27\sqrt{5}\right)v^6$ $\epsilon=\frac{2}{27}\left(422+189\sqrt{5}\right)v^9$
	A_4A_2 $\left(u=w^2,\, w=\frac{1}{2}v^2\left(3-\sqrt{5}\right)\right)$	$\alpha=\frac{1}{2}\left(1-\sqrt{5}\right)v^2$ $\beta=-\frac{1}{3}\left(11-5\sqrt{5}\right)v^5$ $\gamma=-\frac{8}{9}\left(38-17\sqrt{5}\right)v^8$ $\delta=-\frac{1}{6}\left(59-27\sqrt{5}\right)v^6$ $\epsilon=\frac{2}{27}\left(422-189\sqrt{5}\right)v^9$

Table 6 (continued)	Strata in Figure 70	Parametrizations of the strata in $\mathcal{C}(E_6)$
	A_3^2	$\alpha = 0$
		$\beta = 0$
		$\gamma = -u^2$
		$\delta = 0$
		$\epsilon = 0$

5.2 The Straight Projection

We now start analysing contributions of various strata of the E_6 caustic to the roundabout equations corresponding to various generic mappings π of this caustic to a plane. Our plan is to use the maps π_k (see page 150) with increasing k as a sequence of approximations to π. Similar to the situation we had in the $D_6^{\pm}$ cases, the planar bifurcations diagrams $\mathcal{B}_k(E_6)$ of the π_k will serve as successive approximations to the bifurcation diagram $\mathcal{B}(E_6)$ of π. It will be clear from our calculations that once certain strata of the $\mathcal{B}(E_6)$ appear in a sufficiently generic way in certain $\mathcal{B}_k(E_6)$, their co-orientations and contributions to the roundabout equations stay the same for higher k, in spite of possible changes in the circular order of the strata within huge range of the arbitrary coefficients involved.

First of all we will use Table 6 to understand the images of the one-

dimensional strata listed there under the straight projection

$$\pi_0 : (\alpha, \beta, \gamma, \delta, \epsilon) \mapsto (A, B) = (\alpha\,,\ \beta)\,.$$

Eliminating the parameter (w or v) where needed, we obtain the following curves in $\mathcal{B}_0(E_6)$ (see Figure 71):

$$\begin{aligned} A_5 &: B = 0 \\ D_5 &: 9B^2 = -16A^5 \\ A_4A_2 &: 9B^2 = (22 + 10\sqrt{5})A^5 \quad \text{(the dashed curve in Figure 71)} \\ A_4A_2 &: 9B^2 = (22 - 10\sqrt{5})A^5 \end{aligned}$$

Finally, the Table 6 strata D_4A_2 and A_3^2 of the E_6 caustic are mapped by π_0 just to the origin in $\mathbb{R}^2_{A,B}$. This emphasises that π_0 is a rather special mapping on $\mathcal{C}(E_6)$.

Lemma 5.2.1. *Contributions of the strata D_5 and A_4A_2 to the E_6 roundabout equations are trivial.*

Proof. The family $\mathcal{F}$ in (27) defines an (α, β)-family of Lagrangian maps

$$(x, y, \delta) \mapsto (\gamma, \delta, \epsilon) = (-x^2 - \alpha y^2 - \beta y, \delta, -2\alpha xy - \beta x - y^3 - \delta y) \qquad (36)$$

The symmetry $i : (A, B) \mapsto (A, -B)$, that is $(\alpha, \beta) \mapsto (\alpha, -\beta)$, of the target plane of π_0 lifts to the symmetry $(x, y, \gamma, \delta, \epsilon) \mapsto (x, -y, \gamma, \delta, -\epsilon)$ that defines

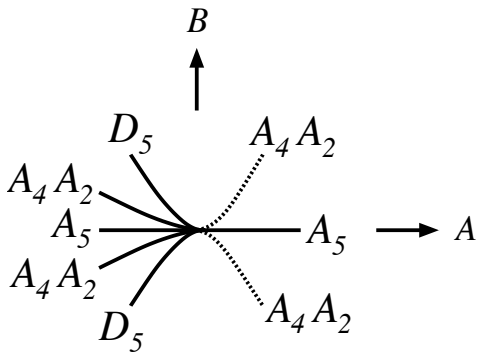

Figure 71: The strata of the bifurcation diagram $\mathcal{B}_0(E_6)$ coming from the Table 6 strata of $\mathcal{C}(E_6)$

orientation-reversing diffeomorphisms of the source and target 3-spaces in (36) under which the family of maps is equivariant. The local degrees of the Lagrangian maps are not changed by such a pair of diffeomorphisms. In particular, this means that both D_5 half-branches in Figure 71 are of the same D_5^g type. Moreover, the equivariance also means that the bifurcations in the 1-parameter families of our maps corresponding to a pair of oriented i-symmetric path-germs in $\mathbb{R}^2_{A,B}$ crossing either the D_5 or A_4A_2 strata are isomorphic. Hence the co-orientations of any pair of i-symmetric half-branches in Figure 71 by the same either positive or negative A-direction. This implies the claim of the Lemma at least on the level of the diagram $\mathcal{B}_0(E_6)$.

Our later calculations will show that, for a generic $\pi : \mathbb{R}^5_{\alpha,\beta,\gamma,\delta,\epsilon} \to \mathbb{R}^2_{A,B}$ (which may be assumed to have the principal part π_0), the D_5 and A_4A_2 strata are the only strata of $\mathcal{B}(E_6)$ with the asymptotics $A^2 = cB^5 + \dots$, where the non-zero coefficients c are different for all three curves and defined

already by π_0. Therefore, validity of the Lemma for π_0 implies its validity for generic π.

□

5.3 Tilted Projections

In the previous section we considered the non-tilted projection π_0 for one-dimensional strata of the E_6 caustic. We have noticed that some of these strata behave badly under π_0. For example $\pi_0(D_4A_2) = \{0\} \subset \mathbb{R}^2_{A,B}$. Moreover, calculations that we are omitting here demonstrate that critical points of generic projections on certain open two-dimensional strata of $\mathcal{C}(E_6)$ do not show up in π_0.

In this section we shall consider generic tiltings of π_0 individually for the closures of the A_2^3, A_4, D_4 and A_3A_2 strata. For the notational convenience, we are assuming that in the space $\mathbb{R}^3_{u,v,w}$ of Figure 70 parametrizing the closure of the A_3 stratum of the E_6 caustic, the region $u < w^2$ corresponds to A_3^σ points, while the $u > w^2$ region corresponds to $A_3^{-\sigma}$. This convention implies that all $D_4^\pm$ points we come across are of the $D_4^{\pm,\sigma}$ types, and all D_5 bifurcations are of the D_5^σ type.

Counting contributions of the individual strata of the bifurcation diagram to our roundabout equations, we will always assume that these equations are read in the $\mathbb{R}^2_{A,B}$ anti-clock-wise.

Remark 5.3.1. Most of our calculations will be restricted to generic maps

π of the E_6 caustic to a plane with the extra-weight 1 part π_1, $(A, B) = (\alpha, \beta + d\delta)$ having the coefficient d positive. Indeed the extension of the planar symmetry $i : (A, B) \mapsto (A, -B)$ introduced in Lemma 5.2.1 may be extended even further by adding the sign change of d. This implies that – as long as no $A_5^{\sigma,s}$ strata of the bifurcation diagram are involved – all the strata contributions to the equations for $d < 0$ are the negatives of those for $d > 0$. The occurrences of the $A_5^{\sigma,s}$ for $d < 0$ will be accompanied by special comments.

5.3.1 The A_2^3 stratum of the E_6 caustic

Consider the three- and four-dimensional diagrams of A_2^3 in $\mathbb{R}^3_{\alpha,\beta,\delta}$ and $\mathbb{R}^4_{\alpha,\beta,\delta,\epsilon}$ in Figures 72 and 73. MAPLE calculations show that the projection of the A_2^3 stratum of $\mathcal{C}(E_6)$ to the $\alpha\beta\delta$-space has equation $3\beta^2 + 4\alpha^2\delta + 4\alpha^5 = 0$. This is a Whitney umbrella. However, only a part of the umbrella corresponds to genuine triple points of the caustic: the remaining part is due to a pair of points in a triplet being complex. The calculations for π_1, $(A, B) = (\alpha, \beta + d\delta)$, $d > 0$, reveal the TA_2^3 stratum $\{3\alpha\beta = 4\alpha^2, \alpha > 0\}$ on the A_2^3 surface which maps to the TA_2^3 stratum of $\mathcal{B}_1(E_6) : 3dB = A^2 - 3\alpha^2 A^3$. Further tilting does not affect the cubic part of this expression $B = B(A)$.

On the other hand, the asymptotics of the A_4A_2 strata in $\mathcal{B}_1(E_6)$ (as well as the result of any further tilting) stays the same as in $\mathcal{B}_0(E_6)$: $B \sim A^{\frac{5}{2}}$, see Figure 71.

The part of the A_2^3 stratum contained in the $\delta\epsilon$-coordinate plane has two-

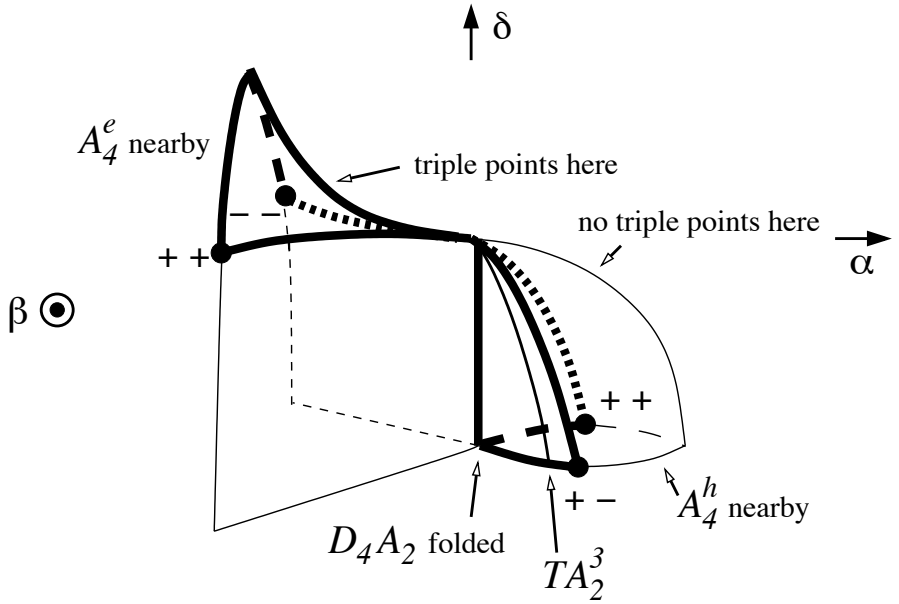

Figure 72: The 3-dimensional plot of $3\beta^2+4\alpha^2\delta+4\alpha^5=0$. The signs $++$ and $+-$ mark the A_4A_2 half-branches in $\mathcal{C}(E_6)$ parametrized by respectively $v>0$ and $v<0$ parts of the A_4A_2 curve $w=\frac{1}{2}v^2\left(3+\sqrt{5}\right)$ of Figure 70. Similarly, $-+$ and $--$ mark the A_4A_2 half-branches $w=\frac{1}{2}v^2\left(3-\sqrt{5}\right)$. These A_4A_2 strata bound the regions of genuine triple points.

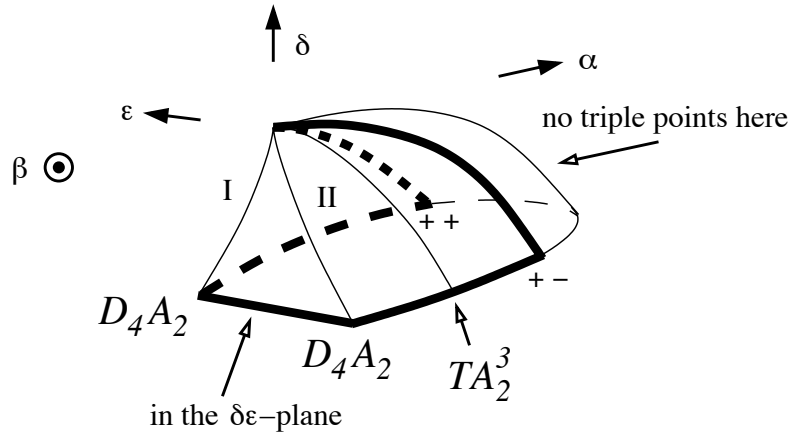

Figure 73: The result of introduction of the 4th coordinate, ϵ, in the $\alpha \geq 0$ part of the previous Figure: the flat component of the A_2^3 stratum described in Section 5.1.2.1 is inserted.

dimensional image under π_4, $(A, B) = (\alpha + k\delta, \beta + d\delta + g\gamma + e\epsilon)$ the earliest. Positions of the π_4-images of the half-branches I and II of the D_4A_2 stratum of $\mathcal{C}(E_6)$ for $d > 0$ and various choices of signs of k and e are shown in Figure 74. The way the part of the A_2^3 stratum of $\mathcal{C}(E_6)$ in Figure 73 is mapped by π_4 is shown in Figure 75 for $d > 0$, $k > 0$, $e < 0$. The contribution of this figure (as well as of each of the other three sign cases) to the roundabout equations is

$$d_{4,1}^{+;\sigma} a_2 - t a_2^3 + [d_{4,2}^{+;\sigma} a_2]$$

which is zero according to the equations **29** and **30**.

The left part of the A_2^3 stratum of $\mathcal{C}(E_6)$ in Figure 72 maps diffeomorphically onto its image in $\mathbb{R}^2_{A,B}$ (the cuspidal sector bounded by the A_4A_2 curve

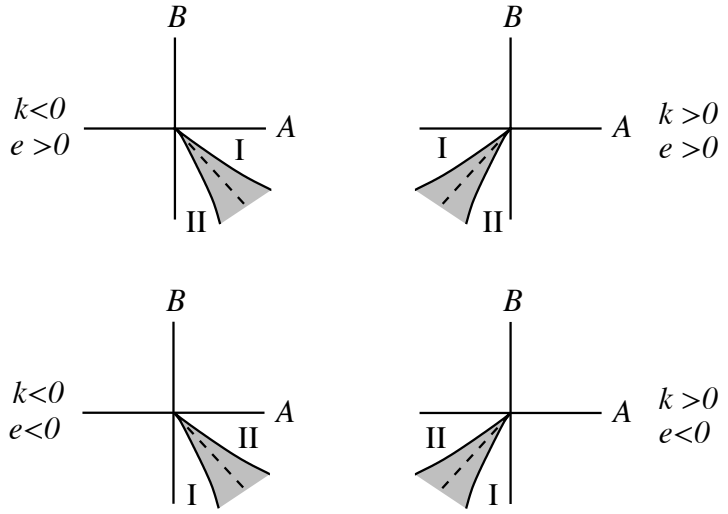

Figure 74: The π_4 images of the flat A_2^3 region in Figure 73 for various parameter options.

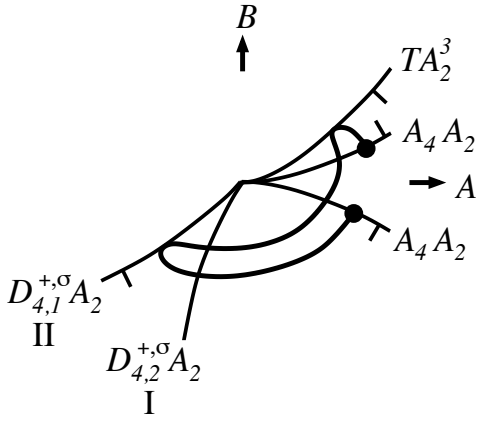

Figure 75: The image of the lower cut of the A_2^3 surface of Figure 73 under generic π_4 (and hence under generic π) for $d > 0$. The way the image folds detects the co-orientations of the bifurcational strata.

in the left part of Figure 71), and contributes nothing to the roundabout equations.

Summarising the results of this subsection we have

Lemma 5.3.2. *The total contribution of the closure of the A_2^3 stratum of $\mathcal{C}(E_6)$ to any roundabout equation is zero.*

5.3.2 The A_4 stratum in the E_6 caustic

In this and two following subsections we will be using the parametrizations of the strata of the E_6 caustic constructed in Section 5.1.2.2 and illustrated in Figure 70. Such a parametrization of a stratum S will be denoted p_S.

The earliest of all the features of $\mathcal{B}(E_6)$ emerging from the closure of the A_4 stratum of $\mathcal{C}(E_6)$ are seen clearly in the projection π_3,

$$(A, B) = (\alpha, \beta + d\delta + g\gamma).$$

To demonstrate this, we now consider what formulae (32) give for π_3 after the A_4 setting $u = w^2$:

$$\pi_3 \circ p_{A_4} : (v, w) \mapsto (\alpha, \beta + d\delta + g\gamma)$$

where

$$\begin{aligned}
\alpha &= w - v^2 \\
\beta &= \frac{4}{3}v^5 - \frac{10}{3}wv^3 \\
\gamma &= -w^4 - w^3v^2 - w^2v^4 + \frac{16}{9}wv^6 - \frac{4}{9}v^8 \\
\delta &= w^2v^2 + 4wv^4 - \frac{4}{3}v^6 - 2w^3
\end{aligned}$$

The critical point set of π_3 is

$$vw\left(v + d(w - 2v^2) + g\left(w^2 + wv^2 - \frac{2}{3}v^4\right)\right) = 0.$$

The factors here correspond in the E_6 caustic to the strata A_5, D_5 and $A_4^{e/h}$. The $\pi_3 \circ p_{A_4}$-images of these curve give us the strata of the planar bifurcation diagram:

$$\begin{aligned}
A_5 &: B = -2dA^3 - gA^4 \quad \text{(see (33) on page 163)} \\
D_5 &: B^2 \sim -\frac{16}{9}A^5 \quad \text{(see (29) on page 156)} \\
A_4^{e/h} &: B = -2dA^3 - \left(g + \frac{5}{3}d^3\right)A^4 + \cdots
\end{aligned}$$

To obtain the last expansion, we determine a few first terms of the Taylor expansion $v = v(w)$ of the solution to the last equation, and use it to obtain the Taylor expansions $A = A(w)$ and $B = B(w)$, from which we then eliminate w. The way the $\pi_3 \circ p_{A_4}$ map folds the vw-plane if $d > 0$ is shown in Figure

76. The folding defines the co-orientations of the strata in the AB-plane.

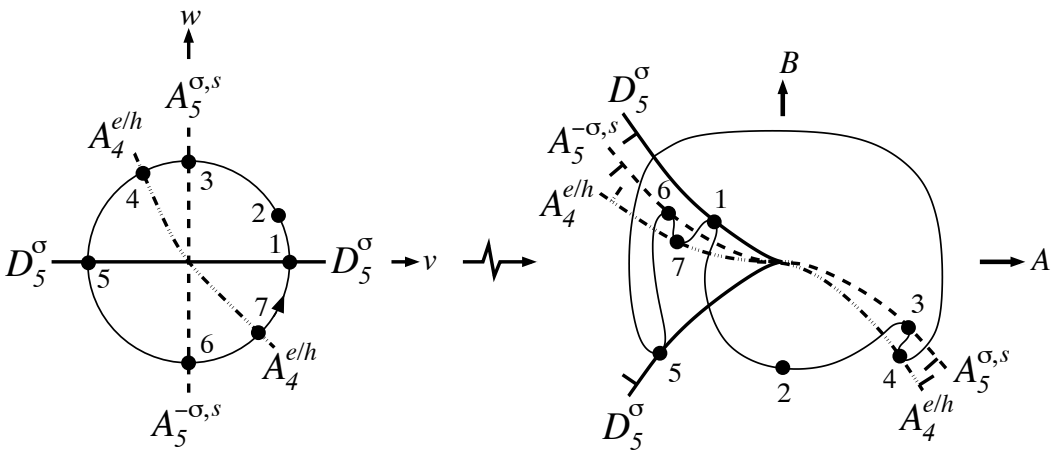

Figure 76: The folding of the uv-plane by the $\pi_3 \circ p_{A_4}$ map when $d > 0$

The MAPLE calculations demonstrate that the decorations of the A_5 half-branches are as shown in Figure 77. The orientation sign of the frame $\gamma\delta\epsilon$ (of

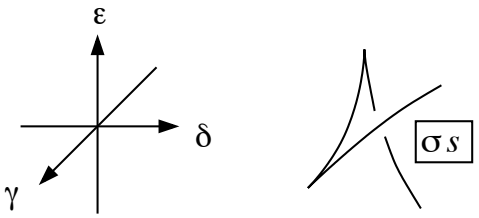

Figure 77: The result of calculations of the local shape of the cuspidal edge of the caustic in $\mathbb{R}^3_{\gamma,\delta,\epsilon}$ for the parameter values (A, B) just below point 3 in the right diagram of Figure 76

the three-space where our caustics live) is then σs. Therefore the contribution

of the A_4 closure to the roundabout equations is

$$a_5^{-\sigma,s} - a_5^{\sigma,s}.$$

According to equation **18**, over $\mathbb{R}$, is equal to $-\sigma a_3^{2,h,+,-}$.

As it was promised at the start of Section 5.3, we now check what happens if we take $d < 0$. In this case, the symmetry mentioned there basically reflects the right diagram in Figure 76 in the horizontal axis. The strata names follow their half-branches, with only one adjustment: the s in the A_5 strata notations becomes $-s$. Thus, the new diagram has total contribution

$$a_5^{\sigma,-s} - a_5^{-\sigma,-s}$$

to the anti-clock-wise equation. Similar to the previous this is equal to $\sigma a_3^{2,h,+,-}$. This is absolutely consistent with our general principle that the anti-clock-wise equations for $d < 0$ should be the negatives of those for $d > 0$. Therefore, consideration of the $d > 0$ case only provides all possible equations coming from the big E_6 caustic.

We conclude this section with a summary of its results:

Lemma 5.3.3. *The total contribution of the closure of the A_4 stratum of $\mathcal{C}(E_6)$ to any roundabout equation is equal to $-sign(d)\sigma a_3^{2,h,+,-}$.*

5.3.3 The D_4 stratum in the E_6 caustic

Figure 78 shows the two parametrizations of the closure of the D_4 stratum of $\mathcal{C}(E_6)$ we have considered earlier. They are are related by the pleat map

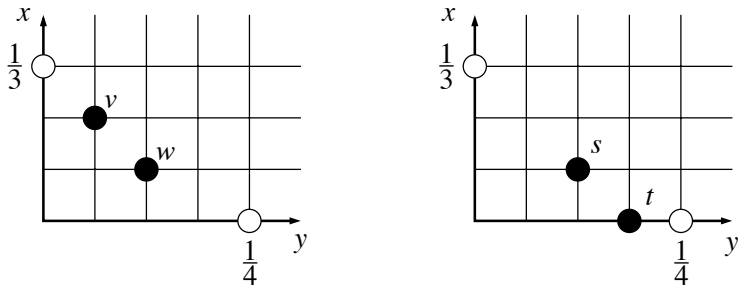

Figure 78: The two parametrizations of the closure of the D_4 stratum of $\mathcal{C}(E_6)$

$$(s,t) = \left(w - v^2, \frac{2}{3}v^3 - vw\right).$$

The participating strata are mapped by it as shown in Figure 79. In this Figure we distinguish the critical point set $D^+_{4,q}$ of the fold map

$$\pi_1 \circ p_{D_4} : (s,t) \mapsto (A,B) = (\alpha, \beta + d\delta) = (s, -2st - 3dt^2),\ d > 0,$$

which is $0 = \frac{\partial B}{\partial t} = -2(s+3dt)$. The corresponding part of the $\mathcal{B}_1(E_6)$ coming from the closure of the D_4 stratum of $\mathcal{C}(E_6)$ is given in Figure 80. MAPLE calculations show that both half-branches of the $D^{+,\sigma}_{4,q}$ strata are $D^{+,\sigma}_{4,a}$. We see from this diagram that the D_5 and $D_{4,q}$ contributions to the roundabout equations are zero. Since the D_4A_2 contribution has already been included in

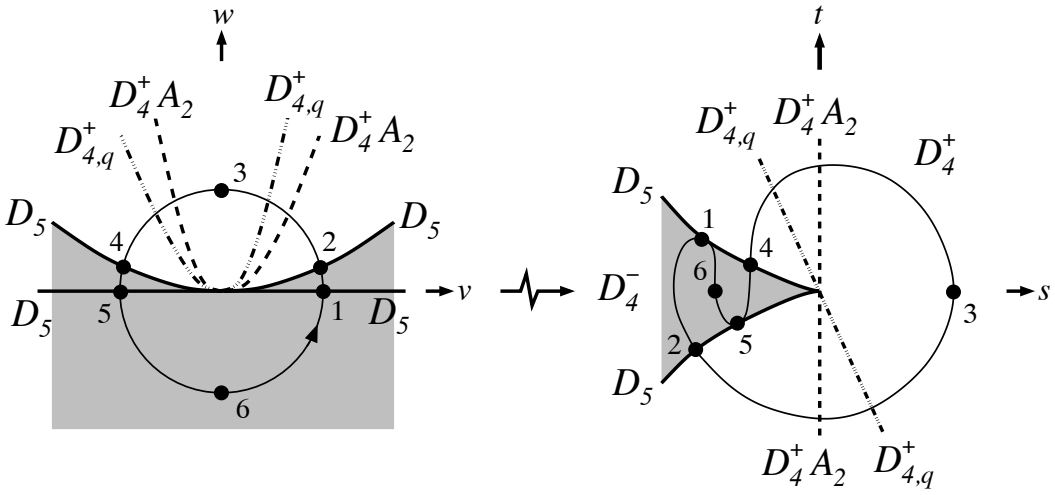

Figure 79: Mapping one parameter space of Figure 78 to the other. The shaded regions represent $D_4^{-,\sigma}$ points, and the non-shaded regions $D_4^{+,\sigma}$

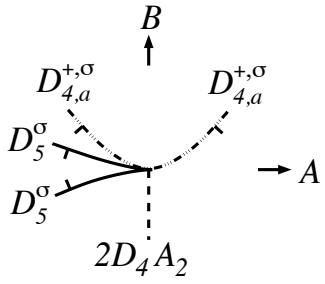

Figure 80: The part of $\mathcal{B}_1(E_6)$ coming from the closure of the D_4 stratum of $\mathcal{C}(E_6)$

the A_2^3 case, we have

Lemma 5.3.4. *Modulo the total contributions to the roundabout equations coming from the closure of the A_2^3 stratum of $\mathcal{C}(E_6)$, similar contributions of the closure of the D_4 stratum are zero.*

5.3.4 The A_3A_2 stratum of the E_6 caustic

Take the map

$$\pi_1 : (\alpha, \beta, \gamma, \delta, \epsilon) \mapsto (A, B) = (\alpha, \beta + d\delta) \tag{37}$$

where α, β, δ are given by formulas (32). We recall that the equation of the A_3A_2 surface is

$$Q := -12w^2uv^2 - 16v^6u - 40v^2w^4 - 9v^6w^2 - 16uw^3 + 33v^4w^3 + 27v^2u^2$$
$$+42v^4wu + 16w^5 = 0.$$

Let us find critical points of π_1 on the A_3A_2 stratum (the open one, without closing that adds A_5, D_5 etc). The critical values corresponding to such critical points are the TA_3A_2 strata of the $\mathcal{B}_1(E_6)$. Taking the determinant of

the Jacobi matrix of α, B and Q with respect to u, v, w results in the equation

$$\begin{aligned} J &:= \begin{vmatrix} \alpha_u & \alpha_v & \alpha_w \\ B_u & B_v & B_w \\ Q_u & Q_v & Q_w \end{vmatrix} \\ &= -48uv^4w + 108uv^2w^2 + 32w^5 - 168v^2w^4 - 32uw^3 - 172v^6w^2 - 8uv^6 \\ &\quad +268v^4w^3 + 120dwuv^5 - 348dw^2uv^3 + 304dw^3uv - 108dwu^2v \\ &\quad -80dv^9w - 740dw^3v^5 + 384dw^2v^7 + 688dw^4v^3 - 256dw^5v + 16dv^7u \\ &\quad +40v^8w = 0 \end{aligned}$$

The resultant of J and Q with respect to u yields

$$\begin{aligned} &-2160\, v^2\, w\, (w^2 - 3v^2w + v^4)\, (4v^4 - 7v^2w + 4w^2)^3\, (4d^2v^6 - 4dv^5 \quad (38) \\ &-16v^4d^2w + v^4 + 10dv^3w + 21v^2d^2w^2 - v^2w - 8dw^2v - 12d^2w^3) = 0. \end{aligned}$$

There is no need to consider $v = 0$, $w = 0$ or $w^2 - 3v^2w + v^4 = 0$ since these have previously been considered in (35). Similarly we have already found that $4v^4 - 7v^2w + 4w^2 = 0$ has a negative discriminant therefore we only consider the remaining bracket. Its Newton diagram is given in Figure 81. The monomials on the faces provide us with the asymptotics of the TA_3A_2

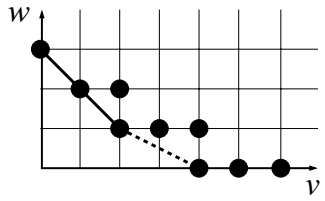

Figure 81: The support of longest bracket in (38)

branches:

$$w(-v^2 - 8dvw - 12d^2w^2) = 0 \quad \Rightarrow \quad v = -2dw + \cdots\,,\ v = -6dw + \cdots$$
$$v^2(-w + v^2) = 0 \quad \Rightarrow \quad w = v^2 + \cdots$$

Extending these Taylor expansions, and using them to find the corresponding Taylor expansions for the solutions u of the equations $Q = J = 0$, we obtain the following three TA_3A_2 curves:

i) $v = -2dw + 5d^3w^2 - \frac{133}{4}d^5w^3 + \cdots\,,\ u = \frac{4w}{27d^2} + \frac{5w^2}{27} - \frac{229}{108}d^2w^3 + \cdots$

ii) $v = -6dw + 27d^3w^2 - \frac{8667}{4}d^5w^3 + \cdots\,,\ u = w^2 - \frac{225}{4}d^2w^3 + \cdots$

iii) $w = v^2 - 2dv^3 + 9d^2v^4 + \cdots\,,\ u = -dv^5 + 8d^2v^6 + \cdots$

emerging respectively from the A_3^2, A_5 and D_4A_2 strata in Figure 70. For $d > 0$, their half-branches are represented by the grey circles in Figure 82. Four of the half-branches are $TA_3^{\sigma}A_2$ and the two others are $TA_3^{-\sigma}A_2$.

Our last task about the closure of the A_3A_2 stratum of $\mathcal{C}(E_6)$ is to understand the A_3^2 stratum in $\mathcal{B}(E_6)$. The A_3^2 stratum in Figure 70 is the u-axis, and

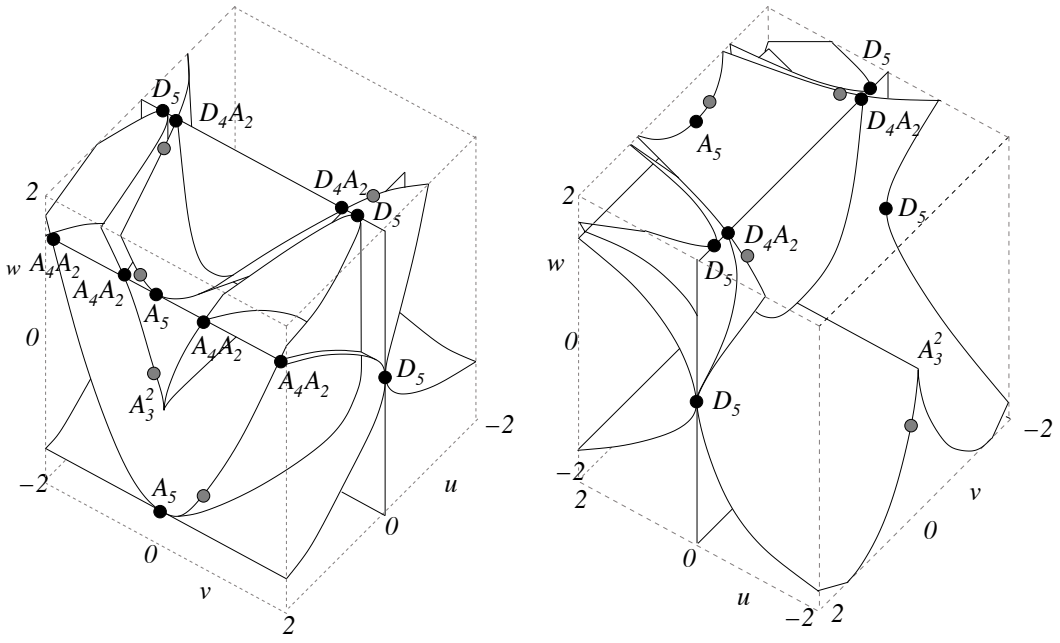

Figure 82: The $\mathbb{R}^3_{u,v,w}$ parametrizing the closure of the A_3 stratum of $\mathcal{C}(E_6)$ with the emerging TA_3A_2 strata found using the π_1 projection when $d > 0$. The TA_3A_2 strata are denoted by grey circles.

it maps 2-to-1, $u \mapsto \gamma = -u^2$, to the negative γ-coordinate ray in $\mathbb{R}^5_{\alpha,\beta,\gamma,\delta,\epsilon}$. This ray is the A_3^2 stratum of $\mathcal{C}(E_6)$. Therefore, the earliest it shows up in the bifurcation diagram of E_6 is under the projection π_3:

$$(A, B) = (\alpha, \beta + d\delta + g\gamma).$$

We have $\mathcal{B}_3(E_6) \supset A_3^2 = \{(A, B) = (0, -gu^2)\} \subset \mathbb{R}^2_{A,B}$ (see Figure 83). Consider the point $(0, -\gamma) \in A_3^2 \subset \mathbb{R}^2_{A,B}$. Its preimages in $A_3^2 \subset \mathbb{R}^3_{u,v,w}$ (which

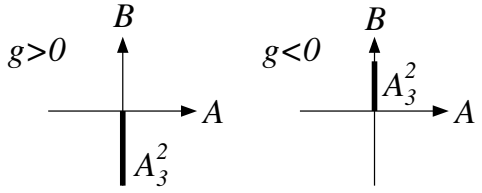

Figure 83: The A_3^2 stratum in $\mathcal{B}_3(E_6)$

parametrizes the A_3 stratum of $\mathcal{C}(E_6)$) are $(\pm 1, 0, 0)$, and its total π_3-preimage in $\mathbb{R}^3_{u,v,w}$ consists of the two A_3 curves

$$\left\{u = \pm 1 - \frac{v}{g} + \cdots, w = v^2.\right\}$$

The $u = +1 - \cdots$ curve is $A_3^{-\sigma}$, and the $u = -1 - \cdots$ is A_3^{σ}. They parametrize the two edges of the three-dimensional caustic meeting at the A_3^2 point. Their vw-projections are shown in Figure 84 by dashed curves. Now take a point $(A, B) = (a, -g)$ with small $a \neq 0$, and check how the dashed curves of Figure 84 move. Since $A = \alpha = w - v^2$ their meeting points with the w-axis $v = 0$

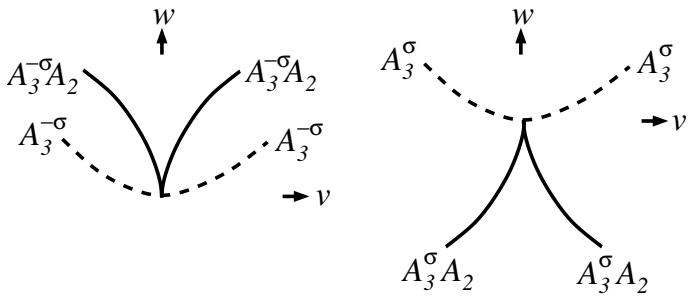

Figure 84: Curves parametrizing edges meeting at an A_3^2 point. Near $(1,0,0)$ and $(-1,0,0)$ respectively

will move to $w = a$, that is, for $a > 0$ the three-dimensional caustic will have two $A_3^{-\sigma}A_2$ points, and for $a < 0$ it will have two $A_3^{\sigma}A_2$ points. Therefore, our A_3^2 point was of the $A_3^{2,h,+,-}$ type, and (since the positive side of an $A_3^{2,h,+,-}$ stratum is where two $A_3^+A_2$ points exist) the co-orientations of the strata are as in Figure 85.

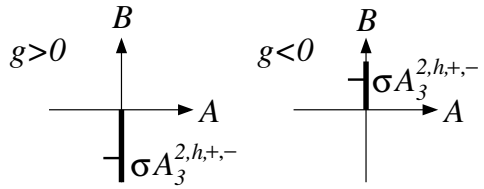

Figure 85: Co-orientation of the A_3^2 stratum of $\mathcal{B}_3(E_6)$.

We summarise the results of this section as

Lemma 5.3.5. *Modulo the contributions to the $\mathcal{B}(E_6)$ coming from the closures of the strata A_2^3, A_4 and D_4 of $\mathcal{C}(E_6)$, similar contributions of the closure*

of the A_3A_2 stratum for $d > 0$ consist of the $A_3^{2,h,+,-}$ stratum as shown in Figure 85, and of four $TA_3^qA_2$ and two $TA_3^{-\sigma}A_2$ half-branches.

5.4 Deriving the E_6 roundabout equations

MAPLE calculations demonstrate that a generic mapping π has no critical points on the open strata A_2^2 and A_3 of $\mathcal{C}(E_6)$. Therefore the strata TA_2^2 and A_3^q of the bifurcation diagram $\mathcal{B}(E_6)$ are empty.

This reduces the participants of the roundabout equations for $d > 0$ just to the summand $-\sigma a_3^{2,h,+,-}$ (see Lemma 5.3.3) and the contributions due to Lemma 5.3.5. From Figure 85, we see that the $a_3^{2,h,+,-}$ enters the roundabout equations with the coefficient -2σ if $g > 0$, and 0 if $g < 0$. The jumps $ta_3^{\pm}a_2$ must enter the equations with the coefficients reflecting the fact that the total increments of the numbers of $A_3^{\pm}A_2$ points along a loop around the origin in $\mathbb{R}^2_{A,B}$ must be zeros.

Thus the equation for $g < 0$ reduces to $0 = 0$, while for $g > 0$ it is

$$-2\sigma a_3^{2,h,+,-} + 2\sigma t a_3^+ a_2 - 2\sigma t a_3^- a_2 = 0.$$

This completes the derivation of the equation **32** from Section 2.3.2.7 and thus our proof of Theorem 2.3.3.

List of Figures

Bibliography

[1] F.Aicardi, 'Discriminants and local invariants of planar fronts', *The Arnold-Gelfand mathematical seminars. Geometry and singularity theory* (eds V.I.Arnold, I.M.Gelfand, V.S.Retakh and M.Smirnov), Birkhäuser Boston, Boston, MA, 1997, 1–76.

[2] F.Aicardi, 'On mod2 local invariants of maps between 3-manifolds', ResearchGate publication 259189520.

[3] V.I.Arnold, 'Wave front evolution and equivariant Morse lemma', *Comm. Pure Appl. Math.* **29** (1976) no. 6, 557–582.

[4] V.I.Arnold, *Singularities of caustics and wave fronts*, Mathematics and its Applications (Soviet Series) **62**, Kluwer, Dordrecht, 1990, xiv+259 pp.

[5] V.I.Arnol'd, 'Plane curves, their invariants, perestroikas and classifications'. With an appendix by F. Aicardi, *Advances in Soviet Mathematics* **21**, Singularities and bifurcations, 33–91, Amer. Math. Soc., Providence, RI, 1994.

[6] V.I. Arnold, 'Invarianty i perestroiki ploskih frontov', Osobennosti gladkikh otobrazheniy s dopolnitel'nymi strukturami, *Trudy Mat. Inst. Steklov.* **209** (1995) 14–64. English translation: 'Invariants and perestroikas of wave fronts on the plane', Singularities of smooth mappings with additional structures, *Proc. Steklov Inst. Math.* **209** (1995) 11–56.

[7] V.I.Arnold, S.M.Gusein-Zade, and A.N.Varchenko, *Singularities of differentiable maps. Vol. I. The classification of critical points, caustics and wave fronts*, Monographs in Mathematics **82**, Birkhäuser Boston, Boston, MA, 1985, xi+382 pp.

[8] J. W. Bruce, 'A classification of 1-parameter families of map germs $\mathbb{R}^3, 0 \to \mathbb{R}^3, 0$ with applications to condensation problems', *Journal of the London Mathematical Society* **33** (1986), 375–384.

[9] J. Callahan, 'Bifurcation geometry of E_6', *Mathematical Modelling* **1** (1980), 283–309.

[10] V.Goryunov, 'Singularities of projections of complete intersections', *Current problems in mathematics*, vol. 22, 167–206, Itogi Nauki i Tekhniki, Akad. Nauk SSSR, VINITI, Moscow, 1983 (Russian). English translation: *Journal of Soviet Mathematics* **27** (1984) no.3, 2785–2811.

[11] V.Goryunov, 'Local invariants of mappings of surfaces into three-space', *The Arnold-Gelfand mathematical seminars. Geometry and singularity*

theory (eds V. I. Arnold, I. M. Gelfand, V. S. Retakh and M. Smirnov), Birkhäuser Boston, Boston, MA, 1997, 223–255.

[12] V.Goryunov, 'Vassiliev type invariants in Arnold's J^+-theory of plane curves without direct self-tangencies', *Topology* **37** (1998), no. 3, 603–620.

[13] V.Goryunov, 'Local invariants of maps between 3-manifolds', *Journal of Topology* **6** (2013) 757–778.

[14] V.Goryunov, 'The cohomology of braid groups of series C and D and certain stratifications', *Functional Analysis and its Applications* **12** (1978) no.2, 139-140.

[15] V.Goryunov, and S.Alsaeed, 'Local invariants of framed fronts in 3-manifolds', *Arnold Mathematical Journal* **1** (2015), no. 3, 211–232.

[16] V.Goryunov, and K.Gallagher, 'On planar caustics', *J. Knot Theory Ramifications* **25** (2016), no. 12, 1642004, 23 pp.

[17] L. Kauffman, *Knots and physics*, 3rd edition. Series on Knots and Everything, 1. World Scientific Publishing, 2001.

[18] A.B.Merkov, 'On the classification of ornaments', Singularities and bifurcations, 199–211, *Advances in Soviet Mathematics* **21**, Amer. Math. Soc., Providence, RI, 1994.

[19] T.Ohmoto, and F.Aicardi, 'First order local invariants of apparent contours', *Topology* **45** (2006) no. 1, 27–45.

[20] R. Oset Sinha, *Topological invariants of stable maps from 3-manifolds to three-space*, PhD dissertation, Valencia, 2009.

[21] V.Tchernov, 'Arnold-type invariants of wave fronts on surfaces', *Topology* **41** (2002) no. 1, 1–45.

[22] V.A.Vassiliev, 'Cohomology of knot spaces', Theory of singularities and its applications, *Advances in Soviet Mathematics* **1**, American Mathematical Society, Providence, RI, 1994, 225–262.

[23] V.A.Vassiliev, 'Invariants of ornaments', Singularities and bifurcations, 225–262, *Advances in Soviet Mathematics* **21**, Amer. Math. Soc., Providence, RI, 1994.

[24] V.A.Vassiliev, *Lagrange and Legendre characteristic classes,* Advanced Studies in Contemporary Mathematics **3**, Gordon and Breach Science Publishers, New York, 1988, x+268 pp.

[25] H.Whitney, 'On Singularities of Mappings of Euclidean Spaces. I. Mappings of the Plane into the Plane', Annals of Mathematics **62** (1955), 374–410.

[26] V.M.Zakalyukin, 'Reconstructions of fronts and caustics depending on a parameter, and versality of mappings'. *Current problems in mathematics*, vol. 22, 56–93, Itogi Nauki i Tekhniki, Akad. Nauk SSSR, VINITI,

Moscow, 1983 (Russian). English translation: *Journal of Soviet Mathematics* **27** (1984) no.3, 2713–2735.